Mangifera Indica Mediated Biogenic Synthesis of Undoped and Doped TiO_2 Nanoparticles and Evaluation of Their Structural, Morphological, Photocatalytic and Antibacterial Properties

BY
ASRAFUZZAMAN
STUDENT ID: 0417112004

MASTER OF SCIENCE IN MATERIALS & METALLURGICAL ENGINEERING

DEPARTMENT OF MATERIALS & METALLURGICAL ENGINEERING
BANGLADESH UNIVERSITY OF ENGINEERING & TECHNOLOGY

24 MAY 2022

CANDIDATE'S DECLARATION

IT IS DECLARED HEREBY THAT, THIS THESIS PAPER OR ANY PART OF IT HAS NOT BEEN SUBMITTED ANYWHERE ELSE FOR THE AWARD OF ANY DEGREE.

ASRAFUZZAMAN

STUDENT ID: 0417112004

APPROVAL PAGE

The thesis entitled "Mangifera Indica Mediated Biogenic Synthesis of Undoped and Doped TiO_2 Nanoparticles and Evaluation of Their Structural, Morphological, Photocatalytic and Antibacterial Properties" submitted by Asrafuzzaman, Roll No: 0417112004, Session: April/2017, has been accepted as satisfactory in partial fulfillment of the requirement for the degree of Masters of Science in Materials and Metallurgical Engineering on May, 2022.

BOARD OF EXAMINERS

1.....Fahmida.....

Dr. Fahmida Gulshan (Supervisor) — Chairman
Professor,
Department of MME, BUET, Dhaka

2.....M.HASAN.....

Head (Ex-officio) — Member
Department of MME, BUET, Dhaka

3.....Rashed.....

Dr. Hossain Mohammad Mamun Al Rashed — Member
Associate Professor,
Department of MME, BUET, Dhaka

4.....Billah.....

Dr. Md. Muktadir Billah — Member
Associate Professor,
Department of MME, BUET, Dhaka

5.....

Dr. Abdul Gafur — Member (External)
Principle Scientific Officer,
PP and PDC, BCSIR, Dhaka

DEDICATION

DEDICATED TO MY BELOVED PARENTS

AND

ALL THE WELL-WISHERS

ACKNOWLEDGEMENTS

First and foremost, I would like to thank the Almighty Allah for blessing me with the means and opportunity to carry out this thesis work successfully and in due time in spite of difficulties.

I express my heartfelt gratitude to my thesis supervisor Dr. Fahmida Gulshan (Professor, DMME, BUET) for giving me the independence in choosing and doing the research according to my own time schedule. As a result, I faced less hindrances regardless of the long distance between my workplace (Rajshahi) and BUET. Perhaps, this was the most important reasons behind the completion of this thesis. Her excellent supervision, and continuous inspiration made me successful in submitting this dissertation. I truly appreciate and value her liberal help, kindness and care. I would also like to thank her endlessly for acceding to my unfair demands of reviewing and correcting this thesis in a very short amount of time.

I would like to thank Dr. Abdul Gafur (Principle Scientific Officer, PP and PDC, BCSIR, Dhaka), for giving me permission to use the Photocatalytic Reactor and the UV-Vis spectrometer in an accessible way. Without the lab facilities provided, a specific part of this research would not have been possible.

I thank Dr. Mahbub Hasan, Professor and Head, Department of Materials and Metallurgical Engineering, BUET, for arranging my thesis defense in a very short time in spite of all his busyness. My examiners also deserve my deepest gratitude for agreeing to hold my thesis defense within an unreasonably short period of time. Thank you Dr. Hossain Mohammad Mamun Al Rashed, Dr. Md. Muktadir Billah, and Dr. Abdul Gafur.

I am immensely grateful to my wife Kazi Faiza Amin for her encouragement and insight through these years. Without her consistent inspiration and co-operation with many experimental aspects this project would have remained incomplete. I am thankful to Dr. Sadia Afrin (Senior Scientific Officer, Industrial Microbiology Section, IFST, BCSIR) and Dr. Md. Abu Reza (Professor, Dept. of Genetic Engineering and Biotechnology, Rajshahi University) for their initial help on the antibacterial activity analysis.

Finally, I would like to thank my parents immensely for supporting me throughout the years and believing in me.

ABSTRACT

Pristine and doped TiO_2 nanoparticles were synthesized utilizing mango leaf extract via a cost effective and eco-friendly biogenic route. As a precursor, titanium isopropoxide (TTIP) was used. The transition metals, Cu and Ag, were added as dopant materials in various concentration levels of 0.5%, 1%, 1.5%, and 2%. To assess the morphological, structural, photocatalytic, and antibacterial properties of the prepared samples, several characterization techniques such as SEM, EDX, XRD, UV-Vis, Kirby-Bauer disk diffusion method were implemented. The observation from SEM analysis revealed that compared to undoped TiO_2, Cu- and Ag-doped TiO_2 nanoparticles showed agglomeration. Evaluation of elemental analysis by EDX confirmed the doping of Cu^{2+} and Ag^{+} ions in the TiO_2 lattice structure. It also ensured the absence of any kind of impurities. According to XRD analysis, pure TiO_2 as well as Cu- and Ag-doped TiO_2 nanoparticles exhibited formation of anatase phase without any rutile phase. Crystallite size and micro-strain of the prepared nanoparticles were determined from XRD results along with W-H plot. At maximum doping percentage (2%), both Cu- and Ag-doped TiO_2 samples showed reduction in crystallite size compared to pure TiO_2. UV-Vis spectroscopy was employed to determine the band gap and photocatalytic efficiency of the prepared samples. Both Cu- and Ag-doped TiO_2 samples showed a gradual decline in band gap in comparison to undoped TiO_2 with the increasing doping percentage. The result of the photo-degradation of methylene blue (MB) demonstrated that doping of TiO_2, whether with Cu/Ag, greatly enhance the photocatalytic performance which is attribute to the "Red-Shift" phenomena along with the reduced photo-generated electron-hole recombination rate. Antibacterial performance of the prepared samples was examined against Gram positive and Gram negative bacteria strain utilizing Kirby-Bauer disk diffusion technique. Cu- and Ag- doped TiO_2 nanoparticles of specific doping percentage showed mentionable zone of inhibition confirming their potential as bactericidal agent. Results obtained suggest that TiO_2 nanoparticles (both undoped and doped) synthesized through a greener approach may have a promising future for water purification, dye remediation, medical sector and food industry owing to better photo-degradation and antibacterial activity.

Keywords: TiO_2 nanoparticles, Mango leaf extract, Biogenic route, Photocatalytic activity, Antibacterial activity.

TABLE OF CONTENT

LIST OF FIGURES

LIST OF TABLES

LIST OF ABBREVIATIONS

NPs	Nanoparticles
MNPs	Metal Nanoparticles
ROS	Reactive Oxygen Species
TiO_2	Titanium Oxide or Titania
MLs	Mango Leaves
E_{BG}	Band gap Energy
V_B	Valence Band
C_B	Conduction Band
e^-	Electron
Ag	Silver
Cu	Copper
TTIP	Titanium Isopropoxide
$AgNO_3$	Silver Nitrate
$CuSO_4$	Copper Sulphate
DW	Distilled Water
MB	Methylene Blue
CFU	Colony Formation Unit
XRD	X-ray Diffraction Spectroscopy
SEM	Scanning Electron Microscopy
EDS	Energy Dispersive X-ray Spectroscopy
UV-Vis	Ultraviolet–visible spectroscopy
W-H Plot	Williamson-Hall Plot

CHAPTER 1: INTRODUCTION

1.1 Background and Research Motivation

The rapid industrialization and urbanization along with unconstrained uses of hazardous and superfluous materials and chemicals are causing our environment to undergo a massive collapse. As a result, to become familiar with the secrets dwelling in nature and its' natural commodities in order to make necessary developments for the synthesis of nanoparticles has become a dire need [1]. There is an inextricable link between green nanotechnology and green synthesis. During the green synthesis of metallic nanoparticles, biological molecules go through sophisticated assembly that are proven to be safe and reliable for environment [2][3]. There are large scopes of research to develop innovative and novel technology for the synthesis of nanoparticles that are metallic and semiconductor in nature [4]. Nanoparticles are rapidly evolving in various domains due to its' enhanced properties, size, shapes, distribution and morphology. The unique physiochemical properties of nanoparticles including high surface to volume ratio, catalytic actions, optical characteristics, antibacterial properties, magnetic and electronic attributes have made the scientist to give a peak interest in this field [5-8].

Among various nanoparticles, TiO_2 nanoparticles (NPs) have promising capability due to their applications in diverse fields from biotechnology to space science [9][10]. Though conventional chemical approaches for TiO_2 NP synthesis are capable of meeting the growing demand, it has also invited degradation of the environment, as a result of the release of toxic substances, during the manufacture and processing of the particles [11]. Moreover, the chemical method is quite costly. As a result, an eco-friendly and cost-effective alternate route has become a pressing need in recent times [12]. The alternative biogenic approach utilizes plant and fruit extracts as reducing and capping agents of nanoparticles from their chemical precursors [13]. The water-soluble metabolites present in the extract not only increase the production process but also facilitates synthesizing bio-mediated TiO_2 NPs of stable morphology and better structural, photocatalytic, and antibacterial properties [14][15]. In this undertaking, mango leaves are utilized for the green synthesis process. The reason for selecting Mangifera Indica plant leaves (mango leaves) is twofold. Firstly, it is abundant in Bangladesh. Secondly, to the best of our knowledge, no studies

have been reported about utilizing mango leaves extract for the synthesis of bio-mediated TiO_2 NPs. These pure TiO_2 NPs possess large band-gap and poor photo and electrochemical properties. The bio-mediated doped TiO_2 NPs showed better optoelectronic and photocatalytic properties [16]. Moreover, the utilization of green synthesized doped TiO_2 NPs is envisaged to be exploited in drug delivery, pharmaceutical, and food industry [17]. Moreover, very few studies have been done on the evaluation of the antibacterial properties of bio-mediated TiO_2 NPs (doped and undoped) by the Kirby-Bauer disk diffusion method [18]. Furthermore, It is proven that the anatase phase of the green synthesized TiO_2 promotes better antibacterial activity on both Gram-positive and/or Gram-negative bacteria strains [19]. Thus, utilization of the mango leaf mediated biogenic route to produce undoped and doped TiO_2 (anatase phase) NPs can be proved to be potentially sustainable as well as economic.

1.2 Objective of the present study

The specific aims of this work was focused on formulating a biogenic/green synthesis route to produce TiO_2 nanoparticles utilizing mango leaf extract. More specifically, the principle aims can be enlisted as follows:

i. Synthesizing un-doped and doped TiO_2 nanoparticles using a biogenic route to study their morphological, structural, photocatalytic, and antibacterial properties.

ii. Assaying the effect of un-doped and doped TiO_2 nanoparticles on Gram-positive and/or Gram-negative bacteria strain by determining the inhibition zone size.

The possible outcome of this research work is the development of a biogenic route to synthesize un-doped and doped TiO_2 nanoparticles using mango leaf extract as an environmentally friendly replacement of the traditional chemical route. Due to the abundance of mango trees in Bangladesh, the synthesis of the aforementioned nanoparticles will be more cost-efficient. Finally, the photocatalytic and antibacterial evaluation would provide an opportunity to utilize the green synthesized TiO_2 nanoparticles in both the industrial and medical sectors of Bangladesh.

1.3 Scope of the Thesis

This thesis is broken up into following chapters including Chapter 1 – Introduction, Chapter 2 – Literature Review, Chapter 3 – Experimental, Chapter 4 – Results and Discussion, Chapter 5 – Conclusion, Chapter 6 – Suggestion for Future Works.

Chapter 1 has started with describing the background and motivation of the thesis. The main concepts along with the aims, objectives, as well as importance of the thesis have been narrated.

Chapter 2 represents the "Literature review" which contains a collection of detailed information regarding green nanotechnology, nanoparticles types and application, different types of synthesis process for nanoparticles, biogenic route of nanoparticles synthesis, metabolites and their importance, mechanism of biogenic synthesis, properties of mango leaf and TiO_2 nanoparticle, photo-catalysis mechanism and antibacterial properties of TiO_2 nanoparticles.

Chapter 3 will outline the required raw materials, process descriptions and experimental details used during the synthesis and characterization of both undoped and doped TiO_2 nanoparticles. It also includes the experimental procedure for photocatalytic and antibacterial test of the prepared nanoparticles.

Chapter 4 contains an elaborate results and discussion along with details explanation for each finding as well as the relevant experimental results and thoroughly explain the relevance of each result.

Chapter 5 a conclusion will be drawn here from the experimental results which are novel to this field of study.

Chapter 6 some recommendations for future works will be enlisted here.

CHAPTER 2: LITERATURE REVIEW

2.1 Green Nanotechnology – An Introduction

Nanotechnology is the science of the structure of materials with sizes ranging from 1 to 100 nm in at least one dimension, as well as the production of nanomaterials. The ability to comprehend, create, and engineer materials, devices, and systems in the nanoscale range is critical to nanoscience and nanotechnology. Actually, nanotechnology is predicated on the premise that humans can manipulate matter at the atomic level [20]. Nanotechnology can now help to solve key sustainability challenges. With the march of time, science and technology is moving at a rapid speed while environment is witnessing drastic changes. Thus, nanotechnology as a field has to be re-envisioned and reinterpreted with scientific rigor today. In the creation of a new field of scientific endeavor known as "Green Nanotechnology", the vision and challenge of environmental engineering science and nanotechnology are broadly merged [21]. The framework of green nanotechnology comprises the creation of nanomaterials, green engineering, green chemistry, indirect and direct environmental applications, as well as the fabrication of nanocatalysts, nanomembranes, and the greater release of harnessed energy. Nanotechnology for green innovation – green nanotechnology – attempts to develop products and processes that are safe, energy efficient, decrease industrial waste, and reduce greenhouse gas emissions. As a result, for the synthesis of nanoparticles green nanotechnology has gained popularity in recent years. Though there are immense challenges in the field of green nanotechnology, it surely opened windows of innovation for the continuance of science in years to come [22].

2.2 Nanoparticles

2.2.1 Definition

By definition, particles that vary from 1 nm to 100 nm in size in at least one dimension out of three, is considered as nanoparticles. The characteristics (biological, physical, and chemical) of nanoparticles alter at the atomic/ molecular level according to the size of this range, making these nanoparticles unique [23]. Metals and their oxides, non-oxide ceramics, silicates, organics, carbon, and polymers are all examples of materials that may be used to make nanoparticles. Nanoparticles

come in a variety of morphologies, including spheres, tubes, cylinders, platelets and so on. These, on the other hand, are designed and customized expressly for the purposes they are utilized for [24]. Figure 2.1 depicts the diversity of nanoparticles based on their form, chemical origin, morphology, medium, surface modification, and state of dispersion. These are the characteristics that have made nanoparticles such a significant component of research in recent years.

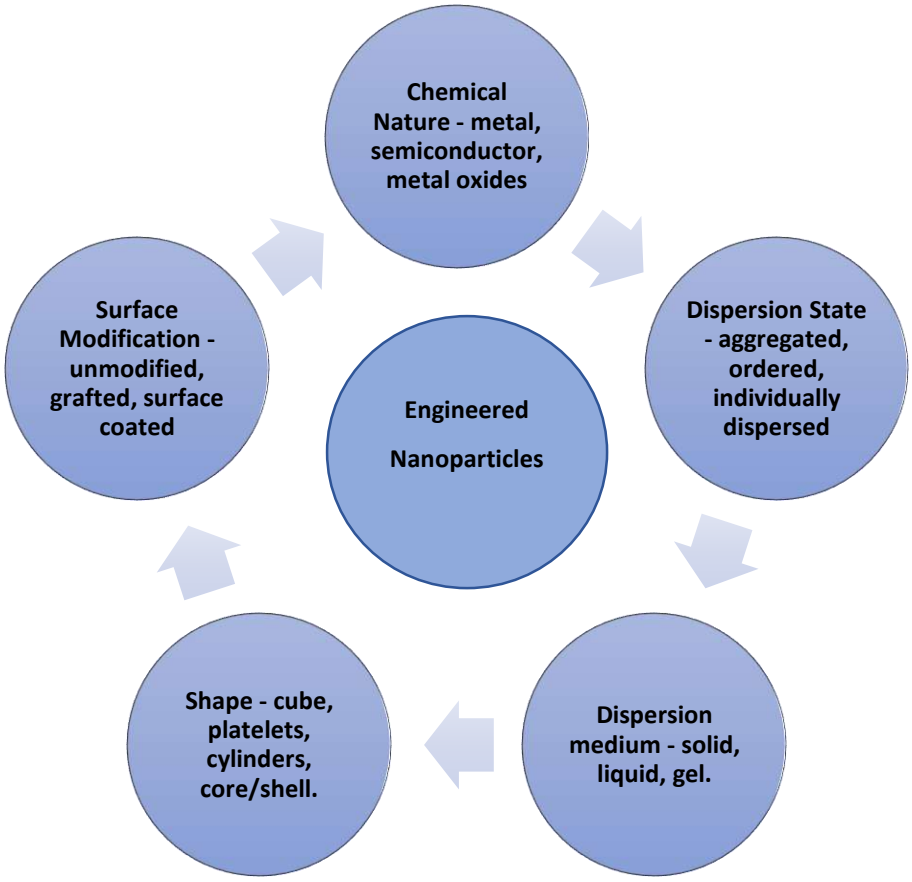

Figure 2.1: The diversity of nanomaterials.

2.2.2 Nanoparticle Categories

The classification of nanoparticles is based on several categories. Depending on dimension, there are zero dimensional nanoparticles – all dimensions are at nanoscale, i.e., no dimensions are greater than 100 nm, one dimensional nanoparticles – two dimensions are at nanoscale and the other is outside the nanoscale, two dimensional nanoparticles – one dimension is at nanoscale and the other

two are outside the nanoscale, three dimensional nanoparticles – they are not confined to the nanoscale in any dimension. Based on origin and composition, nanoparticles are of two types including natural nanoparticles and synthetic nanoparticles. Ocean, dust, fine sand, volcanic ash is the common place to find natural nanoparticles. On the other hand, synthetic nanoparticles are comprised of carbon based, metal based (noble metal including silver, gold, etc.), inorganic (semiconductor nanoparticles like zinc oxide and titanium oxide) based precursors. Inorganic nanoparticles, on the other hand, have piqued the curiosity of researchers due to their many functionalities. Inorganic particles have also been shown to offer a significant potential for application as medical treatments and imaging instruments. Inorganic nanoparticles are also suitable for cellular delivery because they have useful properties such as high functionality, wide accessibility, the ability to administer targeted medications, good compatibility, and precise drug release [25].

2.2.3 Nanoparticle Applications

Sensors, medical diagnostics, catalysts, magnetic recorder, biotechnology, high performance engineering materials, cancer therapeutics, drug delivery, conducting adhesives, and optics are only some of the potential scientific uses of metal oxide nanoparticles presented by scientists. Although nanoparticles cannot be utilized as a food additive, they may have uses in the food industry, such as food safety. Microbe-resistant textiles and nonbiofouling surfaces are the most emerging nanomaterial application in food industry. Nanoparticles have a hazardous effect on the environment because they leach into soil and water, yet it has been shown that they may be cleansed automatically by microbial protein interactions with NPs. For medication delivery systems, nanotechnology has produced a tailored solution. The materials employed in drug delivery systems must be able to bind the substance in question and be quickly digested or excreted through the regular excretory process. The nanoparticles have the capacity to recreate or mend damaged (injured) tissues by stimulating cell proliferation artificially utilizing nano-sized scaffolding and growth factors. Because of their enormous surface to volume ratio, nanoparticles might be used as a catalyst in a variety of applications, including fuel cells, catalytic converters, and photocatalytic devices. For example, TiO_2 NPs (anatase titanium dioxide nanoparticles) are

employed as photo-catalysts and have the ability to convert hazardous organic dyes and CO_2 to non-toxic compounds [26-29].

2.3 Synthesis Approaches of Metal Nanoparticles

In general, there are two ways to synthesize metal nanoparticles (MNPs), namely, top-down approach and bottom-up approach. The "Top-Down" procedures rely heavily on the generation of isolated atoms from bulk materials via various distribution mechanisms. Some of the fundamental techniques used in top-down manufacturing procedures include milling or attrition, repeated quenching, and photolithography [30]. The "Bottom-Up" techniques, on the other hand, begin with a metal salt precursor (dissolved in a solvent) that is reduced in a chemical reaction, and the NPs are created by a nucleation process, followed by cluster formation [31]. A comparative schematic view of the both approaches is illustrated in the figure 2.2.

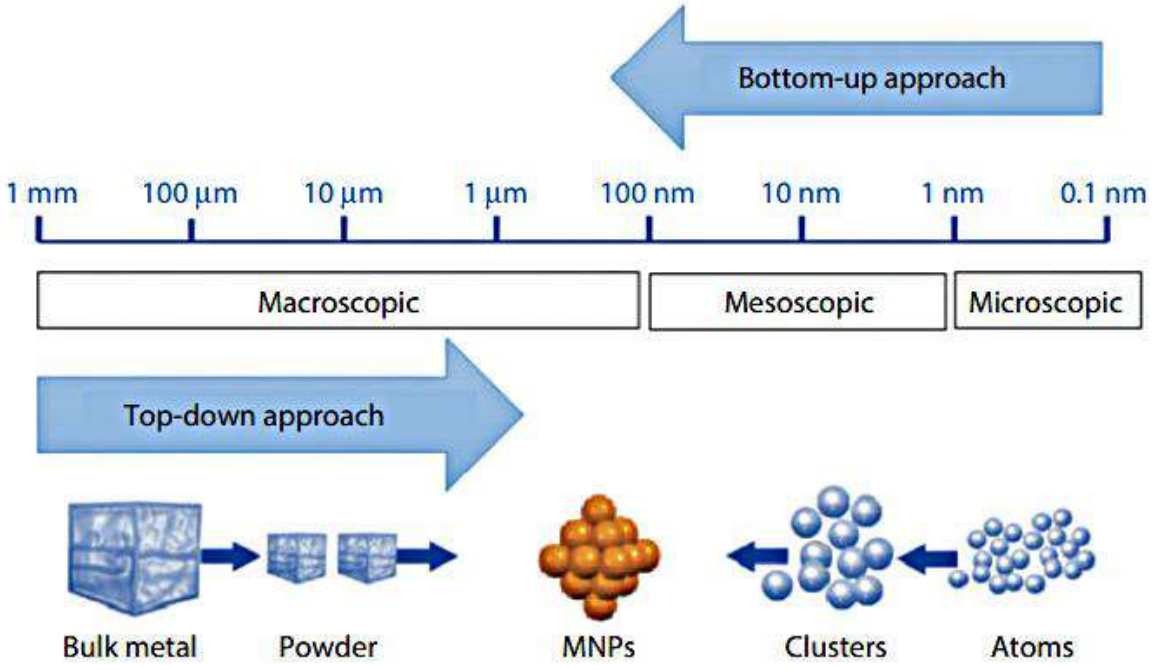

Figure 2.2: Schematic illustration of both top-down and bottom-up approaches for the synthesis of metal nanoparticles.

2.3.1 Top-Down Approaches

The top-down method is a physical technique for producing nanoparticles from bulk materials. The two physical processes employed in the top-down approach for the formation of nanoparticles from their bulk antecedents are cutting and grinding. For the synthesis of very complex structures and the mass manufacture of MNPs, top-down techniques (Figure 2.3) are the preferred methodologies. The fundamental downside of these top-down techniques is that the surface structure might be imperfect, which can have a significant impact on the characteristics of the resultant MNPs [32]. The bottom-up techniques are an effective strategy for resolving this issue.

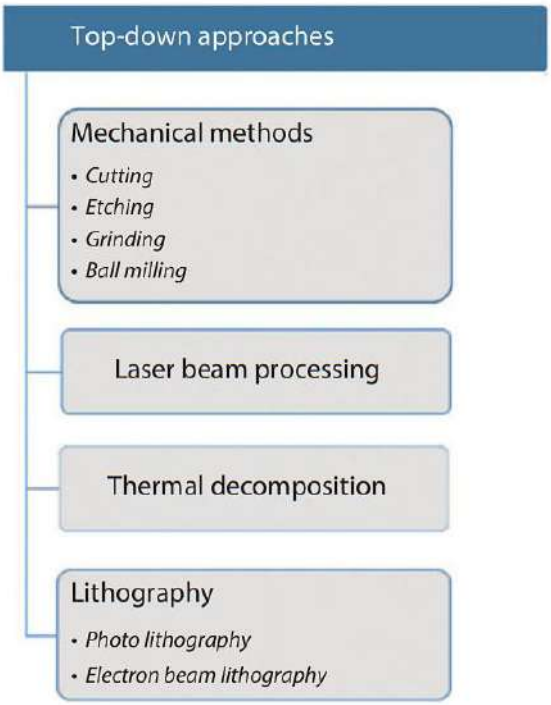

Figure 2.3: Classification of top-down approaches for the synthesis of MNPs.

2.3.2 Bottom-Up Approaches

Bottom-up tactics have been used specifically to avoid the drawbacks of top-down approaches by creating homogeneous and stable MNPs. This process results in the production of target products through the collection (nucleation) and growth of building block units with the desired size, shape, and crystallinity. Self-assembly, chemical synthesis, and colloidal aggregation are classic examples of the bottom-up technique. To synthesis MNPs utilizing wet chemical techniques, the

reaction mixture must contain three key reactants: a metal salt precursor, a capping agent and a reducing agent. Some of the reaction parameters that govern the morphology and surface chemistry of the resultant MNPs are the chemical nature of the capping agent, its molar ratio to the metal salt, and the redox potential of the reducing agent [33]. The concentration of the capping agent, perhaps, may have the greatest influence, notably on the size. Capping agents are sometimes employed as reducing agents for metal salt precursors [31]. The mass manufacture of MNPs is an issue in bottom-up approaches since not all technologies can be employed to mass-produce enough MNPs for industrial usage [31]. A classification of bottom-up approach is depicted in figure 2.4.

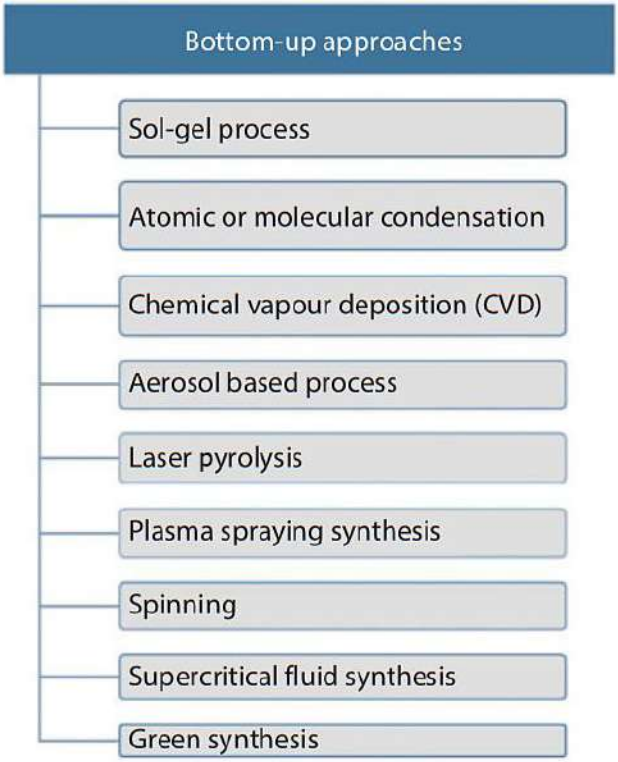

Figure 2.4: Classification of bottom-up approaches for the synthesis of MNPs.

2.3.3 Sub-Category of Nanoparticle Synthesis Routes

The nanoparticles synthesis techniques are sub-divided into three more categories, such as, chemical approaches, physical approaches, and biogenic approaches as shown in figure 2.5. Nanoparticles have been manufactured physically and chemically for many years, but recent

modifications and advancements use microorganisms and a variety of biological systems in the synthesis and production of metal nanoparticles.

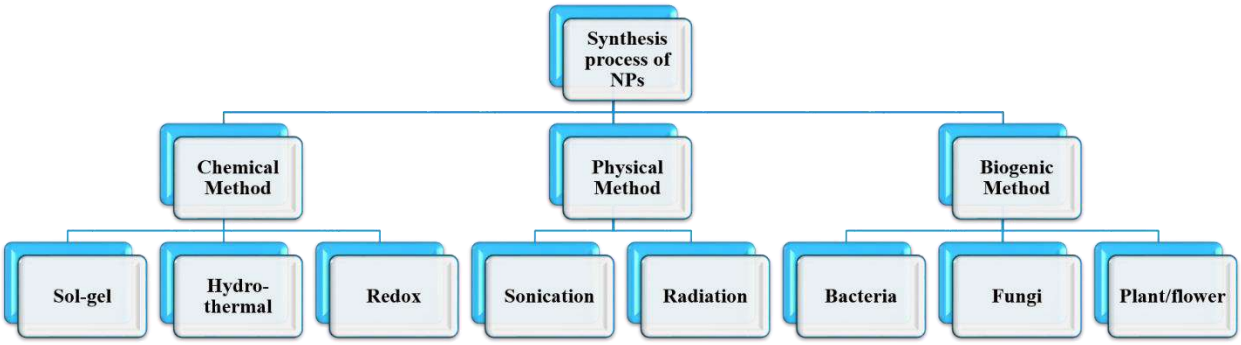

Figure 2.5: Sub-classification of the bottom-up approach.

2.3.3.1 Chemical Approaches

Chemical reduction, chemical precipitation, sol-gel, etc. are well-known methods for producing nanoparticles by employing inorganic and organic reducing agents. In these methods, the use of protective agents allows for the stabilization of dispersive nanoparticles throughout the metal nanoparticle formulation process, as well as the protection of nanoparticles. As a result, they are crucial because they aid in absorption on the desired surface and prevent agglomeration [34].

2.3.3.2 Physical Approaches

The most widely utilized and important physical techniques are evaporation-condensation and laser ablations. Unlike chemical techniques, physical approaches do not have the danger of solvent contamination in thin films and have a homogeneous distribution of nanoparticles [35][36].

2.3.3.3 Biogenic/Green Approach

The biogenic route mitigates the shortcomings of chemical and physical methods by forming and stabilizing MNPs with ecologically friendly ingredients such as biopolymers and plant extracts [37]. The biogenic route conforms the bottom-up approach. The next section will contain elaborate discussion on the definition, types, mechanism of green synthesis or biogenic route of nanoparticle fabrication.

2.4 Biogenic Synthesis of Nanoparticles

Biogenic synthesis is a process in which metal ions get reduced and stabilized in presence of living organisms, such as, fungi, algea, microbes, flower extract, plant extracts as shown in figure 2.6. All these organisms can produce NPs in vivo [38-40]. However, plant extract-mediated in vitro green synthesis of NPs has gained popularity, because of its simplicity, low cost, eco-friendliness, and ease of scale-up [41][42]. In the green synthesis of NPs, extracts taken from various plant species, their organs, and isolated compounds have been effectively employed. NPs synthesized by biogenic route demonstrates better bioactivities [43][44] and catalytic characteristics [45][46] compared to their counterparts fabricated by other methods. The capacity of plant extracts to reduce metal ions might be explained by the ubiquitous presence of phenolic chemicals throughout the plant kingdom [47].

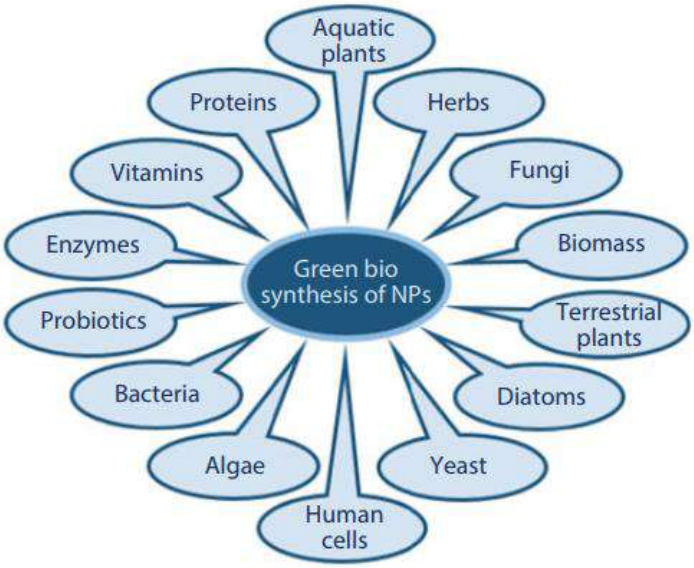

Figure 2.6: Various living organisms to synthesize nanoparticles.

2.4.1 In Vivo Biogenic Synthesis of Nanoparticles

The mechanism of NP production by plants, as shown in figure 2.7, can be explained by a process known as bioaccumulation, which gives plants the ability to detoxify metal ions. When plants receive metal ions at a quicker pace than catabolism can remove them, the excess metal ions build

up in the plant tissues. When metals are present at very high level, excessive reactive oxygen species (ROS) formation in cells and damage to cellular macromolecules can cause major morphological, metabolic, and physiological abnormalities in plants. Plants have complex chelation processes to detoxify metals in order to counteract metal toxicity [48]. When metal poisoning occurs, cellular enzymatic antioxidant mechanisms (Homeostatis) are engaged to preserve ROS equilibrium [49][50]. Plant secondary metabolites, such as phenolic compounds, can help cells maintain ROS homeostasis in addition to enzymatic antioxidant processes [51][52]. In essence, the metabolites present in the plant reduce the metals ions to reduce the toxicity and hence forming NPs in vivo.

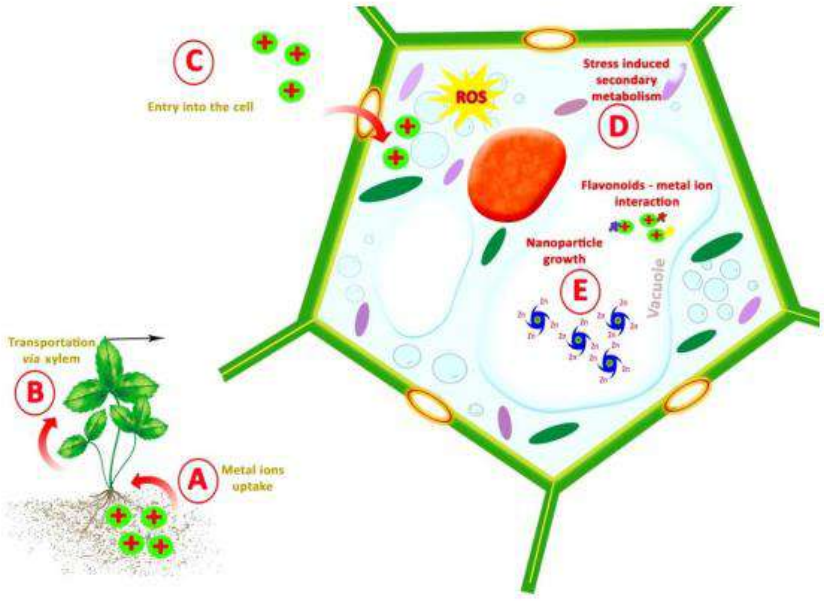

Figure 2.7: Schematics of in vivo synthesis of nanoparticles.

2.4.2 In Vitro Biogenic Synthesis of Nanoparticles

In vitro biogenic/green synthesis of NPs from plant extract utilizes the same principle discussed above. The cations will be saturated to form hydroxyl complexes when a metallic salt dissociates into cation and anion. Crystallite formation of metal with oxygen species begins immediately after the super-saturation of hydroxyl complexes. This causes the creation of crystalline planes with various energy levels. Heat is an important source of energy for the reaction system. The process continues until the plant extracts activate the capping agent, which eventually stops the formation

of high-energy atomic growth planes. As a result, particular types of NPs are formed. The reducing agents usually give electrons to the metal ions and convert them to NPs throughout the synthesis. These NPs are in a high-surface-energy state and tend to aggregate against one other to convert to their low-surface-energy conformations. As a result, the presence of more reducing and stabilizing chemicals reduces nanoparticle aggregation and promotes the formation of smaller NPs [53]. Furthermore, proteins may capture metal ions on their surfaces and convert them to their corresponding nuclei, which can then assemble and form NPs [54]. A flow chart of the whole process is depicted in figure 2.8.

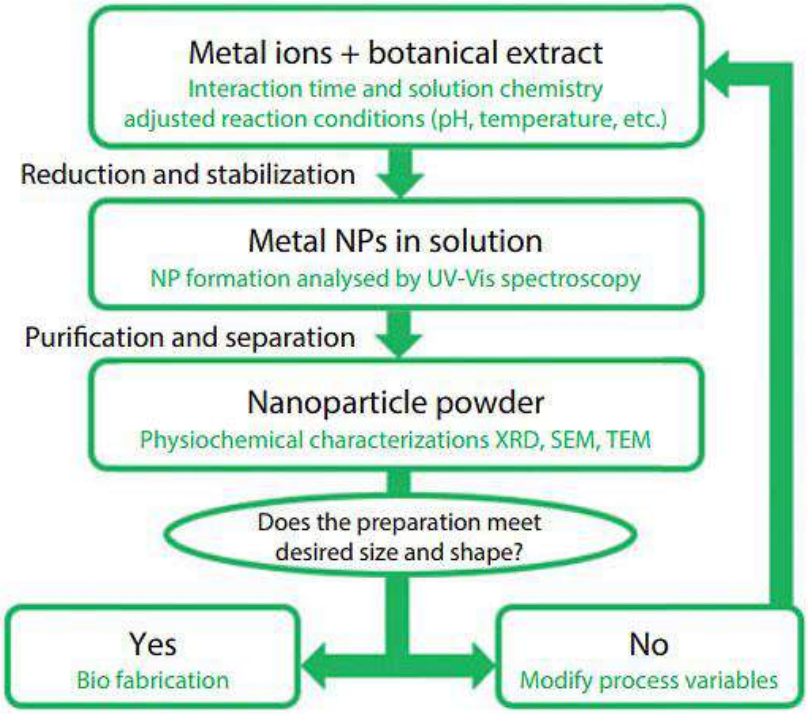

Figure 2.8: Flow chart of the biogenic synthesis route for nanoparticles.

Plant-mediated green NP synthesis process can be divided into three stages as shown in figure 2.9. They are activation phase, growth phase and termination phase [55]. The activation phase is the first step in the process of recovering metal ions from their salt predecessors using plant metabolites, which are biomolecules with reduction abilities. The metal ion's oxidation states are changed from mono-valent/di-valent states to zero-valent states and subsequently nucleation of the condensed metal atoms occurs [56]. The growth stage follows, during which the separated metal atoms merge to form metal NPs, with further biological metal ion reduction taking place.

Nanoparticles accumulate a range of morphologies as they develop, including shapes such as cubes, spheres, triangles, rods, hexagons, pentagons, and wires. The increased thermodynamic stability of NPs occurs as the development stage progresses, but excessive nucleation may cause aggregation of produced NPs, modifying their morphologies. The termination phase is the final stage in the green NP synthesis process. When plant metabolites cap the NPs, they achieve their most promising and stable shape [57]. The working principle of the biogenic synthesis of NPs is illustrated below.

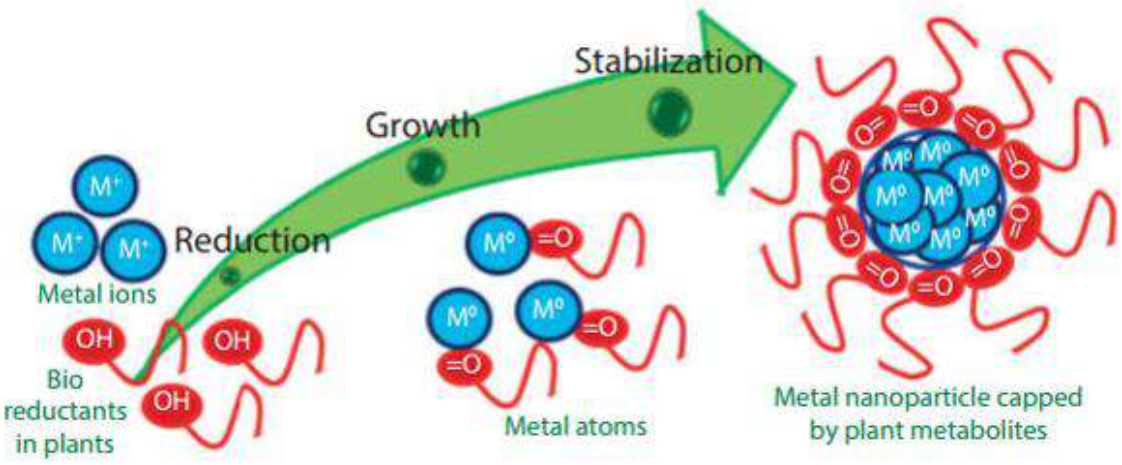

Figure 2.9: Illustration of the step by step formation of NPs in biogenic route.

2.4.3 Importance of Metabolites in Plant Extract – Mediated Biogenic Synthesis of NPs

Metabolites, also known as bio-reductants/phytochemicals, act as the stabilizing and capping agent during the fabrication of NPs in green synthesis route. The inclusion of these compounds may increase the bioactivities of these NPs in addition to giving stability to the NPs as capping agents or stabilizers. A wide range of molecules, ranging from proteins to various low molecular weight compounds such as alkaloids, terpenoids, amino acids, polyphenols (flavones, catechin, taxifolin and phenolic acids), alcoholic compounds, antioxidants, glutathiones, polysaccharides, organic acids (ascorbic, oxalic, malic, tartaric acid), quinones etc., have been reported to play a role in the green synthesis of NPs [47]. Sugars, terpenoids, polyphenols, alkaloids, phenolic acids, and proteins have all been implicated in the reduction of metal ions into NPs and in promoting their

subsequent stability [53]. The key supporting element in the diverse sizes and forms of produced nanoparticles is thought to be the discrepancy in concentration and conformation of these active biomolecules across different plants, as well as their subsequent connection with aqueous metal ions [58]. Among the various metabolites mentioned above, proteins, flavonoids, terpenoids, alkaloids, saponins, phenols are the most important according to some literature. So, before undertaking synthesis of NPs utilizing biogenic route, one must ensure the presence of such metabolites. Figure 2.10 illustrates important metabolites present for NP synthesis.

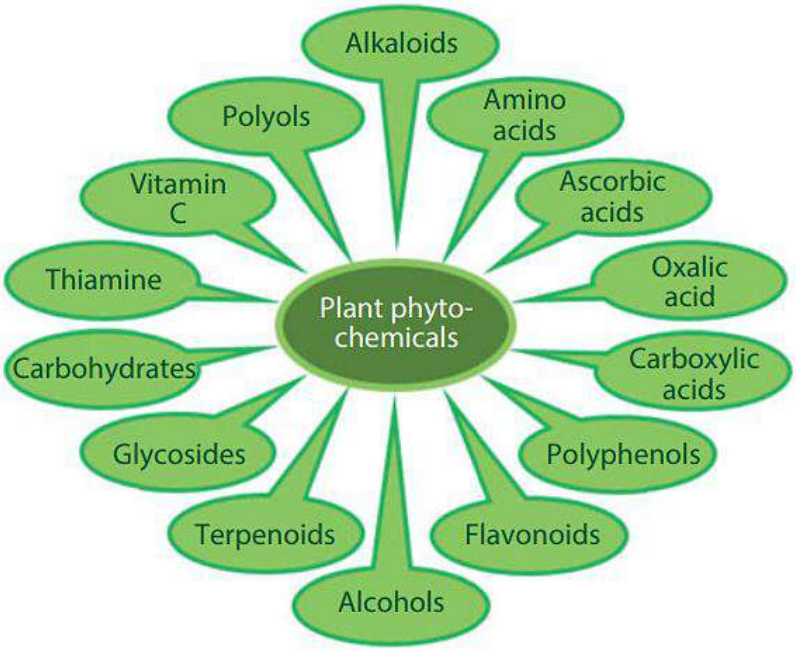

Figure 2.10: Important metabolites of synthesis of NPs.

2.5 Mango (Mangifera indica) Leaves – Phytochemical Profile

Mango (Mangifera indica) is a significant tropical and sub-tropical tree belonging to the Anacardiaceae family [59][60]. Being native to South Asia and Southeast Asia, these tree leaves (shown in figure 2.11) are quite common in Bangladesh, India, Philippines, Thailand, Indonesia, and China. Some species are found in Mexico, Brazil, and Nigeria [61]. Mango leaves (MLs) have plethora of phytochemicals such as mangiferin, followed by phenolic acids, benzophenones, and other antioxidants such as flavonoids, ascorbic acid, carotenoids, and tocopherols [61]. Mangiferin is the main contributor of most of the biological activities of MLs extract. MLs have a great scope

of valorization as they are documented to possess wide-ranging phytochemical, and biological, properties such as anti-microbial and antioxidant characteristics. Flavonoids are a family of natural polyphenolic compounds that include flavonol, flavone, flavanonol, flavanone, and isoflavone derivatives that are quite common in MLs making its' extract suitable for any types of nanoparticle synthesis [61]. The biological, and metabolic capabilities of MLs are quite exceptional. According to literature, mango leaf extract has been utilized for the fabrication of silver nanoparticles [62], iron as well as iron oxide nanoparticles [63][64], gold nanoparticles [65], and zinc oxide nanoparticles [66]. Several studies have mentioned the utilization of mango peels for the synthesis of TiO_2 nanoparticles but none to the best of our knowledge have utilized mango leaf extract for green synthesis of TiO_2. The presence of required metabolites in mango leaf extract inspired the undertaking of this thesis work. The study aimed (i) to produce TiO_2 NPs using a mango flower extract, (ii) to characterize the biosynthesized TiO_2 NPs using various spectroscopic techniques, and (iii) to measure their photocatalytic and antibacterial properties.

Figure 2.11: Mangifera indica leaves.

2.6 Mechanism of Mango Leaf Extract Mediated Biogenic Synthesis of TiO_2 nanoparticles

Albeit the principle of TiO_2 NPs generation through green synthesis is unknown, the synthesis process is similar to the sol-gel method, in which TiO_2 NPs is formed by chemical reactions of hydrolysis and condensation [9][67]. The mechanism of mango leaf extract mediated biogenic synthesis of TiO_2 NPs is proposed to have five stages including hydrolysis, condensation,

nucleation, accumulation, and stabilization. A schematic of the whole process is depicted in figure 2.12.

The first stage is Titanium hydrolysis, which occurs when water molecules break the titanium salt precursor's – Titanium Tetra Isopropoxide (TTIP) – carbon bonds, resulting in $Ti(OH)_4$ molecules [68].

$$Ti[OCH(CH_3)_2]_4 + 4H_2O = Ti(OH)_4 + 4(C_3H_7OH -)$$

The second stage is condensation, which occurs when $Ti(OH)_4$ molecules bind with one another and create H_2O molecules, resulting in Titanium colloids linked by Van der Waals forces. As a result, mechanical agitation, in combination with mango leaf extract compounds, promotes condensation (phytochemicals).

$$Ti(OH)_4 = TiO_2\ x.H_2O + (2\text{-}x)\ H_2O$$

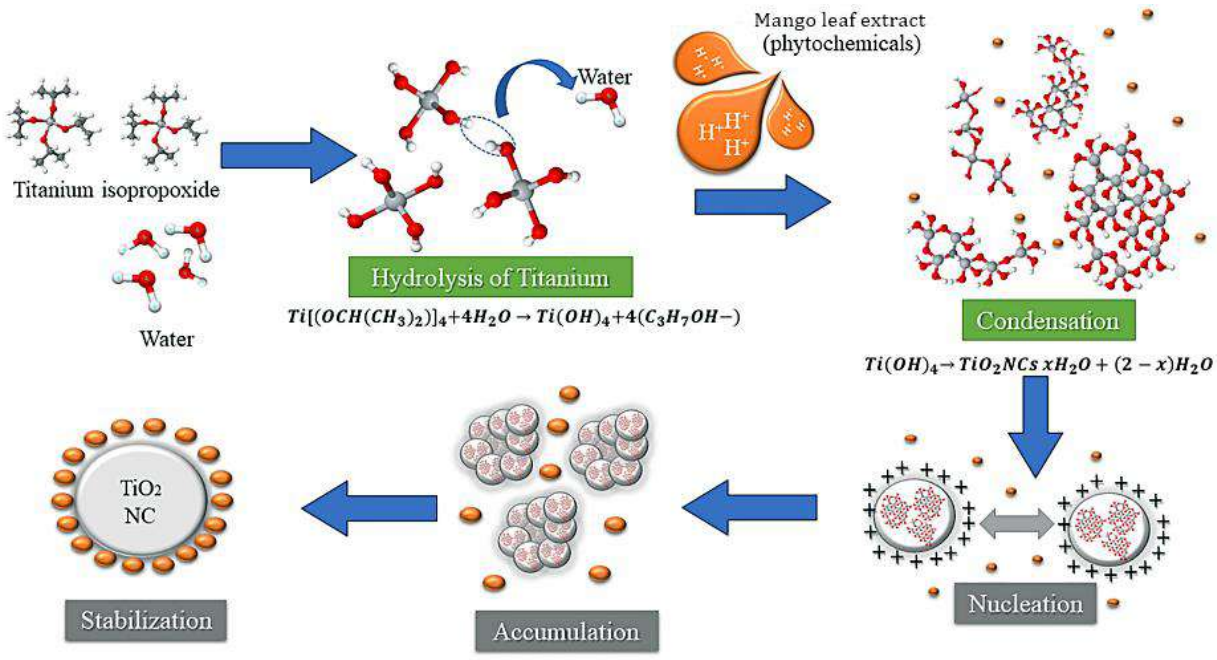

Figure 2.12: Mango leaf extract mediated biogenic synthesis mechanism of TiO_2 nanoparticles.

Because there is enough free energy in the system to create a solid phase, the third stage is nucleation, which occurs as molecules aggregate to form TiO_2 particle nuclei, followed by the production of initial nanocrystals. The usage of mango leaf extract causes heterogeneous nucleation and polydisperse particles in this circumstance [67].

The fourth stage is growth, in which particles begin to develop from their nuclei. The stabilizing electrostatic impact of mango leaf extract and its phytochemicals controls TiO_2 NPs growth. The acidic pH of mango leaf extract, which does not provide the requisite electrostatic repulsion between the nanoparticles to prevent agglomeration, can be attributed for the TiO_2 NPs agglomeration in this study. Moreover, the polymer from the metabolites present in the extract covers the TiO_2 NPs causing them to slow the growth. Finally, in the fifth stage, TiO_2 NPs stabilize, their growth slows, and calcination defines their crystalline structure [9].

2.7 Nanostructured Titanium Dioxide (TiO_2)

Titanium dioxide (salso known as Titania) is a metal oxide semiconductor with the formula TiO_2. It is hard, thermally stable, and chemically resistant, just like other metal oxides. Titania was discovered to be photosensitive to daylight in the 1960s by Juillet and Teichner [69], but it was the work of Fujishima and Honda on TiO_2 based water splitting that popularized its usage as a photocatalyst [70]. Because of its diversified nature and numerous uses in photocatalysis [71], pigments [72], medications and antibacterial usage [73], sensors [74], water purification [75], cosmetics [76], photovoltaics [77], and other fields, interest in nanocrystalline titanium dioxide synthesis has increased. Important properties of TiO_2 is listed in table 2.1.

Anatse, rutile, and brookite are the three polymorphs of titanium dioxide found in nature. The three phases are all made up of TiO_6 octahedra bonded in various ways. Rutile is the most thermodynamically stable of the three, generated by edge-sharing of octahedra to form long chains, whereas anatase is made up mostly of point-sharing octahedra and brookite is made up of both. The most investigated phases for photocatalytic and antimicrobial applications are anatase phase and rutile phase [78]. In the interest of brevity, the nature of brookite will not be described here because it is typically difficult to synthesize reliably [79] and is generally photo-catalytically inert [80]. Figure 2.13 illustrates crystal structures of Anatase and Rutile phase of TiO_2.

Rutile, a direct-bandgap semiconductor with a band gap of 3.0 eV, is the most common and stable form of TiO_2. Despite having a lower band gap than other titanium dioxide polymorphs, rutile is not a good option for photocatalysis due to the high rate of electron-hole recombination [81].

Despite being less stable than rutile, anatase TiO_2 is metastable up to 600°C and hence has a wide range of applications. Anatase has a band gap of 3.2 eV, which limits its activity to UV light, yet it is still the most commonly used titania phase for photocatalytic applications [82]. Anatase is an indirect band-gap semiconductor, which, in combination with its proclivity for hole-trapping on the particle surface [83], considerably extends the lifespan of photo-excited electron-hole pairs in the material. On anatase phase, excited electrons are energetic enough to participate in the reduction of H^+ to hydrogen, whereas holes can oxidize water to oxygen and aid in the breakdown of a variety of organic contaminants [84].

Table 2.1: Important properties of various phases of TiO_2

Properties	**Anatase**	**Rutile**	**Brookite**
Crystal structure	Tetragonal	Tetragonal	Orthorhombic
Color	Mineral is dark. Fine powder is white.	Mineral is deep red. Fine powder is white.	Mineral is deep brown/reddish. Fine powder is white.
Density	3.79	4.13	3.99
Ti–O bond length (Å)	1.937 1.965	1.949 1.980	1.87–2.04
O–Ti–O bond angle	77.7° – 92.6°	81.2° – 90.0°	77.0° – 105°
Lattice constant (Å)	a = b = 3.784 c = 9.515	a = b = 4.5936 c = 2.9587	a = 9.184 b = 5.447 c = 5.154
Density (g cm_{-3})	3.79	4.13	3.99
Volume/ molecule ($Å_3$)	34.061	31.2160	32.172

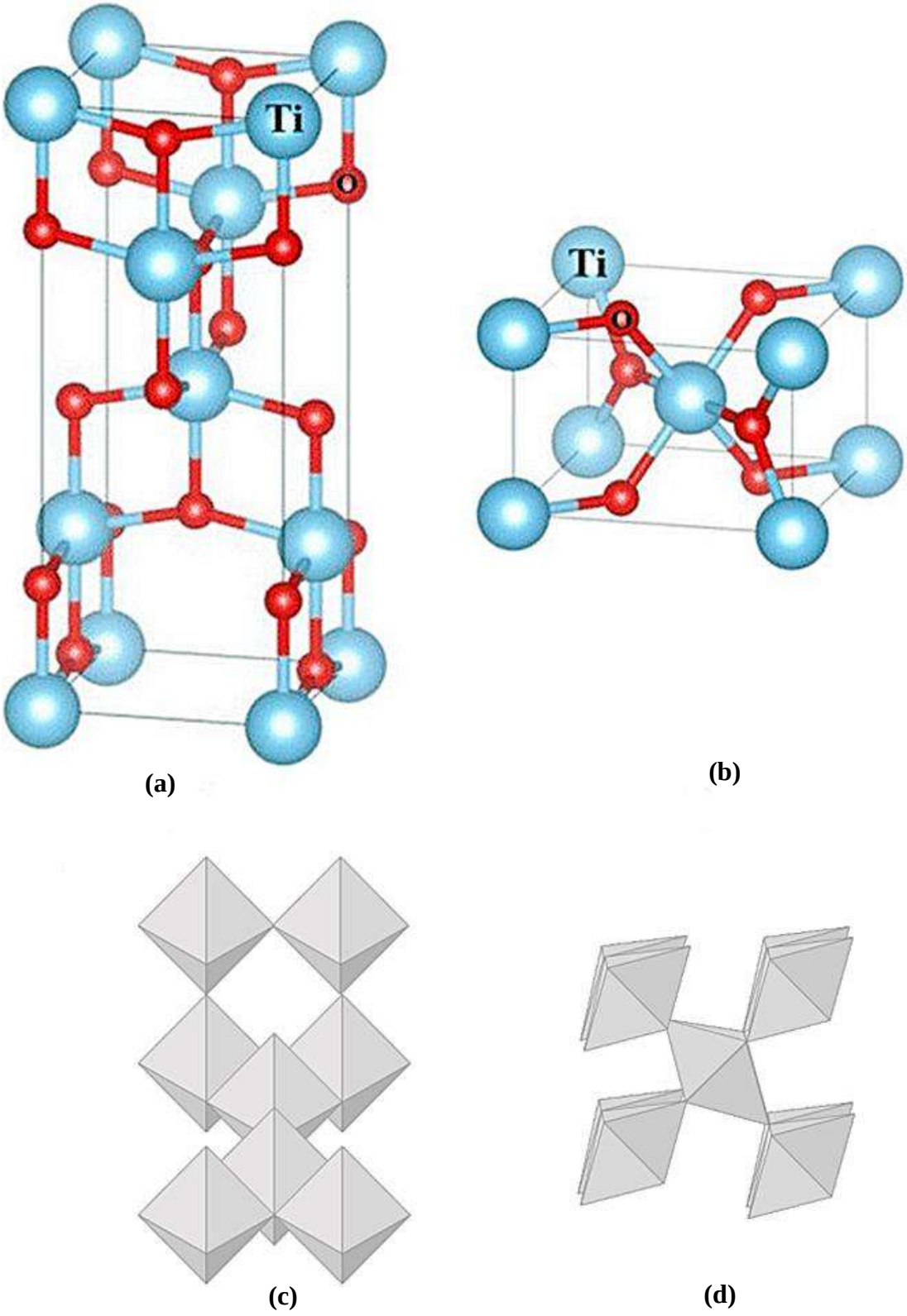

Figure 2.13: Crystal structure of TiO_2 (a) Anatase (b) Rutile; Large light-blue and small red spheres are Ti^{4+} and O^{2-} ions, respectively. (c) Arrangement of point-sharing of TiO_6 octahedra in Anatase (d) Arrangement of edge-sharing of TiO_6 octahedra in Rutile.

2.7.1 Why is Anatase TiO_2 a Better Photocatalyst than Rutile TiO_2?

As stated above, TiO_2 is chemically stable and biologically benign and as such, it has widespread usage as a photocatalyst for the decomposition of the organic pollutants [85]. When comparing pure phases, anatase is thought to have a higher photocatalytic activity than rutile TiO_2 [86]. Moreover, the two polymorphs not only show different photoactivities but also due to their difference in crystallographic orientation, they demonstrate variety in other properties too [87][88]. Possible explanation for the differences of photocatalytic activities of anatase and rutlile are pointed out below.

- The band gap of anatase is greater than that of rutile TiO_2. While this reduces the amount of light that can be absorbed, it may elevate the valence band maximum to higher energy levels in comparison to adsorbed molecules' redox potentials [89].

- Surface characteristics may influence molecule adsorption and subsequent charge transfer to the molecule. Surface properties may not only be polymorph dependent, but may also vary significantly for the identical material for dissimilar surface orientations or reconstructions. As a result, it may contribute to the observation of prominent surface effects in photocatalytic activities [90].

- The indirect band gap of anatase is smaller than its direct band gap. The fundamental band gap of rutile (whether direct or indirect) are very similar. When compared to direct band gap materials, indirect band gap semiconductors have a longer charge carrier life duration. Charge carriers would be more likely to engage in surface processes in anatase than in rutile due to the longer electron-hole pair life [91].

- Charge transport may vary depending on the polymorph. The exciton mobility must be considered in addition to the exciton lifespan. Anatase is hypothesized to show better property due to better preferential diffusion of excitons along certain crystallographic directions that explains surface orientation dependencies in their oxidation/reduction behavior [92].

2.8 Enhancement of TiO_2 Activity

Despite the fact that titanium dioxide is a good photocatalyst, it is not widely used due to two major problems [93].

First of all, the large band-gap of TiO_2 restricts light absorption to the UV ($\lambda \leq 390nm$). Due to the fact that such light makes up around 5% of the solar spectrum, the efficacy of such catalysts under solar irradiation is limited: given the efficiency of present systems, TiO_2 based photocatalysts seldom achieve 1% solar energy conversion [94][95]. It may be able to use up to 40% of the solar spectrum by reducing the band gap sufficiently so that the catalyst can absorb visible light [96].

Secondly, both in the bulk and on its surface, titanium dioxide still shows large-scale charge recombination. This is most common near grain boundaries and bulk or surface flaws, and it can significantly impair the material's photocatalytic activity [95][97].

As a result, substantial study has been conducted in recent years to solve the aforementioned issues. Many researchers have sought to minimize the recombination rate of titanium dioxide catalysts by doping with both metals and non-metals, adding charge traps, improving crystallinity, or regulating the size and form of the particles. These strategies will be briefly covered in the remainder of this section.

2.8.1 Doping of TiO_2

Doping is one of the most extensively-studied techniques by which TiO_2 has been altered in the literature. It is the process of introducing small amounts of foreign materials into a semiconductor in order to change its electronic properties, usually by forming small bands (mid-gap states) inside the band gap. This approach can change a semiconductor's photoresponse because photons of energy $E < E_{BG}$ (E_{BG} = Band Gap Energy) can excite electrons from the valence band to mid-gap states, or from mid-gap states to the conduction band as shown in figure 2.14.

Doping in TiO_2 may take place in one of two forms, namely, substitutional – in which the dopant atom replaces a lattice atom, or interstitial – in which it is located between existing lattice atoms. While dopant increases the photoresponse of TiO_2, it also produces bulk defects, or irregularities in the crystal structure, which stimulate electron-hole recombination [98]. General observation suggests that photoactivity of TiO_2 rise with the dopant concentration to a certain point, after which

it declines due to excessive exciton recombination [99]. TiO_2 doping mechanisms can be broadly divided into four groups: cationic doping, anionic doping, multi-element doping, and self-doping.

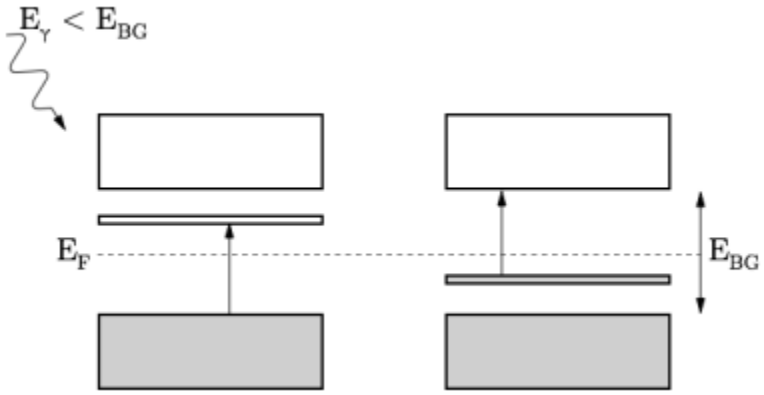

Figure 2.14: Introduction of mid-gap states by doping.

[These states allow the material to absorb light of energy $E < E_{BG}$, either by exciting electrons from the valence band to the mid-gap state (if it lies above the E_F, Fermi level) or from the mid-gap state to the conduction band (if it lies below the E_F, Fermi level).]

2.8.1.1 Cationic Doping

In the crystal lattice, cationic dopants replace Ti^{4+}, either by hybridizing with the TiO_2 3d-like conduction band or by introducing new bands into the bandgap [98]. In order to increase the photoresponse of TiO_2, cationic doping has been widely employed, with current publications focusing on the use of alkalai [99], transition metals [99], noble metals [99], metalloids [99] and rare-earth elements [100]. The type and amount of dopant used, as well as the doping method and reaction under observation, all influence the outcome. These systems are complicated, and in many situations, the characteristics of the dopant must be taken into account in order to construct a complete picture of the doped system: for instance, Oropeza et al. discovered that doping TiO_2 with Sn(IV) on the surface resulted in a small widening of the band gap; the electrical nature of the dopants moved to mid-band states slightly above the TiO_2 valence band when Sn(IV) reduced to Sn(II), resulting in visible-light activity [101]. Despite a substantial amount of research on cationic doping of TiO_2, these materials have a high recombination rate and are thermally unstable [102] which lead to the investigation of anionic and co-doped TiO_2.

2.8.1.2 Anionic Doping

Cationic doping focuses on the substitution of Ti centres for dopants while anionic doping looks at the O centre. Till 2001, the main focus was on the metal doped TiO_2 when Asahi et al. investigated on the study of nitrogen doping in TiO_2 [103]. Asahi looked on the theoretical and experimental applicability of dopants such as carbon, nitrogen, phosphorus, fluorine, and sulfur [104-106]. The scientists came to the conclusion that nitrogen was the best of the dopants tested for boosting TiO_2's visible light activity. When compared to the oxygen atom it would replace, sulfur's ionic radius was excessively big whereas carbon and phosphorous easily occupy the space left by a vacant oxygen center. These dopants' mid-gap states would occur too deep into the band gap, making them effective exciton recombination centers. Moreover, fluorine has no propensity to increase mid-gap states or to shorten the band gap in any other way. Experiments revealed that nitrogen-doped TiO_2 was significantly more active than undoped TiO_2 in degrading methylene blue, and additional research revealed that this activity was due to substitutionally-doped, rather than interstitially-doped, nitrogen [107].

2.8.1.3 Multi-Element Doping

Given the wide range of cationic and anionic dopant materials known, it's only natural that researchers look into the effects of multi-doping or co-doping on TiO_2. A mixture of two anionic dopants, two cationic dopants, and one of each has been successfully tested in two-element doping [108]. Co-doping can be used in a variety of ways to provide advantageous synergistic effects. Charge separation may be aided by the use of numerous dopants. Because the distinct dopants function as electron (iron) and hole (europium) traps, research on europium/iron co-doped TiO_2 have shown decreased electron-hole recombination [99]. Niu and colleagues reported a similar occurrence in Fe and S co-doped TiO_2 [109]. While some of these materials have an excellent photo-response, the rising complexity of their chemical makeup predicts that bulk recombination may become a problem. The advantage of any dopant synergy must balance not only the increased synthetic complexity of the materials, but also any resulting increase in electron-hole recombination.

2.8.1.4 Self-Doping

Ti^{3+}-rich TiO_2 compounds have lately attracted attention as a potential way of extending TiO_2's photoresponse [110]. The development of oxygen vacancies in the material results in the formation of a localized mid-gap state below the conduction band edge, resulting in the generation of Ti^{3+} [111]. Oxygen vacancies, like other kinds of doping, function as bulk defects that increase the rate of recombination, therefore any advantage from doping must be balanced against this.

2.8.2 Elements to Improve Photocatalytic and Antibacterial Performance of TiO_2 NPs

Research studies suggest that TiO_2 doped with metals as well as non-metals show enhanced characteristics. Among various metals, silver (Ag) and copper (Cu) are considered as potential doping element to augment the photocatalytic and antibacterial properties of TiO_2 NPs. The creation of trap charge from the transition metal ions (Ag and Cu ions) in TiO_2 enhances the efficiency of metal-doped catalysts. The metals or dopants (Ag and Cu) operate as electron traps, increasing visible light absorption and enhancing surface electron excitation via plasmon resonance stimulated by visible light. This deposition subsequently creates traps to remove photo-induced electrons or holes, resulting in a decrease in the photocatalytic process's electron-hole recombination rate and an increase in TiO_2's visible light absorption capacity [112][113]. Enhanced antibacterial activity of the Ag and Cu doped TiO_2 is also investigated in several studies [114][115].

2.8.2.1 Ag (Silver) Doped TiO_2

Silver NPs, among the other noble metal NPs, have gained a lot of interest in recent decades due to their effectiveness as bactericidal agents [116] and their capacity to improve semiconductor photocatalytic activity [112]. As a result, Ag-doped TiO_2 have become very popular in the field of dye degradation, water purification, food industry, and medical sector. The ability of silver to trap electrons at Schottky barriers at each Ag-TiO_2 contact site is attributed with improving photocatalytic activity by reducing recombination of electrons and holes produced at the TiO_2 surface. As a result, charge separation is improved, and more electrons are transferred, resulting in longer electron – hole pair lifetimes [112]. After entering the bacterial membrane, silver NPs produce highly oxidative free radicals, killing the bacterium [116]. Additionally, certain noble metals, such as Au, Pd, Pt, and Rh, are too expensive to be employed on a large scale, but silver is

a less expensive metal that performs similarly. Moreover, quite recently, the disadvantages of the conventional synthesis mechanisms of Ag-doped TiO_2 such as sol-gel process and hydrothermal process are outweighed by the introduction of a novel, facile biogenic system for the preparation of such with non-toxic and biocompatible matrices [117].

2.8.2.2 Cu (Copper) Doped TiO_2

Copper has recently received a lot of attention as a titania dopant. Because of its relative abundance, strong electrical conductivity, and inexpensive cost compared to noble metals (Au, Pt, Pd, Ag), it is one of the best potential metal dopants for TiO_2 surfaces. Several studies on Cu-TiO_2 applications in solar energy, environmental remediation for chemical pollutants removal, and microbiological treatment have been published. The presence of Cu increases the light response of TiO_2 towards the visible area, enhancing its photoelectrochemical characteristics and boosting its activity as a catalyst. Just like Ag-doped TiO_2, copper was shown to be an efficient electron trapper, capable of preventing electron–hole pair recombination and therefore considerably increasing photo-efficiency [118]. Cu species can also be employed as an impurity material in microbial treatment to increase TiO_2 activity for the treatment of water containing dangerous biological pollutants [115]. Because Cu might alter the particle size, optical or electrical characteristics of TiO_2, as well as the amount of oxygen or intermediate species on the TiO_2 surface, the presence of Cu species in the TiO_2 matrix has an effect on the overall activity [119].

2.9 Application of TiO_2 Nanoparticles

TiO_2 NPs have diverse application. A few notable applications are discussed here in brief.

2.9.1 Application in Waste Water Treatment and Remediation of Organic Dye

The use of modified and unmodified TiO_2 NPs as an adsorbent and photo catalyst in the removal of organic and inorganic contaminants from water and wastewater has been effectively tested. Heavy metals such as chromium and lead have been reported to be removed with 96 percent effectiveness from electroplating waste water using TiO_2 NPs [120]. In the presence of a light source (UV/Visible), anatase titanium dioxides are employed as photocatalysts for the breakdown of toxic organic dyes and insecticides. When light comes reaches titanium dioxide, a chemical reaction happens in the immediate vicinity, breaking down organic toxins, odors, and other things.

2.9.2 Application in Biomedical Sector

Modified and unmodified TiO_2 medical uses may be categorized based on their biological capabilities, which range from antibacterial to hard tissue replacement, cardiac and cardiovascular, cancer therapeutics, drug delivery, medical implants, and other applications. The self-cleaning property of TiO_2 has recently been reported to be used in photo catalytic coatings for the decontamination and sterilization of re-usable surgical instruments by the health industry [121]. To solve some of the topological difficulties surrounding medical implants, TiO_2 nanostructures have been effectively employed in vital medical items such as bone and dental implants. Because of its capacity to break cell membranes, regulate virus activity, and trap infectious particles, titanium dioxide photocatalyst is frequently used for sterilization and virus restraint.

2.9.3 Application in Photovoltaic Devices

There has been a lot of interest in the study field of using TiO_2 NPs as a photo anode in the fabrication of dye- and quantum dot-sensitized solar cells during the last decade [122]. Because of its simple availability, nontoxicity, low cost, and ability to conduct electrons as a broad band gap semiconductor, TiO_2 NPs are preferred as a semiconductor in the fabrication of dye- and quantum dot-sensitized solar cells.

2.9.4 Application in Environmental Remediation

The conversion of air pollutants such as nitrogen oxides (NOx), sulpher oxides (SOx), volatile organic compounds (VOCs), carbon monoxide (CO), and ozone to more environmentally acceptable products such as calcium nitrate and carbon dioxide has been successfully conducted in a series of studies on the solar activation of TiO_2 NPs for the purification of automobile exhaust, waste burners, and atmospheric air [123]. Because of its high hydrophilic surface, TiO_2's photo catalytic self-cleaning ability has increased its use in the fabrication of TiO_2 coated building materials. TiO_2 Photocatalytic oxidation has also been reported to be used as an anti-fogging agent and for the primary breakdown of organic molecules into CO_2 and water.

2.9.5 Other Application of TiO_2 Nanoparticles

The powder TiO_2 is used as an opacity agent in a variety of goods, including paints, coatings, toothpastes, food, cosmetics, and medications. TiO_2 NPs is also used in capacitors and electrode of photochemical solar cells.

2.10 **Photocatalysis**

The term “Photocatalysis” was first coined by Doerffler and Hauffe to define the oxidation of CO on ZnO in the presence of light [124]. However, it was not until Fujishima and Honda's work on the photocatalytic water-splitting characteristics of titanium dioxide was published in 1972 that the field of photocatalysis gained international academic prominence [70]. The word “Photocatalysis” is of greek origin. The prefix “Photo” means light whereas the suffix “Catalysis” is a process in which a material alters the pace of a chemical transformation of the reactants without changing the end product. By lowering the activation energy, the material that is known to be a catalyst improves the pace of the reaction. As a result, photocatalysis is a method of aiding or accelerating up a chemical reaction by combining light with catalysts. As a result, photocatalysis is defined as the catalysis-driven acceleration of a light-induced process. Photocatalysis is a remarkable process that can be utilized for a variety of applications, including the degradation of numerous organic contaminants in wastewater, air purification, hydrogen production and antibacterial activity [125][126]. The rate of photo catalysis is primarily determined by the properties of the catalyst, such as its structure, size, shape, area of the surface, reaction temperature, light intensity pH, and catalyst quantity. In general, it is sub-divided into two categories: homogeneous and heterogeneous process [127].

In case of homogenous photocatalysis, the reactants and photocatalyst are in the same phase. Under photon and temperature conditions, the higher oxidation state of metal ion complexes generates hydroxyl radicals in this process. These hydroxyl radicals react with organic materials, causing hazardous substances to be destroyed [128].

On the other hand, in the heterogeneous photocatalysis, the catalyst is in different phase than the reactants. It has several positive aspects in comparison to homogeneous one due to low cost, complete mineralization, and no waste disposal problem. Because of their promising combination of electronic structures, which are characterized by a filled valence band and an empty conduction band, light absorption characteristics, charge transport properties, and excited states lifespan, semiconducting materials such as TiO_2, CeO_2, ZnO are primarily used as heterogeneous photocatalysts. The ultimate purpose of heterogeneous photocatalyst design is to initiate reactions between excited electrons and oxidants, resulting in reduced products, and/or reactions between produced holes and reductants, resulting in oxidized products. At the surface of semiconductors,

oxidation-reduction events occur due to the creation of positive holes and electrons. Heterogeneous photocatalysis is a technically advanced process for degrading a wide range of organic contaminants in wastewater [129][130].

2.10.1 Photocatalysis Mechanism of TiO_2

The wavelength or energy of light (photon) and the catalyst are the most important factors in photocatalytic reactions. Due to their electronic structure, which is defined by a filled valence band and a vacant conduction band, semiconducting materials (such as TiO_2) are utilized as a catalyst that acts as sensitizers for the irradiation of light triggered redox processes. A schematic illustration of the photocatalysis mechanism is depicted in figure 2.15.

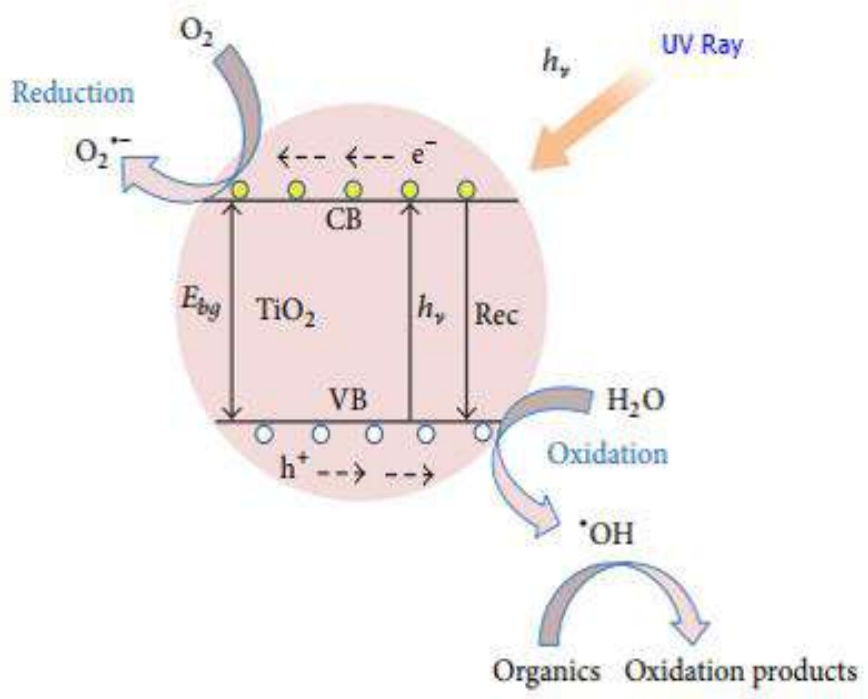

Figure 2.15: Illustration of photocatalysis mechanism of TiO_2.

In heterogeneous photocatalysis on the surface of TiO_2, there are five fundamental key steps: (1) photoexcitation (light absorption and charge carrier production), (2) diffusion, (3) trapping, (4) recombination, and (5) oxidation [130][131]. In a typical photocatalysis process, photons with energy greater than the band gap (E_{BG}) can excite electrons (e^-) on the photocatalyst surface from

the valence band (VB) to the conduction band (CB). As a result, electron (e^-) and holes (h^+) are formed on CB and VB, respectively. The photogenerated electrons and holes move to the photocatalyst's surface, where they participate in redox reactions with adsorbed species, forming superoxide radical anion ($\cdot O_2^-$) and hydroxyl radical ($\cdot OH$), respectively, as follows [132][133]:

$$TiO_2 \xrightarrow{solar} e^- + h^+$$

$$h^+ + H_2O \longrightarrow \bullet OH + H^+$$

$$h^+ + OH^- \longrightarrow \bullet OH$$

$$e^- + O_2 \longrightarrow \bullet O_2^-$$

The photogenerated reactive oxygen species are powerful oxidizers that play a key role in the breakdown of organic contaminants in wastewater. There is no secondary contamination since organics in wastewater can be entirely reduced to CO_2 and H_2O. Many e^- and h^+, on the other hand, recombine and release energy as heat before participating in redox processes, severely limiting the practical photocatalytic activity of photocatalysts [134].

2.10.1.1 Oxidation Step of Photocatalysis

The absorbed water on the photocatalyst surface is oxidized by positive holes formed in the valence band as electrons shift to the conduction band as a result of light irradiation, allowing the creation of hydroxyl ($\cdot OH$) radicals with strong oxidative decomposing power. Following that, the hydroxyl radicals react with the organic contents in the dyes. If oxygen is present at the time of this reaction, the intermediate radicals in organic compounds, as well as the oxygen molecules, may undergo radical chain reactions, consuming oxygen in some situations. The organic matter eventually decomposes into carbon dioxide and water in this situation. Organic substances can react directly with the positive holes in such conditions, resulting in oxidative breakdown [135].

2.10.1.2 Reduction Step of Photocatalysis

A pairing reaction happens in this stage, which results in the reduction of oxygen in the air. Due to the fact that oxygen is a readily reducible substance, it is used as an alternative to hydrogen generation. Superoxide anions are formed when electrons in the conduction band react with dissolved oxygen species. These superoxide anions bind to the intermediate products of the oxidative process, generating peroxide or converting to hydrogen peroxide and then to water. The

reduction is more likely to happen easily in organic matter than in water. As a result, higher organic matter concentrations tend to increase the number of positive holes. This lowers carrier recombination while increasing photocatalytic activity [135]. Figure 2.16 depicts the oxidation and reduction steps of photocatalysis.

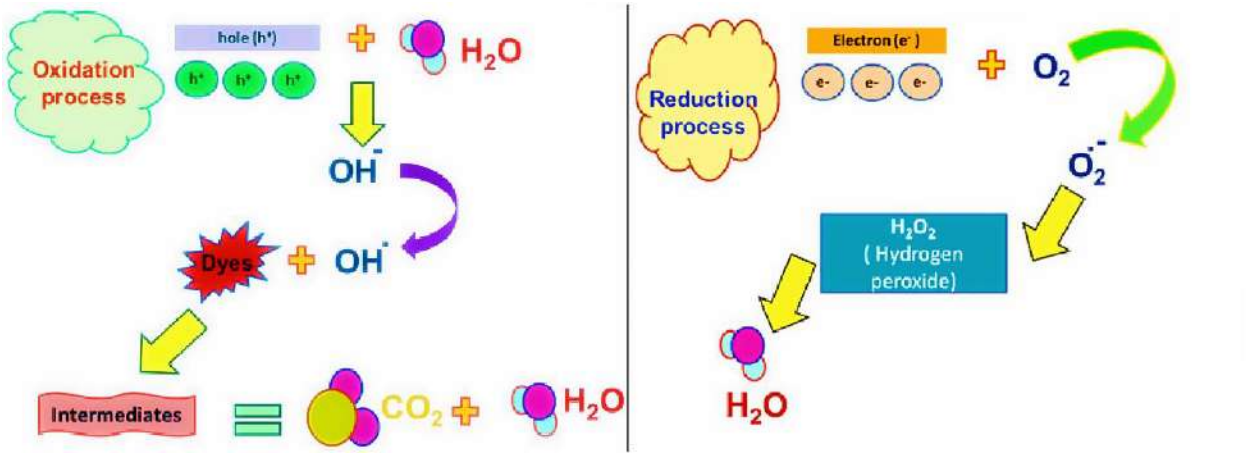

Figure 2.16: Schematics of oxidation and reduction steps of photocatalysis.

2.10.2 TiO_2 Photocatalysis – Limitation and Countermeasures

TiO_2 photocatalysis is remarkably efficient in destroying organic contents. However, its' use is limited due to its narrow photocatalytic zone ($\lambda < 400$ nm) and capacity to absorb only a miniscule fraction (5%) of incident solar irradiation and indoor light, which is due to its relatively large band gap (anatase, 3.2 eV). Because photocatalytic degradation happens mostly on TiO_2's surface, mass transfer limitations must be avoided for TiO_2 's use in water treatment to be effective. The adsorption of organic pollutants on TiO_2 surface is generally low due to its limited affinity for organic pollutants (particularly hydrophobic organic pollutants), result in slow photocatalytic degradation rates. Furthermore, due to the instability of the nanosized particle, the TiO_2 nanoparticles may aggregate during the photocatalytic degradation process, obstructing light incidence on the active centers and lowering catalytic activity. Furthermore, one major practical problem for the slurry system is to recover the nanosized TiO_2 particles from the treated water, which is both an economic and a safety concern. The following countermeasures can be used to overcome the limits of TiO_2 based photocatalysis: (1) TiO_2 catalyst modification/alteration in order

to achieve visible light utilization; (2) catalyst synthesis optimization in order to generate catalysts with a defined crystal structure, reduced particle sizes, and a high affinity for diverse organic pollutants; (3) design and development of a second generation TiO_2 catalyst with strong separation capability and the capacity to be recovered and regenerated. Table 2.2 summarizes the countermeasures for overcoming these constraints, as well as the mechanisms and downsides of each countermeasure.

Table 2.2: The counter measures to enhance TiO_2 photocatalytic process and their respective disadvantages

Countermeasures		**Drawbacks**	**References**
Enhancing the visible-light photocatalytic activity of TiO_2 particles	Doping of Metals Doping of Non-metals Co-doping Surface Organic Modification	• Thermal instability • Dopant concentration dependent • Costly • Multistep experimental process • Competitive adsorption of other coexisting species	[136] [137] [138]
Enhancing adsorption of organic pollutants on TiO_2 particles	Doping of carbon based NPs Surface Organic Modification	• Concern on the remobilization of carbon-based materials during photocatalysis • remobilization of surface coating during photocatalysis	[139] [140]
Stabilization of TiO_2 particles	Stabilization by support structures Stabilization by surface modification	• Lower activity of supported TiO_2 compared to unrestricted TiO_2 • In presence of cation, stability decreases	[141] [142]
Separation of TiO_2 particles	Immobilization on support structures Magnetic Separation	• Lower activity of supported TiO_2 compared to unrestricted TiO_2 • Magnetic core size and calcination temperature influence the photocatalysis	[143] [144]

2.10.3 Effect of Doping on TiO_2 Photo-catalyst

Due to the large band gap, TiO_2 can only be energized by UV photons, which account for less than 5% of the solar spectrum's energy [145]. As a result, it's essential to produce TiO_2 based materials that can harness more solar energy. To address this issue, various metals and their derivatives, such as Ag, Cu, Au, Co, and others, have been combined with TiO_2 to generate hybrid photocatalysts that extend photocatalytic activity into the visible light spectrum. The mechanism can be elucidated by two features and depicted in figure 2.17.

- Because of the presence of integrated materials, the recombination rate of e^- and h^+ is suppressed, which enhances interfacial electron transport and so improves the separation of e^- and h^+ [145].
- The band gap in TiO_2 has been decreased, making TiO_2 excitation easier. It will make it easier for electrons to move from the valence band to the conduction band, potentially resulting in more oxidative species. There are various reports that concluded the lowering of TiO_2 band gap due to doping [146].

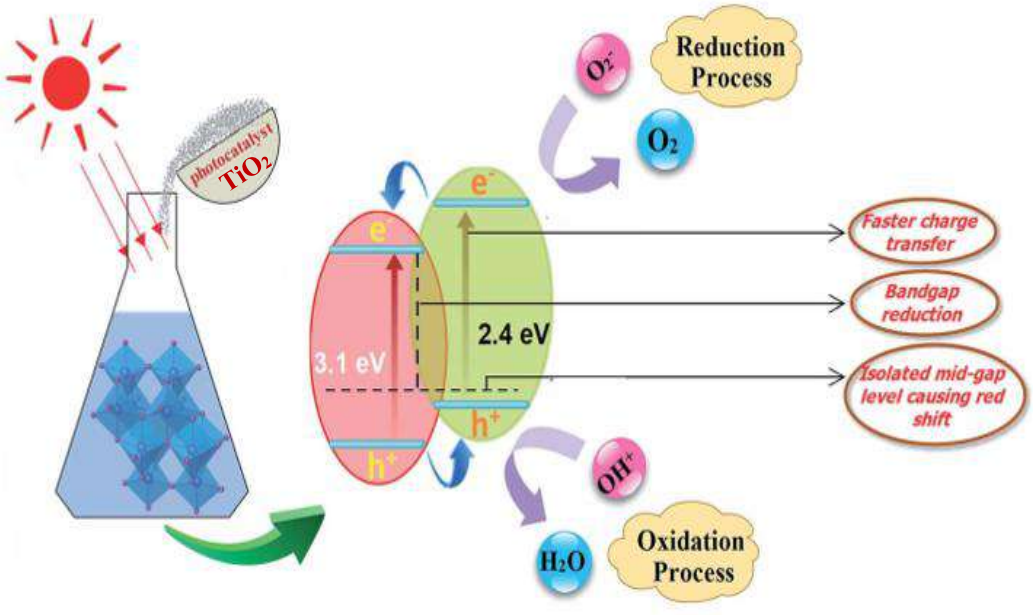

Figure 2.17: Effect of doping on photocatalysis.

2.11 **Antibacterial Effect of TiO_2 Nanoparticles**

Antibiotic usage has resulted in the emergence of multidrug-resistant bacterial strains. As a result, food safety and human health are both at risk. Metal oxide nanoparticles, especially, TiO_2 NPs, have sparked curiosity as a potential novel antibacterial material owing to photocatalytic nature chemical stability, non-toxicity, low-cost. Titania NPs has been shown in several tests to have good antibacterial activity against a wide range of Gram-positive and Gram-negative bacteria. Gram-positive bacteria have many layers of peptidoglycan and teichoic acid, while Gram-negative bacteria have a thin layer of peptidoglycan surrounded by a secondary lipid membrane with transmembrane lipopolysaccharides and lipoproteins [147]. TiO_2 NPs promote the inactivation of microorganisms due to their strong oxidizing capacity by free radical formation, such as hydroxyl and superoxide anion radicals exhibiting reduced growth against numerous pathogens, including Escherichia coli and Staphylococcus aureus. Figure 2.18 compares Gram-positive and Gram-negative bacteria.

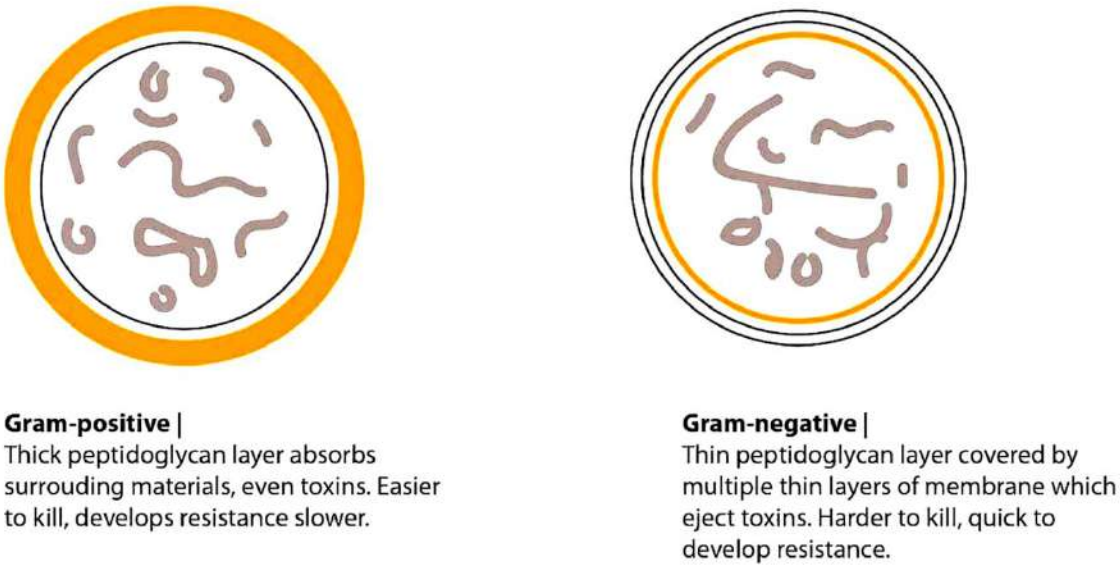

Figure 2.18: Schematic comparison between Gram-positive and Gram-negative bacteria.

Being a thermally stable and biocompatible chemical compound with significant photocatalytic activity, TiO_2 has shown promising antibacterial performance. The antibacterial activity of TiO_2 NPs was primarily differentiated by their shape, crystal structure, and size. According to several studies, because of the increased specific surface area, hollow TiO_2 nanotubes showed promising

antibacterial reduction. This is due to the nature of titanium dioxide, which produces reactive oxygen species (ROS) on its surface during photocatalysis when exposed to light of the right wavelength. It's worth noting that, due to the photocatalytic nature of TiO_2 NPs, several studies have found that their antibacterial activity enhanced when they were exposed to UV-A light [148]. Table 2.3 summarizes some of the investigations on the antibacterial properties of TiO_2 NPs.

Table 2.3: TiO_2 nanoparticles against different bacterial strain and their antibacterial activities

Bacteria Strain	**Nanoparticles**	**Results**	**References**
Escherichia coli	TiO_2 nanotubes (~ 20 nm)	97.53% of reduction	[149]
Staphylococcus aureus	TiO2 nanotubes (~ 20 nm)	99.94% of reduction	[149]
Pseudomonas aeruginosa	TiO_2 NPs (10–25 nm)	Although they were not fully terminated, their chances of surviving were greatly reduced.	[150]
Bacillus subtilis	TiO_2 NPs doped with silver (19–39 nm)	1% Ag-N-TiO_2 had the highest antibacterial activity with antibacterial diameter reduction of 22.8 mm	[151]
Shewanella oneidensis	TiO_2 NPs doped with copper (~20 nm)	The percentage of inhibition was around 11%	[152]

2.11.1 Understanding the Antibacterial Mechanism of TiO_2 Nanoparticles

The antibacterial action mechanism of TiO_2 NPs is typically related with reactive oxygen species (ROS) with high oxidative potentials formed under band-gap irradiation photo-induces charge in the presence of O_2. ROS cause bacterial cells to die through a variety of methods. TiO_2 generates ROS with the advantage of being in nanoscale. This nanoscale nature suggests a significant increase in surface area-to-volume ratio, allowing for maximal interaction with the environment's water and oxygen, as well as a small size that may readily penetrate the cell wall and cell membrane, allowing for an increase in internal oxidative damage. Bacteria contain enzymatic

antioxidant defense mechanisms such as superoxide dismutase and catalases, as well as natural antioxidants such as carotene, ascorbic acid, and tocopherol that limit lipid peroxidation and the impacts of ROS radicals. When such systems are breached, a series of redox events can result in cell death through the modification of many critical structures such as cell wall, cell membrane, DNA, and so on [147]. Figure 2.19 illustrates antibacterial mechanism of TiO_2 NPs.

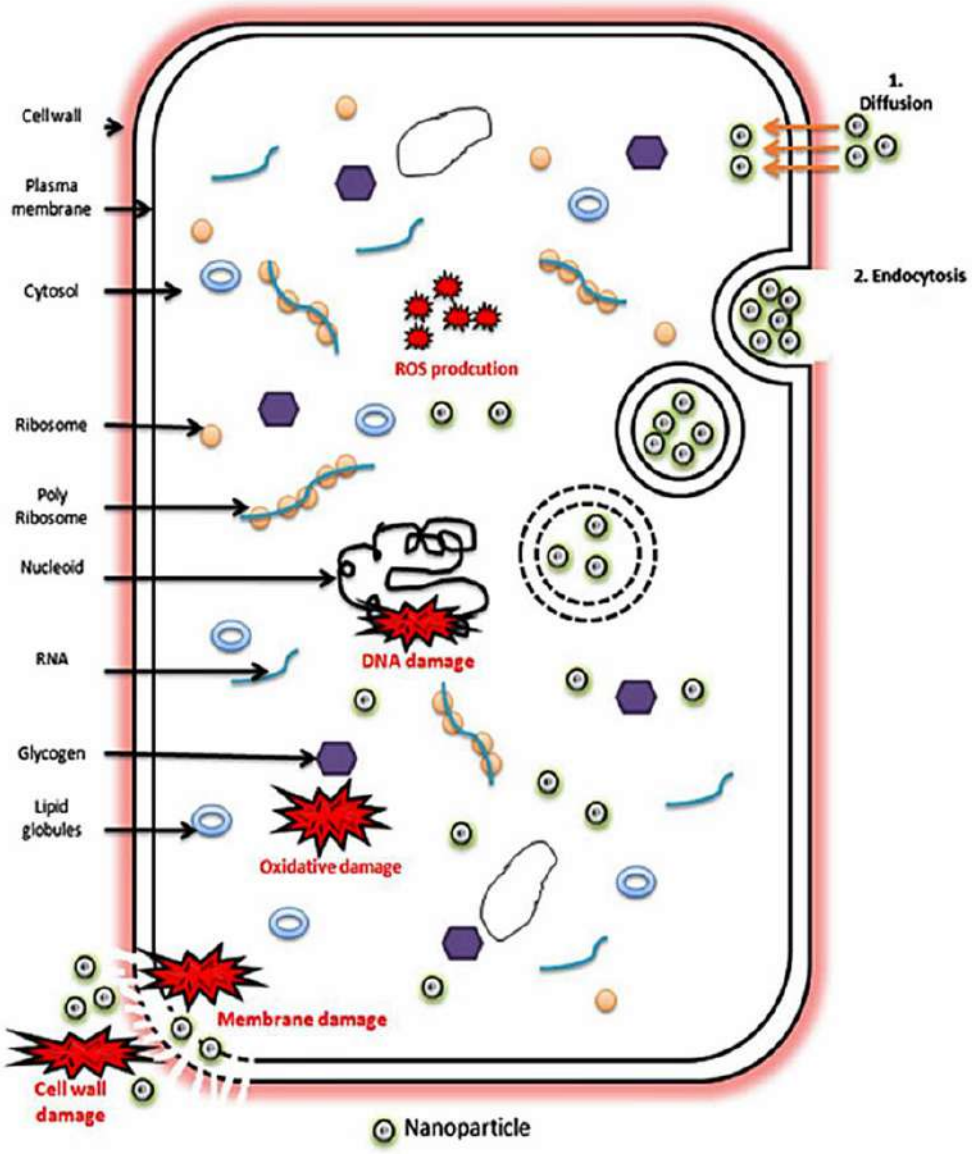

Figure 2.19: Effect of bio-mediated TiO_2 nanoparticles on bacteria.

In essence, When TiO_2 NPs come into contact with bacterial cells, they produce reactive oxygen species (ROS). These ROS kill bacteria by compromising cell wall integrity, mostly by phospholipid oxidation, resulting in decreased adhesion and irregular ionic equilibrium. It inhibits respiratory cytosolic enzymes and modifies macromolecule structures in the cytosol, having a significant impact on cellular integrity and gene expression. It also reduces phosphate absorption and cellular communication across the cell [10].

Whether chemically derived or green synthesized, TiO_2 NPs kill bacteria, however biologically derived NPs have superior antibacterial action. The capping agents produced by the plant extracts are responsible for their remarkable antibacterial capability. Both gram-positive and gram-negative bacteria are effectively inhibited by green TiO_2 NPs. However, it is more reactive against gram-positive bacteria due to the relative structural complexity of gram-negative bacterial cell walls [10].

CHAPTER 3: EXPERIMENTAL

3.1 Raw Materials

For this thesis work, analytical grade chemicals and reagents were utilized. The required raw materials for this thesis is listed in table 3.1.

Table 3.1: List of raw materials with purpose and specification.

Raw Materials	Purpose	Specification
1. Titanium Tetraisopropoxide (TTIP), $Ti\{OCH(CH_3)_2\}_4$	Metal Salt Precursor	Purity ≥ 99.9 %, Merck, India
2. Copper Sulphate, $CuSO_4.5H_2O$	Copper Doping Element	Purity ≥ 99.9 %, Merck, India
3. Silver Nitrate, $AgNO_3$	Silver Doping Element	Purity ≥ 99.9 %, Merck, India
4. Distilled Water (DW)	TiO_2 Nanoparticle Synthesis	Purity ≥ 99.9 %, Merck, India
5. Ethanol, C_2H_5OH		Purity ≥ 99.9 %, Merck, India
6. Acetone, C_3H_6O		Purity ≥ 99.9 %, Merck, India
7. Hydrochloric Acid, HCl	Metabolites Screening Test	Purity ≥ 99.9 %, Merck, India
8. Picric Acid, $(O_2N)_3C_6H_2OH$		Purity ≥ 99.9 %, Merck, India
9. Nitric Acid, HNO_3		Purity ≥ 99.9 %, Merck, India
10. Sodium Hydroxide, NaOH		Purity ≥ 99.9 %, Merck, India
11. Ferric Chloride, $FeCl_3$		Purity ≥ 99.9 %, Merck, India
12. Sulfuric Acid, H_2SO_4		Purity ≥ 99.9 %, Merck, India
13. Chloroform, $CHCl_3$		Purity ≥ 99.9 %, Merck, India

Raw Materials	Purpose	Specification
14. Methylene Blue (MB), $C_{16}H_{18}ClN_3S$	Photocatalytic Experiment	Purity ≥ 99.9 %, Merck, India
15. Staphylococcus aureus (Gram +ve)	Bacteria Strain for Antibacterial Assay	-
16. Escherichia coli (Gram -ve)		-
17. Bacillus subtilis (Gram +ve)		-
18. Klebsiella pneumonia (Gram -ve)		-

3.2 Synthesis Procedure

The overall TiO_2 NP green synthesis process involve several stages including extract preparation, phytochemical screening test, stirring, doping, centrifugation, drying, calcination and so on. The step by step procedure of the whole process is discussed in the following sub-section. The figure 3.1 below illustrates the overview of the whole process.

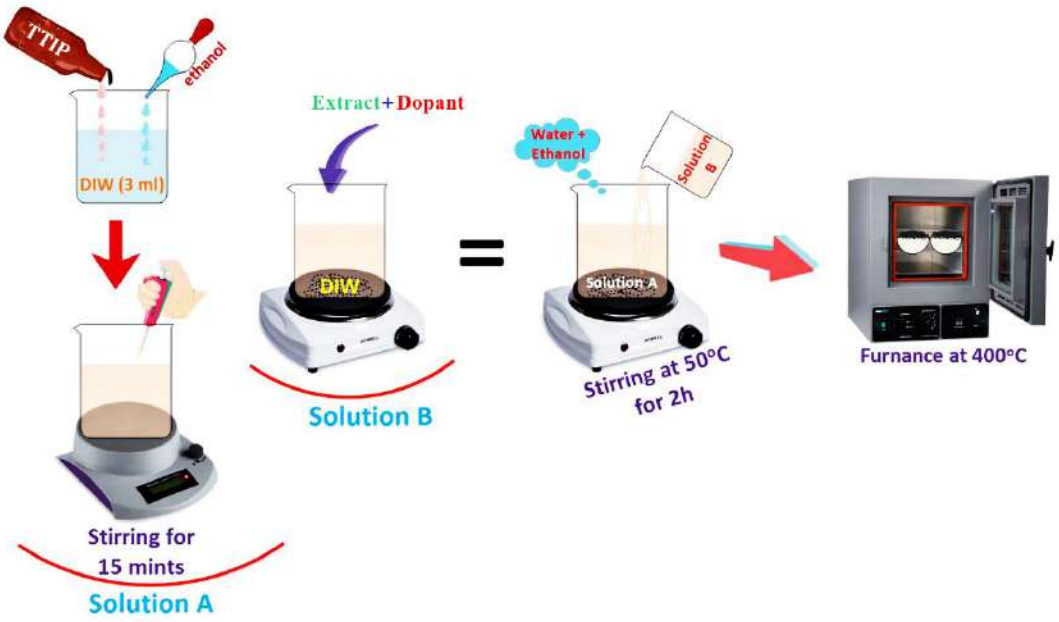

Figure 3.1: Overview of the TiO_2 green synthesis procedure.

3.2.1 Stage 1: Mango Leaf Extract Preparation

Fresh and healthy mango leaves were collected from the Rajshahi district. Leaves were washed with distilled water (DW) to removed dust and dirt. Then they were dried at room temperature for 7-10 days. After that, the leaves were cut to small pieces with knife (cleaned with acetone). About 20g of the chopped leaves were mixed with 100 ml DW. The mixture was boiled above 100^{o}C for 30-40 minutes. After cooling, Whatman filter paper was utilized for the filtration of the solution and the extract was stored in a refrigerator at 4^{o}C for further use. Figure 3.2 depicts stage 1 of the experimental steps.

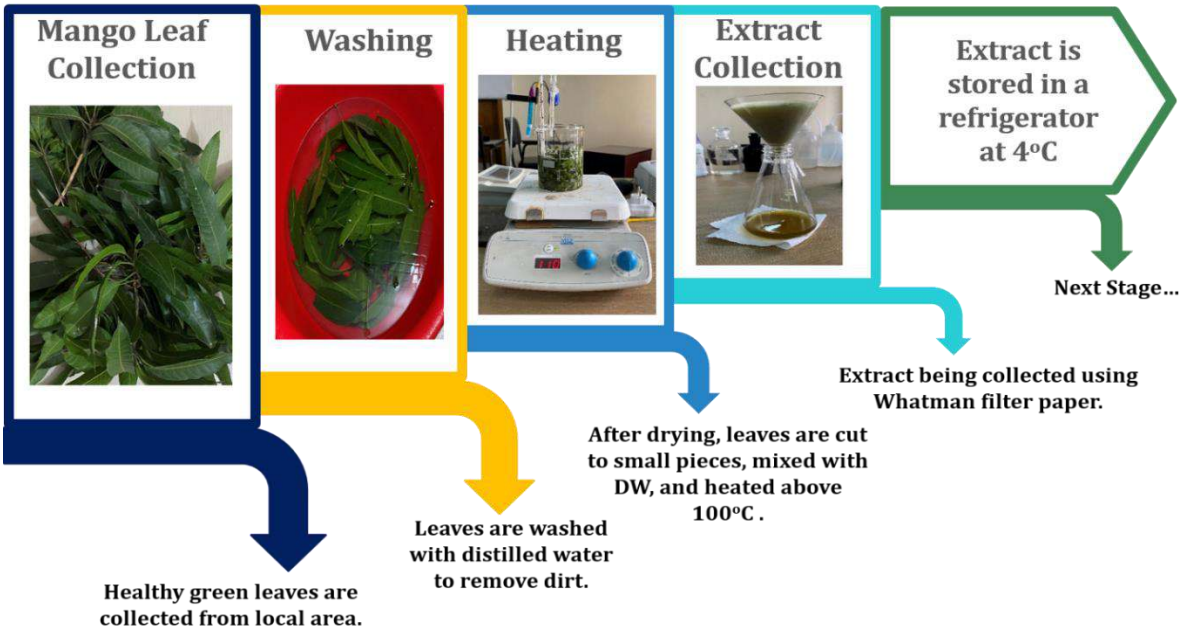

Figure 3.2: Mango leaf extract preparation.

3.2.1.1 Metabolites Screening Test

- Test for saponins: 2/3 drops of DW were mixed with 1mL mango leaf extract. The formation of foam confirmed the presence of saponin in the extract.
- Test for alkaloids: 2 mL extract was mixed with 1 mL HCl and heated for around 30 minutes and cooled to room temperature. After that, the resultant solution was filtered and the filtrate was mixed with Hager's Reagent (Picric Acid). Formation of the yellow color confirmed the presence of alkaloids.
- Test for terpenoids: 3 mL extract was mixed with 5 mL chloroform and 5 mL H_2SO_4. Formation of reddish brown color confirms the presence of terpenoids.

- Test for proteins: 2 mL extract was mixed with a few drops of HNO_3. Formation of yellow color confirms the presence of protein.
- Test for phenols: Formation of bluish black color due to the mixing of 2 mL extract with a few drops of $FeCl_3$ confirms the presence of phenols.
- Test for flavonoids: Emergence of intense yellow color due to the mixing of 2 mL extract with 5 mL NaOH confirmed the presence of flavonoids in the extract.

3.2.2 Stage 2: Biogenic Synthesis of TiO_2 Nanoparticles

As shown in figure 3.3, 10 mL of the metal salt precursor, TTIP, was added dropwise in in a mixture of DW and 50 mL ethanol followed by the addition of 10 mL mango leaf extract under constant stirring at 50°C for 4-5 hours. A few drops of NaOH have been added to control the pH of the solution. To prepare (0.5%, 1%, 1.5%, and 2% mole fraction) Cu doped TiO_2 and (0.5%, 1%, 1.5%, and 2% mole fraction) Ag doped TiO_2, stoichiometric amount of $CuSO_4.5H_2O$ solution and $AgNO_3$ solution have been added, respectively, in this stage. Finally, the prepared solution is kept for gelation and aging for 1 day. The obtained orange colored gel is washed and centrifuged at 2500 RPM for around 20 minutes using DW and ethanol, consecutively, for several times.

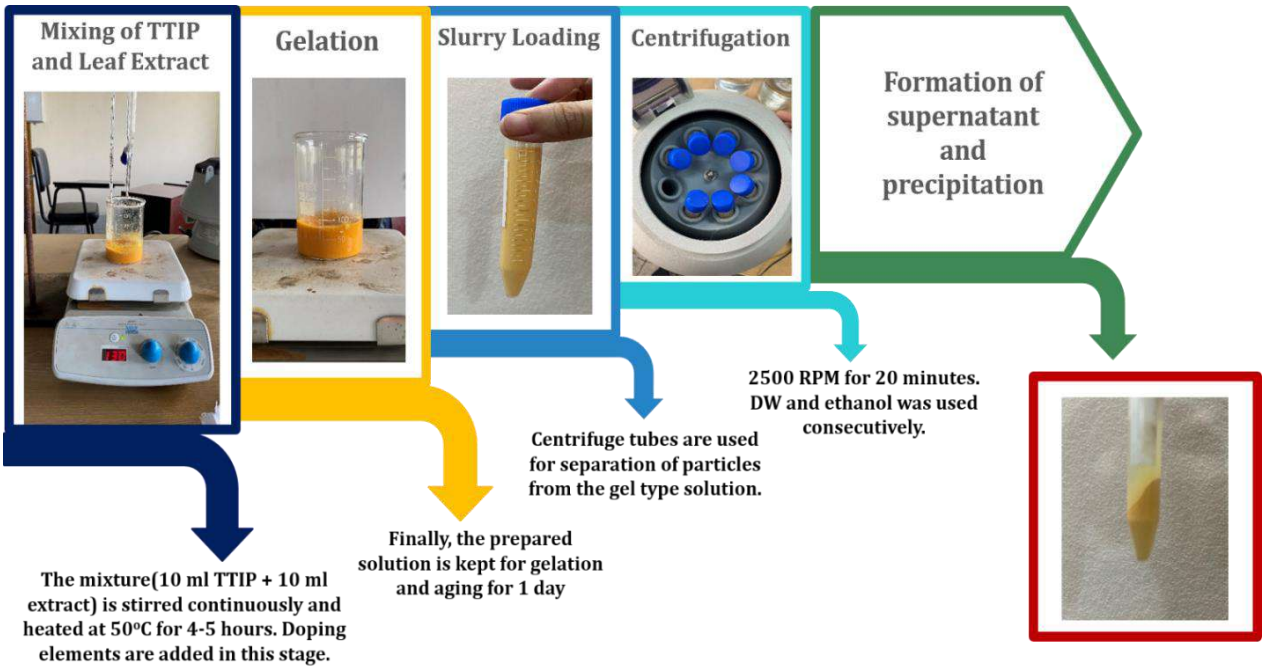

Figure 3.3: Biogenic synthesis of TiO_2 nanoparticles – Mixing, Gelation, and Centrifugation.

3.2.3 Stage 3: Drying, Calcination, and Collection

The centrifuged wet particles were dried overnight in an oven at 100°C. The flake type particles were ground using mortar and pestle for uniform distribution of heat during calcination. Finally, it was calcined in a furnace at 400°C (to ensure the formation of anatase phase) for 4 hours and the calcined powder was collected for characterization, photocatalytic experiment, and antibacterial test. Stage 3 is illustrated in figure 3.4.

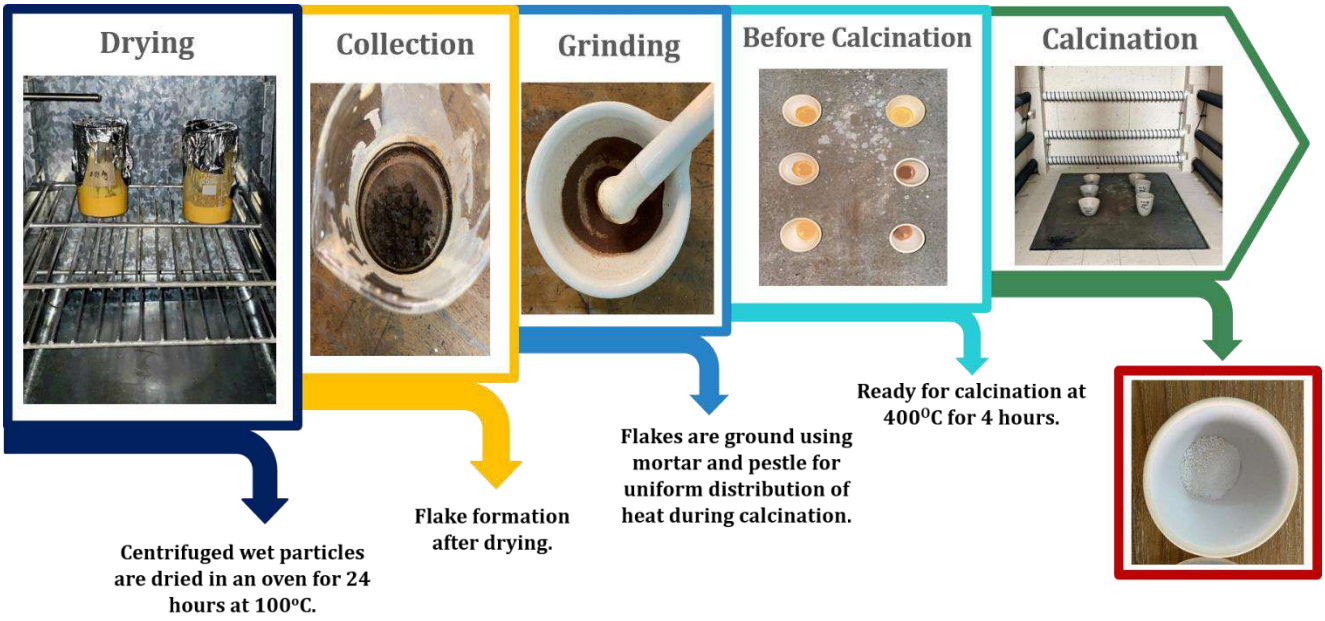

Figure 3.4: Drying, calcination, and collection of the biogenically prepared TiO_2 nanoparticles.

3.3 Procedure for Photocatalytic Experiment

The photocatalytic oxidation of methylene blue (MB) in TiO_2 suspension (both undoped and doped) under UV illumination was investigated in order to evaluate the photocatalytic activity of the as-prepared undoped and doped TiO_2 nanoparticles as shown in figure 3.5. The MB solution was prepared by adding appropriate amount of dye in DW to get the 0.01 mM stock solution. 50 mL of the stock MB solution was taken into a reaction vessel containing 10 mg of the TiO_2 catalyst. The solution mixture was kept inside the reactor without UV illumination and stirred for 30 min to established adsorption/desorption equilibrium. After the attainment of the equilibrium, the UV light was on (24 watt) and after a specific interval of time (15, 30, 45, 60, 75, and 90 minutes) 5 mL of the solution was taken from the reaction vessel and it was filtered to remove the catalyst.

The UV–Vis spectroscopy was used (wavelength range of 200 – 800 nm) for monitoring the progress of the reaction by measuring maximum absorbance of MB dye at previously specified time interims. The highest absorbance at 664 nm was recorded for MB. The same procedure has been employed for the undoped as well as the doped (both Cu and Ag doped) TiO_2 samples. The percentage dye degradation (Efficiency) was calculated using the following equation:

$$\text{Photocatalytic Degradation Efficiency (\%)} = [1 - \frac{C}{C_o}] * 100$$

where C_o is the initial MB dye concentration and C is the MB dye concentration in the reactor at a particular time.

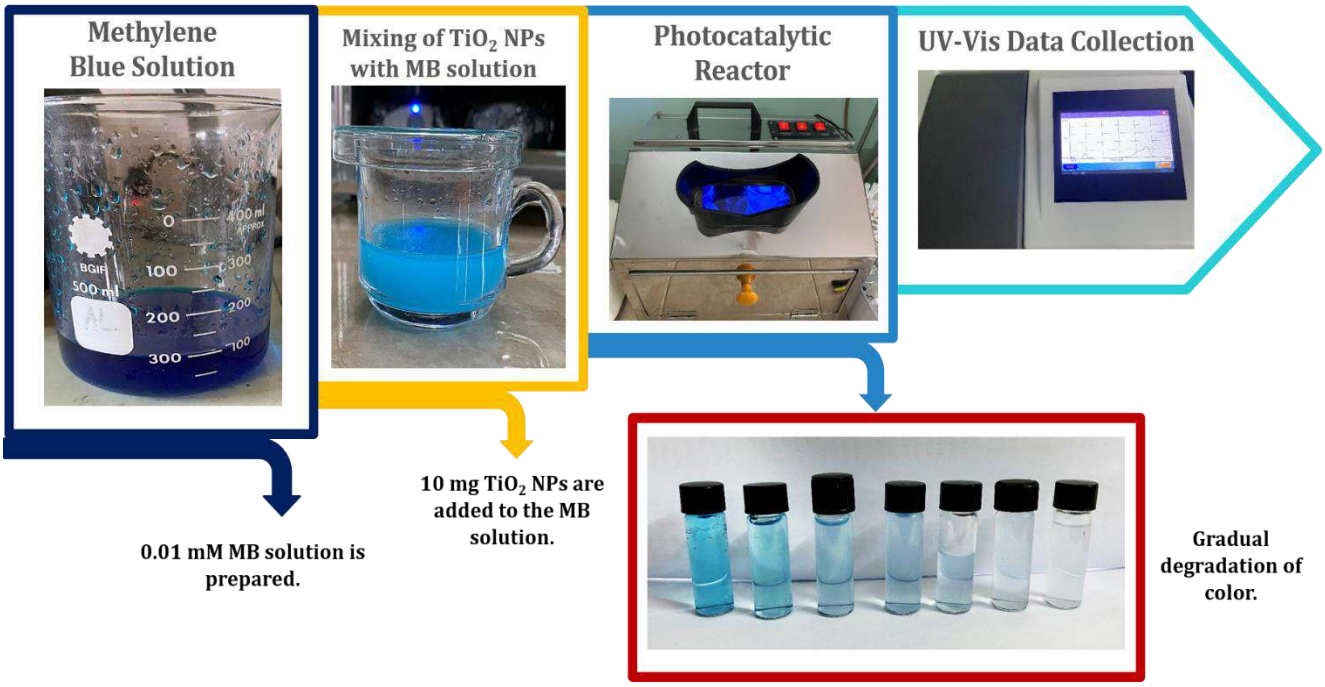

Figure 3.5: Photocatalytic performance evaluation of the undoped and doped TiO_2 NPs.

3.4 Procedure for Antibacterial Test

The antibacterial test was carried out by "Kirby – Bauer Disk Diffusion Method". Figure 3.6 gives an illustration of the method. To make the appropriate combination for bacterial culture, 10g nutritional agar was dissolved in 50 ml deionized water and heated at 40°C for 10 minutes. The mixed solution was then dried in an autoclave at 121°C for another 15 minutes. Four different bacterial strains (Accoding to McFarlands standard - 10^6 CFU/mL), Staphylococcus aureus (Gram +ve), Escherichia coli (Gram -ve), Bacillus subtilis (Gram +ve), Klebsiella pneumonia (Gram -ve)

were introduced on the dried plate with the help of a cotton-tipped stick. Suspension of undoped TiO_2, Cu doped TiO_2, and Ag doped TiO_2 were prepared by dissolving 0.1 mg of undoped TiO_2, Cu doped TiO_2, and Ag doped TiO_2 in 1 mL DW for antibacterial assessment of Bacillus subtilis (Gram +ve) and Klebsiella pneumonia (Gram -ve). Similarly, suspension of undoped TiO_2, Cu doped TiO_2, and Ag doped TiO_2 were prepared by dissolving 2 mg of undoped TiO_2, Cu doped TiO_2, and Ag doped TiO_2 in 1 mL DW for antibacterial assessment of Staphylococcus aureus (Gram +ve) and Escherichia coli (Gram -ve). The suspensions were sonicated for 10 minutes before using. Each dried standard antibiotic disc was impregnated with these suspensions (50 µl). To analyze the antibacterial activity against four distinct bacterial strains, disks containing the test materials were placed on the surface of the agar plate using sterile forceps. The plates were incubated at 37 °C for 24 h to check the antibacterial activity. This activity (inhibition zone) was measured using slide calipers in millimeters.

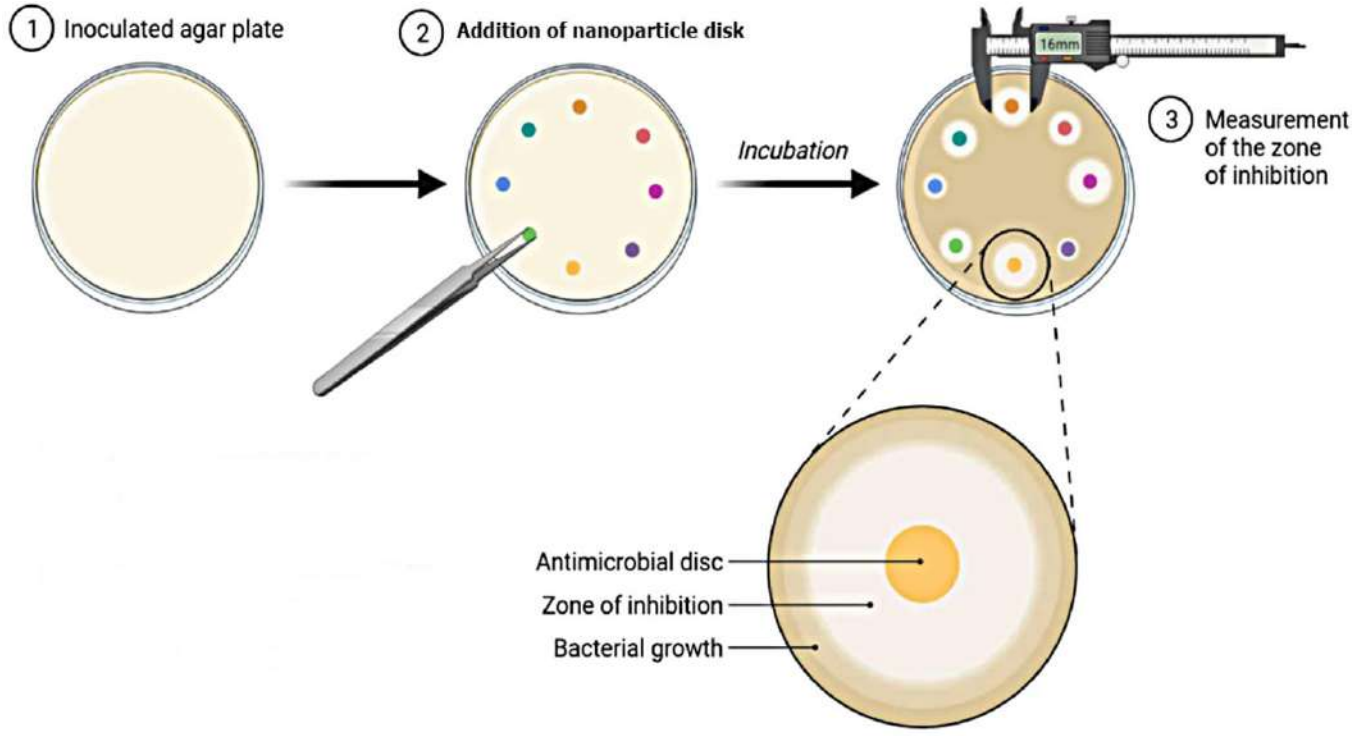

Figure 3.6: Schematic illustration of Kirby-Bauer disk diffusion antibacterial test for TiO_2 NPs.

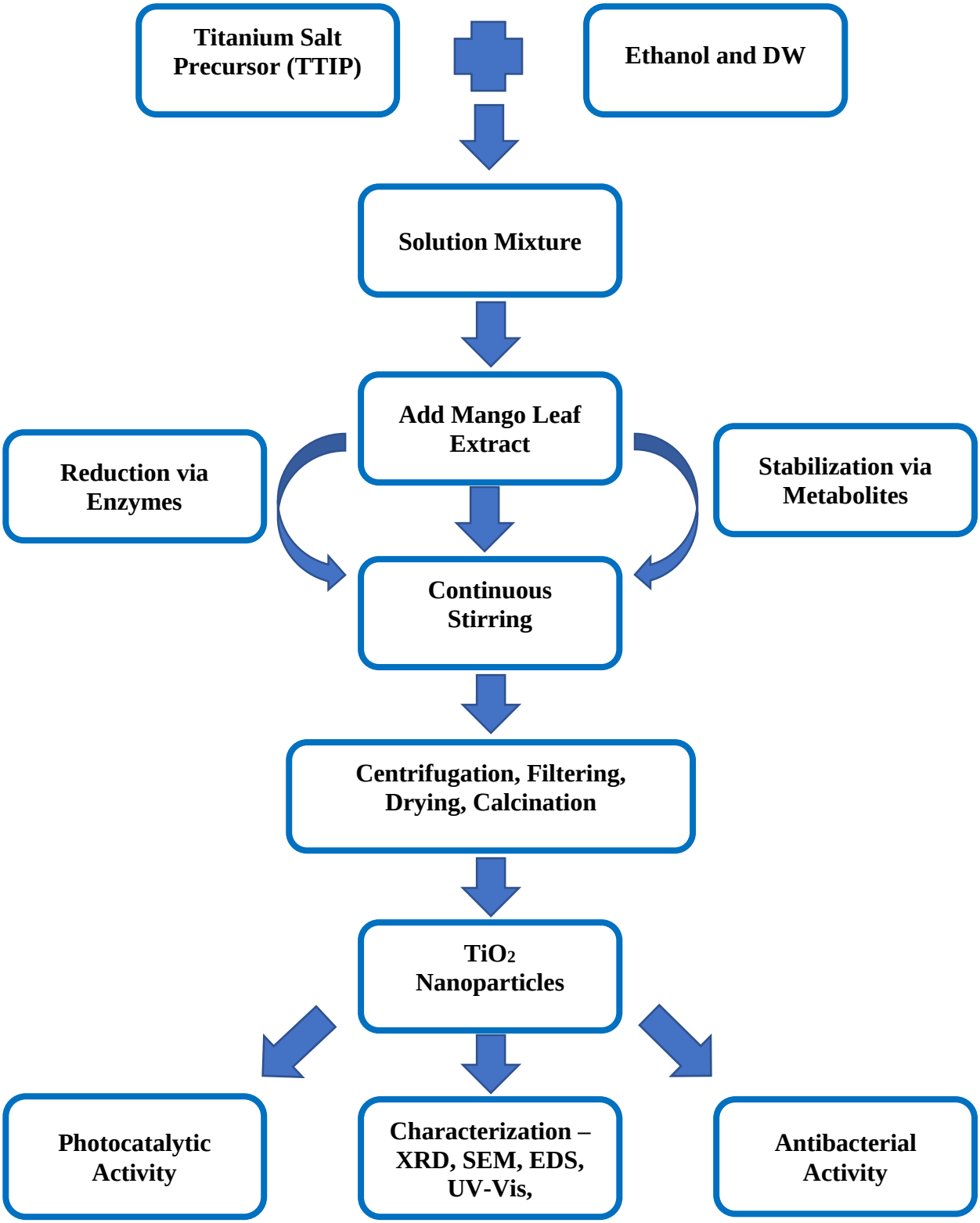

Figure 3.7: Flowchart of the overall experimental work.

3.5 Characterizations

3.5.1 X-Ray Diffraction (XRD) analysis

X-ray diffraction analysis was done using RIGAKU SmartLab x-ray diffractometer (Figure 3.8) having a Cu x-ray source (wavelength: $K_{\alpha 1}$ = 1.540598Å and $K_{\alpha 2}$ = 1.544426Å). The diffraction was performed using Bragg angles between 2θ = 10° to 80° at a scanning rate of 0.2°/min. It is a fast analytical method that may offer information on unit cell dimensions and is mostly utilized for phase identification of crystalline materials. For this study, bulk powder samples were employed as specimens.

Figure 3.8: XRD machine.

3.5.2 Scanning Electron Microscopy (SEM)

The surface morphology of the prepared samples was examined using a scanning electron microscope (ZEISS-EVO 18, UK) (Figure 3.9) in this experiment. The attached energy dispersive X-ray spectroscopy (EDS) was used for elemental analysis of the nanoparticles. The grain sizes and grain distribution were determined using ImageJ software.

Figure 3.9: Scanning Electron Microscope.

3.5.3 UV-vis Spectroscopy

Absorbance and transmittance spectra were measured using UV 1800 UV-VIS Spectrophotometer (Figure 3.10) in the range of 200-800 nm. Band gap was calculated using Tauc Plot from the absorbance spectra.

Figure 3.10: UV-vis spectrophotometer.

CHAPTER 4: RESULTS & DISCUSSION

The findings of the thesis work are presented in this chapter with the help of graphical representations and data tables with proper explanation gathered from existing theories and literatures. Comparison of this thesis work with other reported studies are also provided here.

4.1 Structural Analysis – XRD

4.1.1 Major Peaks and Effects of Incorporating Doping Elements

For the investigation of crystal structure of pure TiO_2 as well as Cu-doped and Ag-doped TiO_2 fabricated via biogenic route (calcined at 400^{o}C), XRD analysis has been carried out in the range of $2\theta = 10^o – 80^o$. Figure 4.1 and 4.2 represents the XRD spectra of the undoped and doped samples. For the pure TiO_2 XRD spectra, well defined peaks are observed at 25.54^o, 37.93^o, 48.29 ^{o}, 54.11^o, 55.35^o, 62.99^o, 69.07^o, 70.69^o, and 75.42 ^{o} related to planes (101 – predominant), (004), (200), (105), (211), (204), (116), (220), and (215), respectively. According to JCPDS Card No: 021-1272, all the diffraction peaks corresponds to the tetragonal anatase phase of TiO_2 [113][153][154]. The diffractive maximum of Cu doped TiO_2 and Ag doped TiO_2 were identical to those of untreated (pure) TiO_2 confirming that the crystalline phase of anatase TiO_2 did not change after doping. In essence, no extra peaks were observed due to the presence of impurities such as Cu, Ag and their oxides (as they might be too less as well as small in size to be detected), even at highest doping concentration, stating that the anatase phase is not disturbed upon doping. Furthermore, the lack of impurity phases demonstrated the effective integration of Cu and Ag ions into the anatase TiO_2 matrix structure. This observation does not rule out the possibility of Cu-based planes/phases as well as Ag-based planes/phases in the synthesized product. On the contrary, it might imply that Cu and Ag ions are evenly distributed as small clusters within anatase crystallites. Additionally, with the increasing doping percentage of both Cu and Ag, a gradual decrease in the predominant peak intensity was observed indicating the degradation of TiO_2 crystallinity resulted from the substitution of Ti^{4+} ions with Cu^{2+} ions and Ag^+ ions, respectively. Only the anatase TiO_2 phase has been detected in the synthesized material, with no rutile phase. This might be owing to a low concentration of oxygen vacancies during development due to a high concentration of gaseous oxygen, delaying the transition from anatase to rutile phase [155].

4.1.2 Shifting of Peak Position Due to Doping

However, with increased Cu and Ag doping ion concentration, major diffraction peaks move towards the lower 2θ value and peak broadening occurs, which might be attributed to lattice strain originated in the host materials [156]. The reason for this peak shifting is due to the difference in the ionic radii as well as the charges of the dopants and the host materials [157]. The ionic radius of Cu^{2+} (0.73 Å) is slightly larger than that of Ti^{4+} (0.61 Å) [157]. As a result, Cu^{2+} ions occupy the interstitial position of host lattice leading to a change in the lattice structure and the d-spacing between atoms increases. Consequently, 2θ values move to lower angle. For Cu doped TiO_2, a notable shift of the major peak (101) was observed from higher angle to lower angle (25.54° to 25.26°) with increasing doping concentration from 0.5% to 2%.

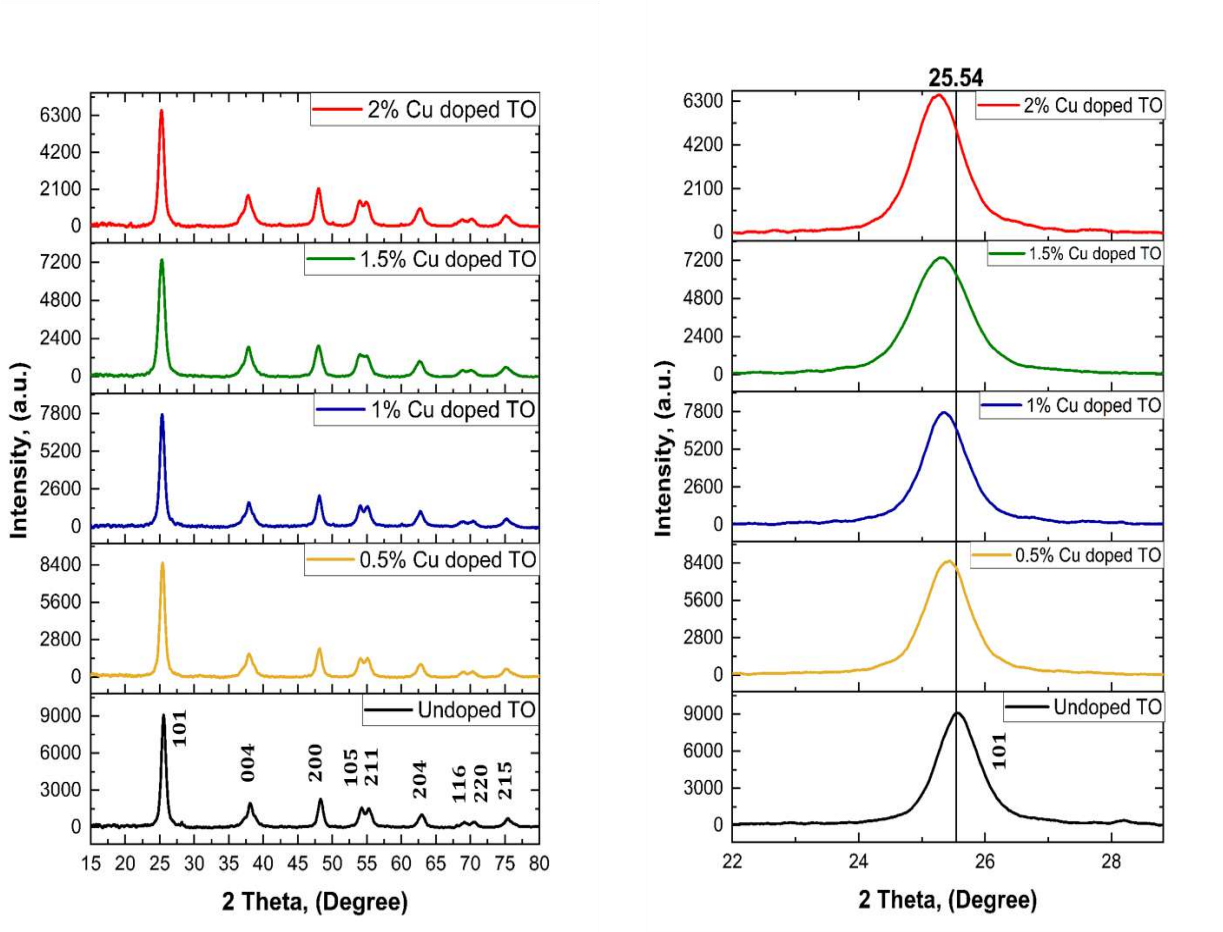

Figure 4.1: (a) XRD spectra of Undoped and (0.5%, 1%, 1.5%, 2%) Cu-doped TiO_2 samples showing no extra peaks due to doping, (b) Peak shifting to lower angle and peak broadening due to Cu doping in TiO_2 nanoparticles.

Similar trend has been found in the case of (0.5%, 1%, 1.5%, 2%) Ag doped TiO_2 samples. Compared to the ionic radius of Ti^{4+} (0.61 Å), the ionic radius of Ag^{+} is much larger (1.25 Å) [158]. As a result, Ag^{+} ions cannot occupy the interstitial position of host lattice rather replace Ti^{4+} ion substitutionally leading to a change in the lattice structure and the d-spacing between atoms increases [159]. Consequently, 2θ values move to lower angle. For Ag doped TiO_2, a notable shift of the major peak (101) was observed from higher angle to lower angle (25.54° to 25.22°) with increasing doping concentration from 0.5% to 2%. In addition to the ionic radii difference, incorporation of both Cu^{2+} and Ag^{+} ion in the TiO_2 lattice induces imbalance of charges due to replacement of Ti^{4+}. To compensate the charge imbalance, oxygen vacancies are formed that causes lattice defects (strain – both tensile and compressive) [157].

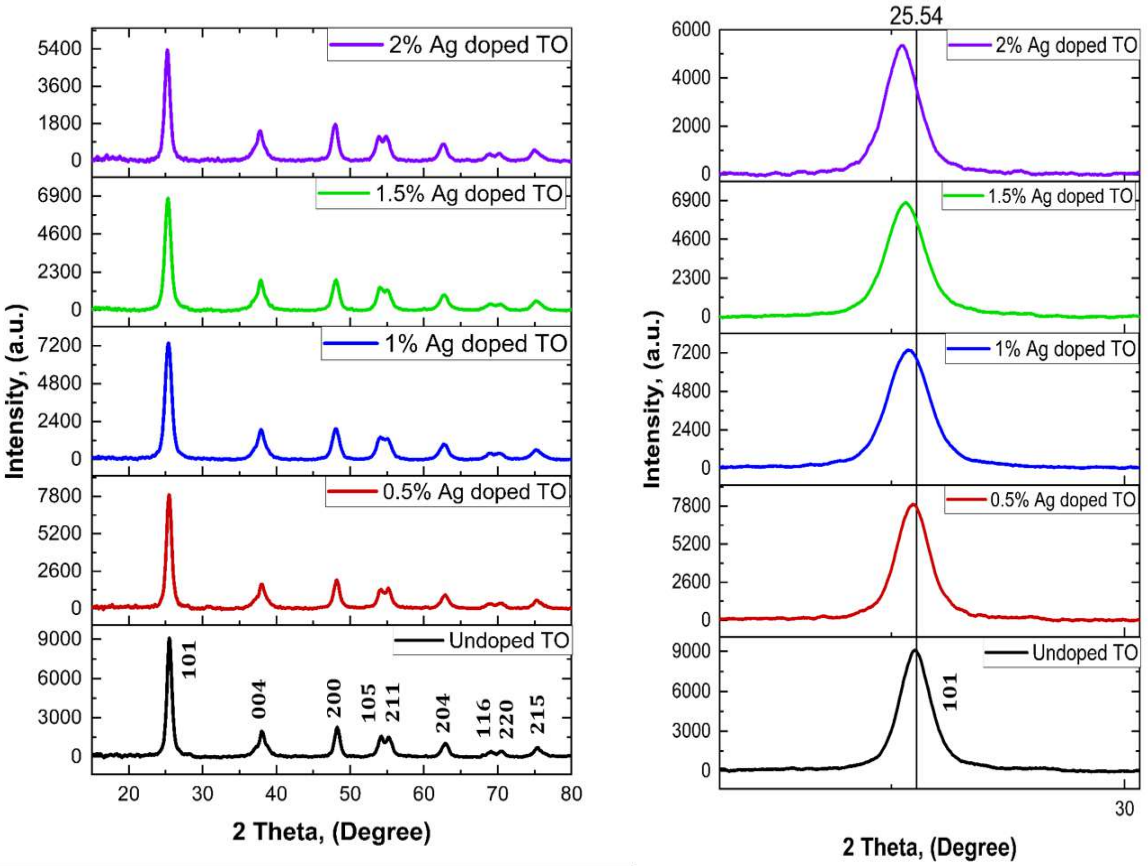

Figure 4.2: (a) XRD spectra of Undoped and (0.5%, 1%, 1.5%, 2%) Ag-doped TiO_2 samples showing no extra peaks due to doping, (b) Peak shifting to lower angle and peak broadening due to Ag doping in TiO_2 nanoparticles.

4.1.3 Williamson – Hall Plot: Crystallite Size and Micro-strain

In XRD diffraction pattern, peak broadening occurs due to several reasons including crystallite size, micro-strain (due to deformation of lattice), lattice faulting (extended defects), and instrumental broadening. If we consider, synthesized TiO_2 is free of faulting and instrumental broadening, then by using the Williamson–Hall (W-H) relation, as indicated in the following equation, the average crystallite size (D) and lattice strain may be calculated from the full-widths at half-maximum (FWHM) of the diffraction peaks [160]. Figure 4.3 and Figure 4.4 illustrate W-H plots of the prepared undoped and doped TiO_2 nanoparticles.

$\beta \cos\theta = \varepsilon\,(4\sin\theta) + \frac{K\lambda}{D}$ [Williamson – Hall Equation: it resembles a straight line equation]

where β indicates full-width at half-maximum (FWHM), θ is diffraction angle, K denotes shape factor, ε stands for strain, λ is wavelength of Cu $_{K\alpha}$ and D presents crystallite size. A straight line graph was attained from each sample by plotting $\beta \cos\theta$ vs $4 \sin\theta$. From the graph, the y-intercept provided crystallite size and slope of straight line indicated strain. The average crystallite size and the micro-strain associated with undoped and doped TiO_2 samples are listed in table 4.1.

Table 4.1: XRD data assessment for prepared samples.

Serial No	Sample	2θ (degree) of (101) Peak	Crystallite Size, nm	Average Micro-strain
1	Undoped TiO_2	25.54	10.74	0.348
2	0.5% Ag doped TiO_2	25.50	15.80	0.222
3	1% Ag doped TiO_2	25.36	11.25	0.264
4	1.5% Ag doped TiO_2	25.32	10.51	0.303
5	2% Ag doped TiO_2	25.22	9.25	0.415
6	0.5% Cu doped TiO_2	25.38	13.14	0.187
7	1% Cu doped TiO_2	25.36	12.06	0.258
8	1.5% Cu doped TiO_2	25.31	11.31	0.271
9	2% Cu doped TiO_2	25.26	10.63	0.367

It has been observed that with increasing percentage of both Cu and Ag (from 0% to 0.5%), there is an increase in crystallite size while the lattice strain decreases. It might be due to the fact that with the incorporation of dopant elements (Cu^{2+} and Ag^{+} ions), they occupy the interstices of the TiO_2 host lattice since both of them are larger in size than Ti^{4+} ions. As a result, they produce stress in the lattice. To neutralize the effect, lattice become larger to release the stress, hence the increase of crystallite size and decrease of lattice strain. Compared to the undoped TiO_2, the crystallite size of both 0.5% Cu doped TiO_2 and 0.5% Ag doped TiO_2 samples increased from 10.74 nm to 13.14 nm and 15.80 nm, respectively.

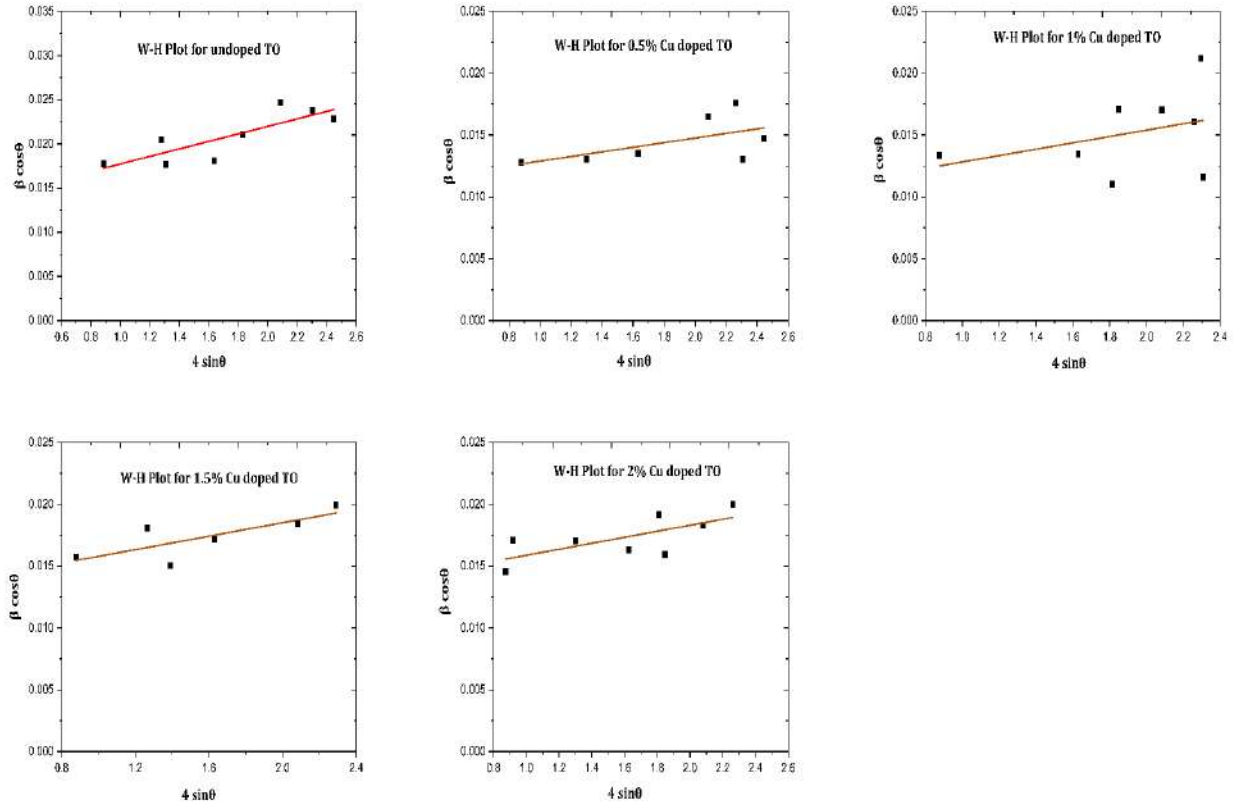

Figure 4.3: Williamson – Hall Plot for undoped and Cu doped TiO_2.

However, with increasing doping percentage (1% to 2%) for both Cu and Ag, optimal concentration of metal dopants is achieved and as such the crystallite growth is hindered due to grain boundary pinning [159]. As a result, it supersedes the previous crystallite growth effect. The impact of Cu and Ag substitution on TiO_2 crystallite size reduction is due to grain-boundary

restraining by dopant ions, which inhibits grain development due to the symmetry-breaking actions of the dopant at the boundary [161], resulting in smaller crystallite sizes while increasing the strain. Furthermore, the repulsion between crystallites caused by the presence of Cu and Ag ions in the crystallites may be responsible for crystallite growth regulation. For 1%, 1.5%, and 2% Cu and Ag doped TiO_2 samples, crystallite size decreased gradually while strain increased which confirms the theory stated above.

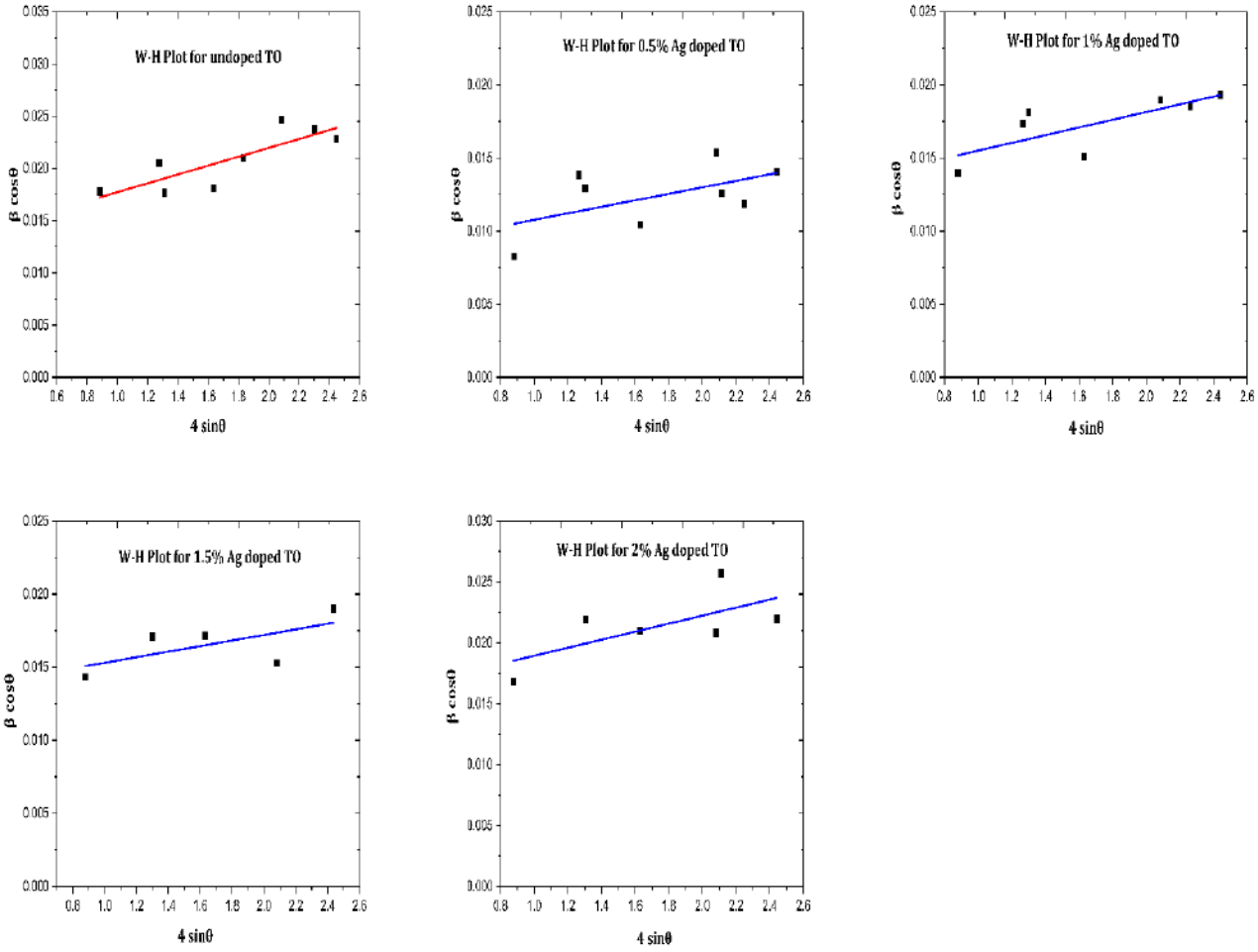

Figure 4.4: Williamson – Hall Plot for undoped and Ag doped TiO_2.

4.2 Morphological and Elemental Analysis

4.2.1 SEM Analysis

SEM analysis has been undertaken to observe the microstructure and the morphology of the prepared undoped TiO_2 along with Cu doped TiO_2 and Ag doped TiO_2. In the figures 4.5(a), 4.6., and 4.7, the SEM micrographs at a magnification of 25,000X for undoped TiO_2, (0.5%, 1%, 1.5%, 2%) Cu doped TiO_2 and (0.5%, 1%, 1.5%, 2%) Ag doped TiO_2 samples are displayed, respectively. Particle size and its distribution was calculated utilizing ImageJ software. The figures 4.5(b), 4.8, 4.9 shows particle size distribution curves for undoped TiO_2, (0.5%, 1%, 1.5%, 2%) Cu doped TiO_2 and (0.5%, 1%, 1.5%, 2%) Ag doped TiO_2 samples, respectively. Table 4.2 summarizes the particle size of the prepared samples. The undoped TiO_2 exhibited somewhat spherical shape with average particle size 31.85 nm. However, with increasing doping percentage (0.5%, 1%, 1.5%, 2%), both Cu doped samples and Ag doped samples showed intense agglomeration compared to pure TiO_2 samples. As a result, particle size increased gradually for both Cu doped samples and Ag doped samples with increasing percentage of doping. This result is consistent with a previously reported study [162]. Understanding the surface forces at the particle's interface with the aqueous part of the particle is critical for understanding particle agglomeration. The zero charged particles in aqueous solution tends to aggregate and form large clusters. However, if each particle carries similar charges, a force of repulsion is generated causing them stay away from each other. The reason behind the agglomeration, which in turn increases particles size, is perhaps associated with the electric charge of the particles as well as the pH of the aqueous solution during synthesis procedure. Without strong electrostatic repulsion, some nanoparticles tend to aggregate. Many nanoparticles exhibit an effective charge change in aqueous conditions, from positive (at low pH) to negative (at high pH,) with an isoelectric point in between. In essence, higher pH is required for the prevention of the nanoparticle agglomeration because at pH level around 7-8, nanoparticles have lower isoelectric point that renders overall particle charge negative, and thus help the avoidance of agglomeration/aggregation [163]. During the experiment, a few drops of NaOH was added into the extract, metal salt precursor, and dopant mixture to control the pH of the solution in the range 7 to 8. However, due to the lack of a pH meter in the laboratory, the exact value of the pH of the solution could not be determined. So, it was very difficult to maintain the pH in the desired the range. As a result, agglomeration of the particles was observed.

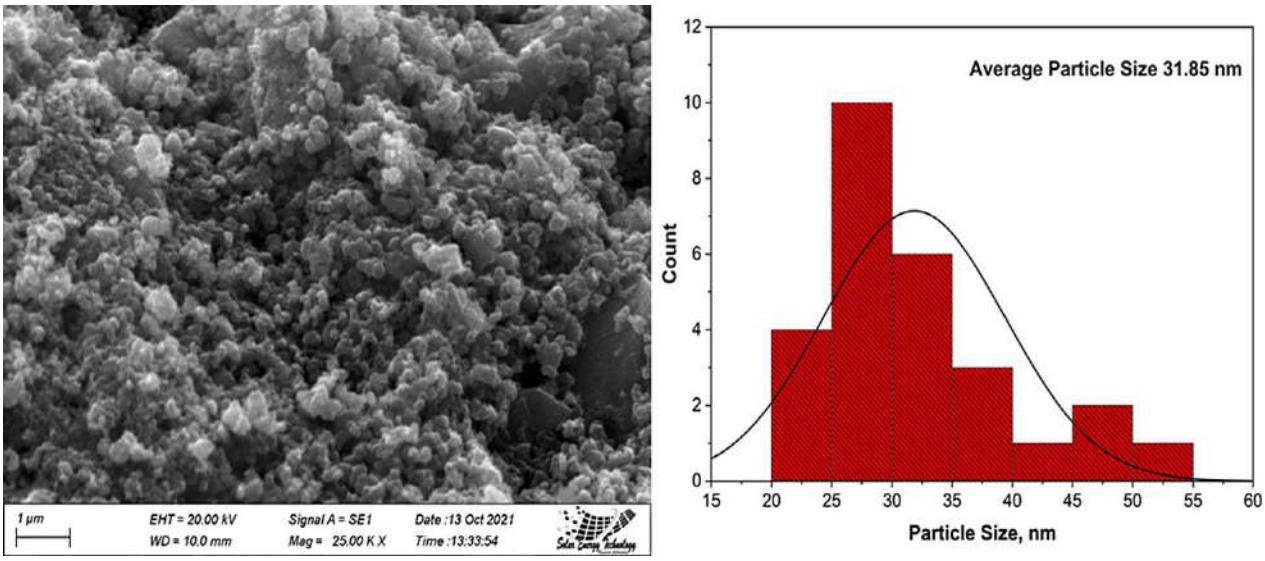

Figure 4.5: (a) SEM micrograph of undoped TiO_2, (b) Particle size distribution of undoped TiO_2.

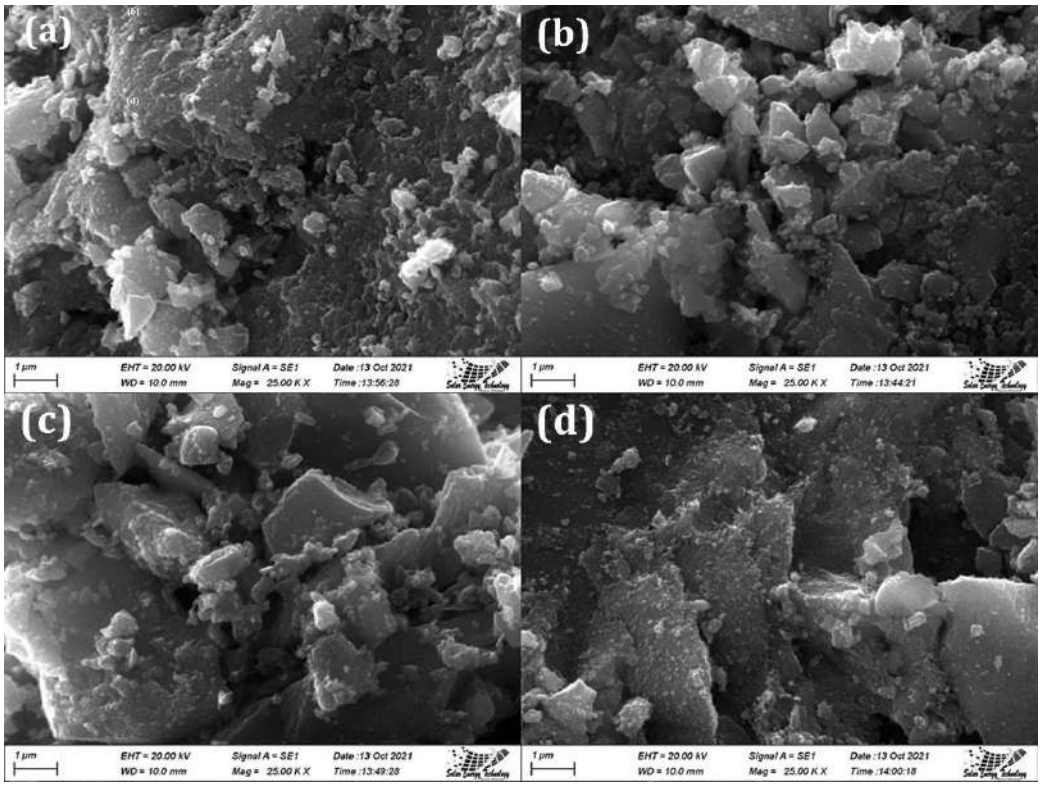

Figure 4.6: SEM micrograph of (a) 0.5%, (b) 1%, (c) 1.5%, and (d) 2% Cu doped TiO_2.

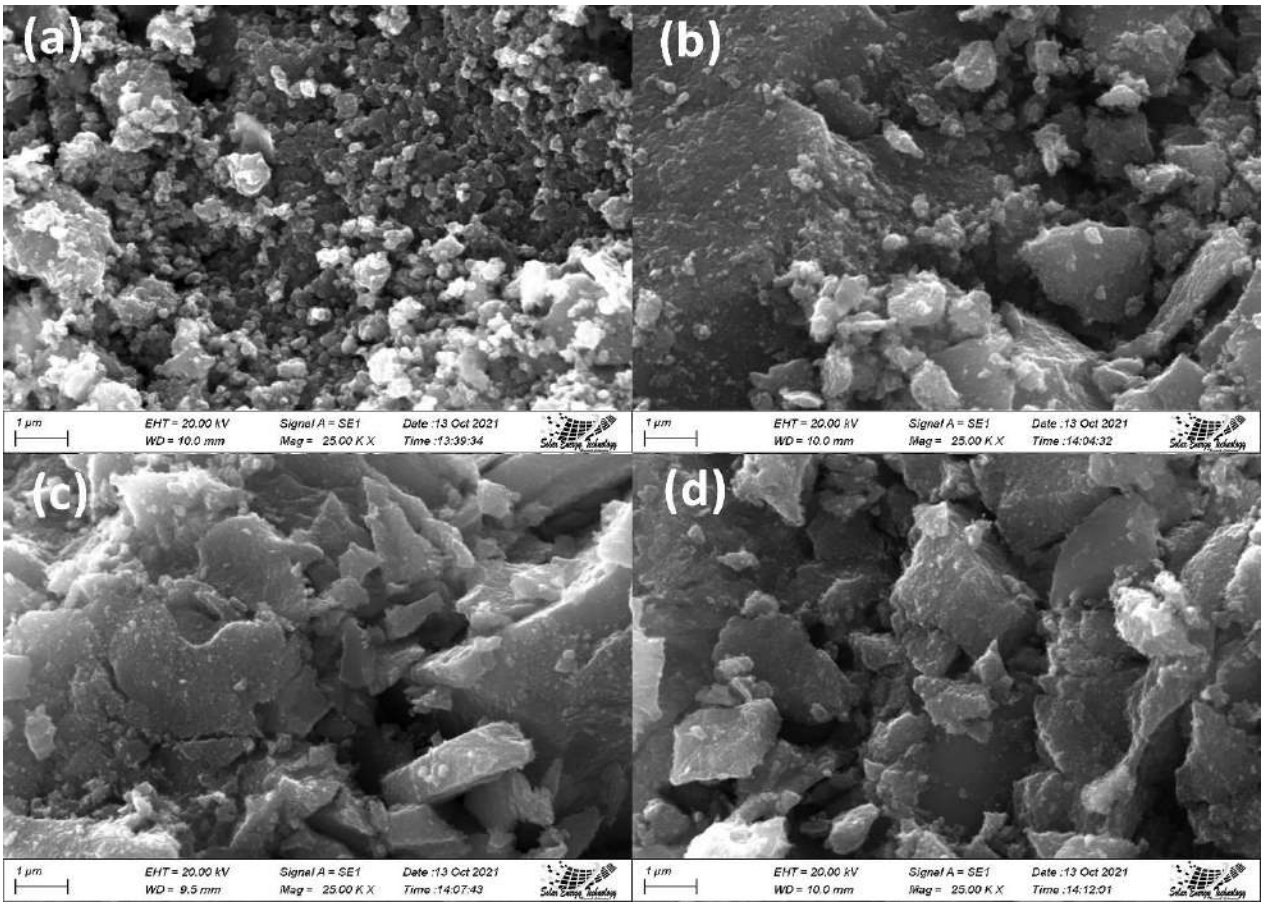

Figure 4.7: SEM micrograph of (a) 0.5%, (b) 1%, (c) 1.5%, and (d) 2% Ag doped TiO_2.

Table 4.2: Particle size of undoped, Cu doped and Ag doped TiO_2 samples.

Sample	**Particle Size, nm**
Undoped TiO_2	31.85
0.5% Cu doped TiO_2	49.06
1% Cu doped TiO_2	69.61
1.5% Cu doped TiO_2	81.36
2% Cu doped TiO_2	97.14
0.5% Ag doped TiO_2	44.76
1% Ag doped TiO_2	61.62
1.5% Ag doped TiO_2	79.25
2% Ag doped TiO_2	93.16

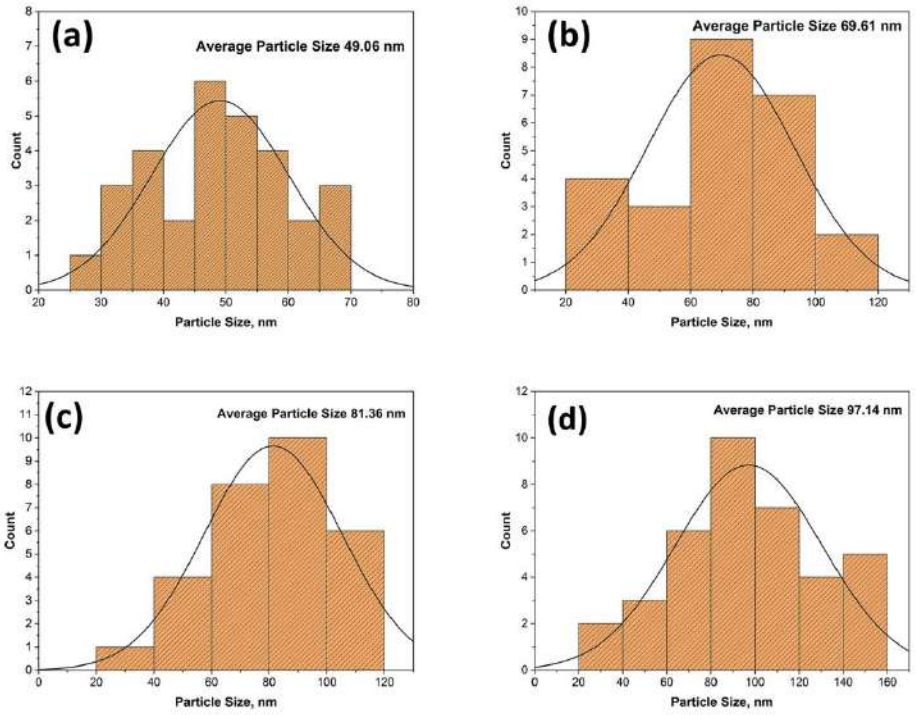

Figure 4.8: Particle distribution histogram of Cu doped TiO_2.

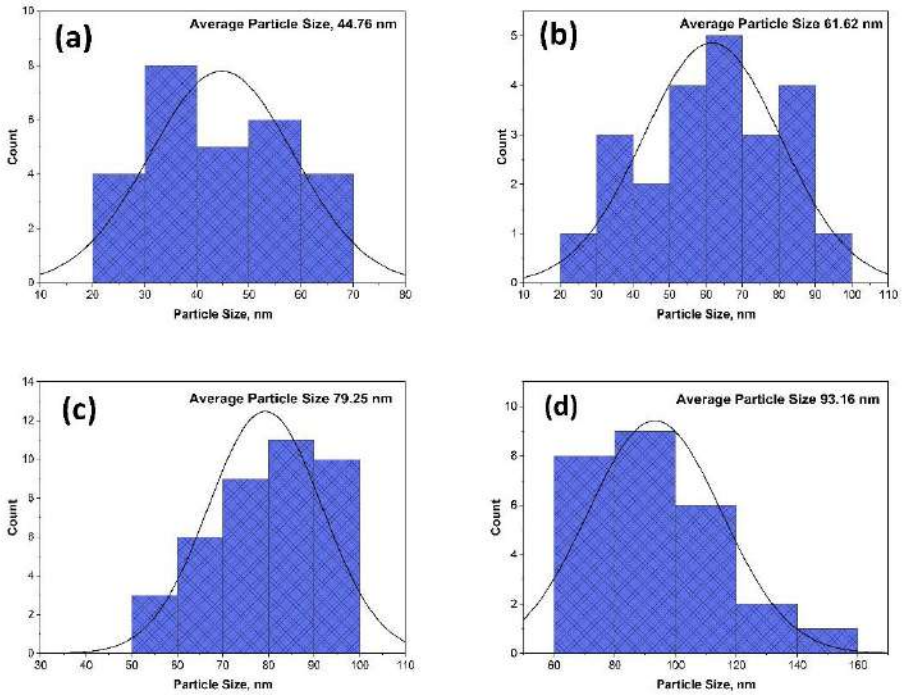

Figure 4.9: Particle distribution histogram of Ag doped TiO_2.

4.2.2 EDX Analysis

The energy dispersive X-ray spectroscopy (EDX) was utilized to determine the elemental composition of the prepared undoped and doped TiO_2 nanoparticles that provides information on how much percentage in the nanoparticles is occupied by every element. The figure 4.10 shows the EDX spectra of the undoped TiO_2 which confirms the presence of pure titanium dioxide nanoparticle due to the emergence of titanium and oxygen peaks from the sample. For the doped TiO_2 samples (both Cu doped and Ag doped), XRD result could not evidently confirm Cu and Ag in the doped products. However, EDX images, figure 4.11, confirmed the presence of dopants (Cu and Ag) in the TiO_2 lattice. The EDX analysis of the doped samples reveal the presence of Cu and Ag along with primary constituents Ti and O. The presence of distinct signals from these elements indicates that both Cu and Ag have been effectively incorporated into the TiO_2 host structure. Moreover, the EDX spectra of both undoped and doped samples showed no other additional peaks confirming the absence of impurity. This observation was in good agreement with XRD results, which confirmed the phase purity of undoped and doped TiO_2 nanoparticles.

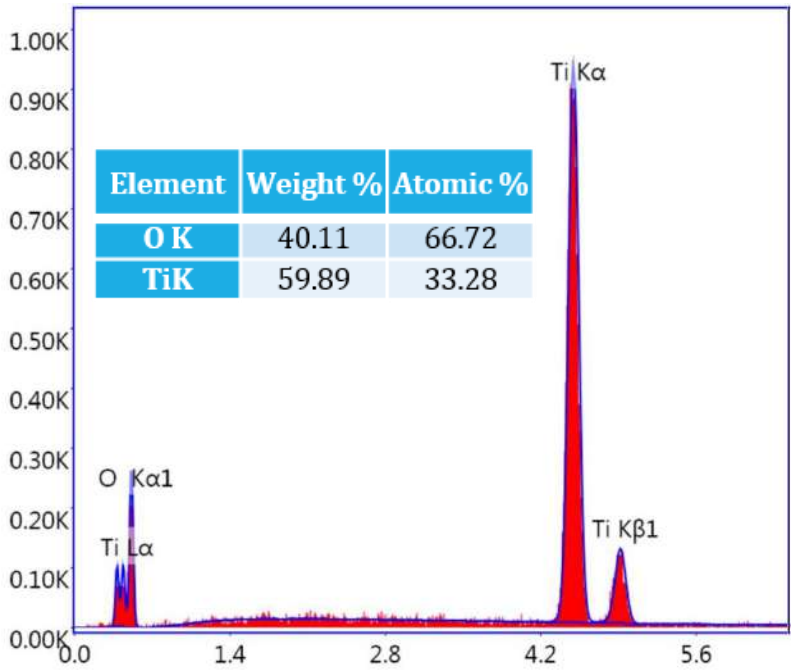

Figure 4.10: EDX spectra of undoped TiO_2.

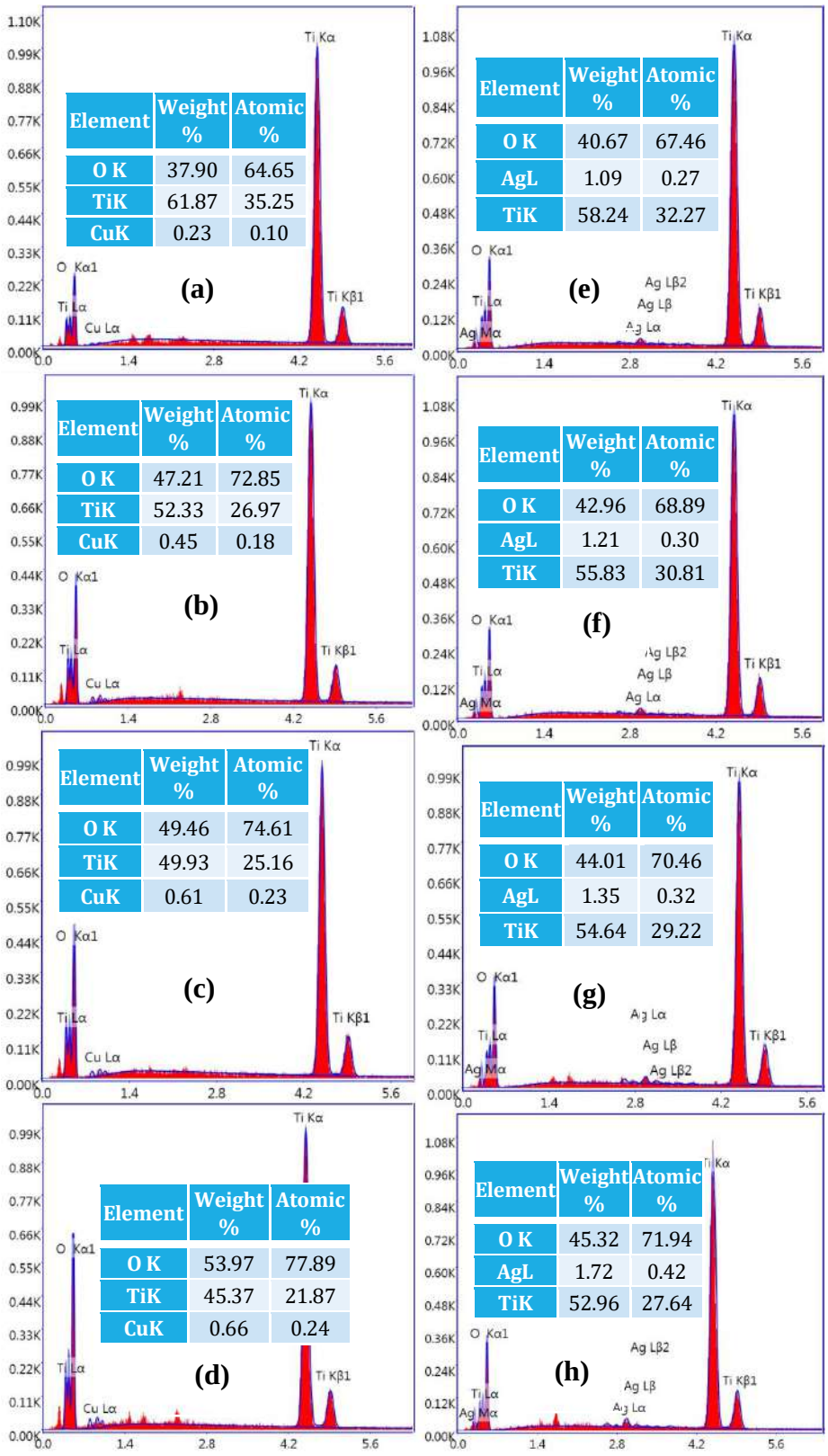

Figure 4.11: EDX spectra of (a) 0.5%, (b) 1%, (c) 1.5%, (d) 2% Cu doped TiO_2; (e) 0.5%, (f) 1%, (g) 1.5%, (h) 2% Ag doped TiO_2.

4.3 UV-Vis Analysis

For the determination of nanoparticle band gap (both undoped and doped) as well as the photocatalytic performance evaluation, UV-Vis analysis was performed.

4.3.1 Effect of Cu and Ag Doping on the Band Gap Energy of TiO_2

The UV-Vis spectroscopy was employed to determine the band gap of the prepared samples as well as to study the effect of Cu and Ag doping on TiO_2 lattice. The UV-Vis absorbance spectra of pure TiO_2 along with different amount of dopant concentration (0.5%, 1%, 1.5%, and 2%) of Cu and Ag is show in the figure 4.12. For the undoped TiO_2, there was no absorption in the visible light region rather it showed typical anatase absorbance in the UV region. However, doping TiO_2 with both Cu and Ag showed a "Red-Shift" of the absorbance spectra to the visible region [71][113]. The doped samples have better light harvesting performance, as evidenced by not only a wider UV absorbance peak, but also an increase in light absorbance across the entire visible spectrum [164]. When the doping concentration was increased from 0.5% to 2%, the visible light absorption ability of the Cu- and Ag- doped TiO_2 also increased as indicated in the figure 4.12.

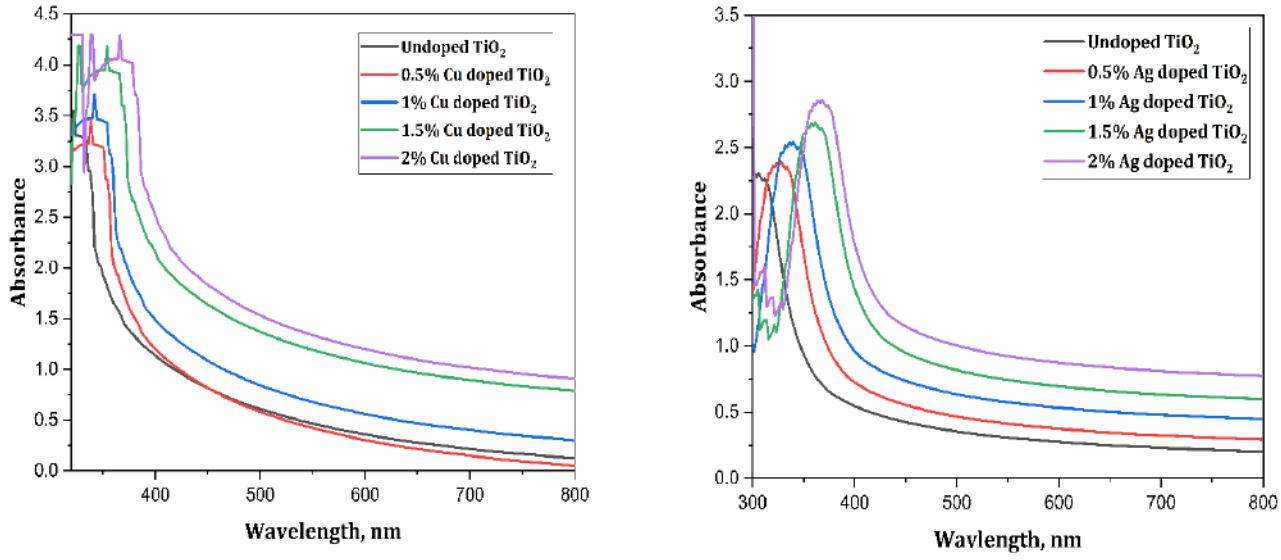

Figure 4.12: UV-vis absorbance spectra of undoped and doped TiO_2 nanoparticles.

Additionally, due to this red shift phenomena, a decrease of the band gap energy has been observed for all the doped samples whether doped with Cu or Ag as shown by the figure 4.13. Compared

to the band gap of undoped TiO_2 (3.50 eV), Cu doped TiO_2 showed band gap of 3.05 eV whereas, Ag doped TiO_2 exhibited band gap of 2.91 eV for maximum amount of doping concentration. The introduction of Cu and Ag dopants in the mother lattice causes the formation of localized energy levels in between the VB and CB of TiO_2 NPs which in turn causes the reduction of the band gap [71]. Band gap energies were evaluated by using Tauc equation:

$$\alpha h\nu = A(h\nu - E_g)^2$$

where a is absorption coefficient, h denotes Planck's constant, ν is photon frequency and A is proportionality constant/absorption index.

The decrease of the band gap energy with increasing doping percentage is well corroborated by various studies [165][166]. Doping with a transition metal like Cu or Ag can create new electronic phases in the actual band gap, implying that e^- is activated by a defect state of TiO_2 conduction band with lower photon energy [166]. Cu^{2+} and Ag^+ ions intercalated between host lattices of TiO_2 and formed oxygen vacancies due to charge compensation effect, resulting in a decrease in band gap energy as Cu and Ag concentration increased [113]. Additionally, Cu and Ag provide numerous additional doping sites near the valance band of TiO_2 and so enriches the visible absorption spectrum by Cu 3d – Ti 3d and Ag 3d – Ti 3d optical transition, respectively, lowering the band gap energies [113]. Table 4.3 summarizes the band gap energy of the prepared samples.

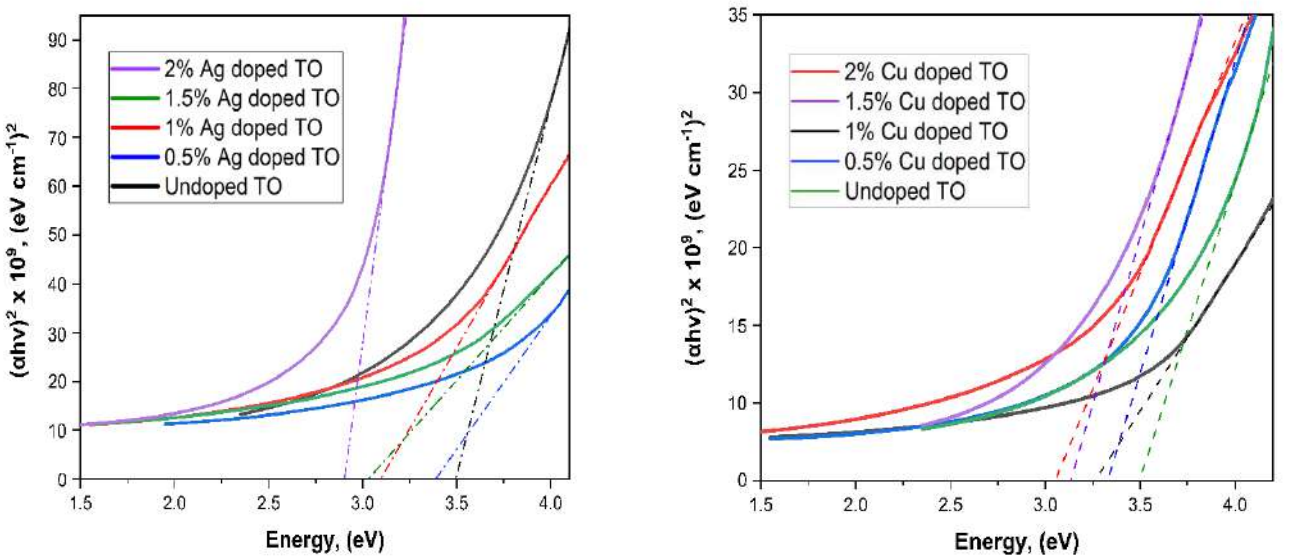

Figure 4.13: Band gap energy of undoped, Cu doped and Ag doped TiO_2 nanoparticles.

Table 4.3: Band gap energy of undoped and doped TiO_2 nanoparticles.

Sample	Bandgap Energy (E_g), eV
Undoped TiO_2	3.50
0.5% Cu doped TiO_2	3.32
1% Cu doped TiO_2	3.26
1.5% Cu doped TiO_2	3.13
2% Cu doped TiO_2	3.05
0.5% Ag doped TiO_2	3.39
1% Ag doped TiO_2	3.10
1.5% Ag doped TiO_2	3.02
2% Ag doped TiO_2	2.91

4.3.2 Photocatalytic Performance Evaluation

According to literature, the red shift phenomena along with the reduction of band gap due to doping enhances the activity of photo-catalyst [71]. The photocatalytic activity of the undoped and doped TiO_2 NPs was measured against methylene blue (MB) solution under UV light irradiation. Figure 4.14 shows the absorption spectra of MB solution that shows characteristics absorption peaks at 664 nm and 614 nm. The peak at 664 nm was used for observing the photo degradation procedure.

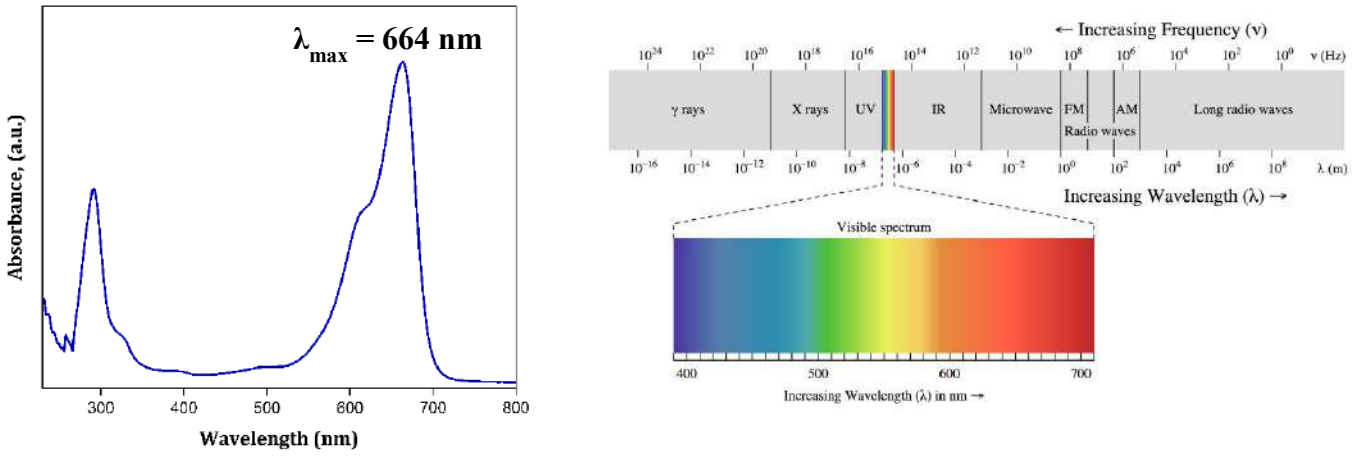

Figure 4.14: Absorbance spectra of MB solution and electromagnetic spectrum.

The figure 4.15 shows the absorbance spectra of MB solution at different time intervals under UV illumination for untreated TiO_2 NPs. Evidently, the strong peak of MB solution at 664 nm reduced gradually with UV radiation with the progress of time. Pristine TiO_2 exhibited 26% degradation after 90 minutes.

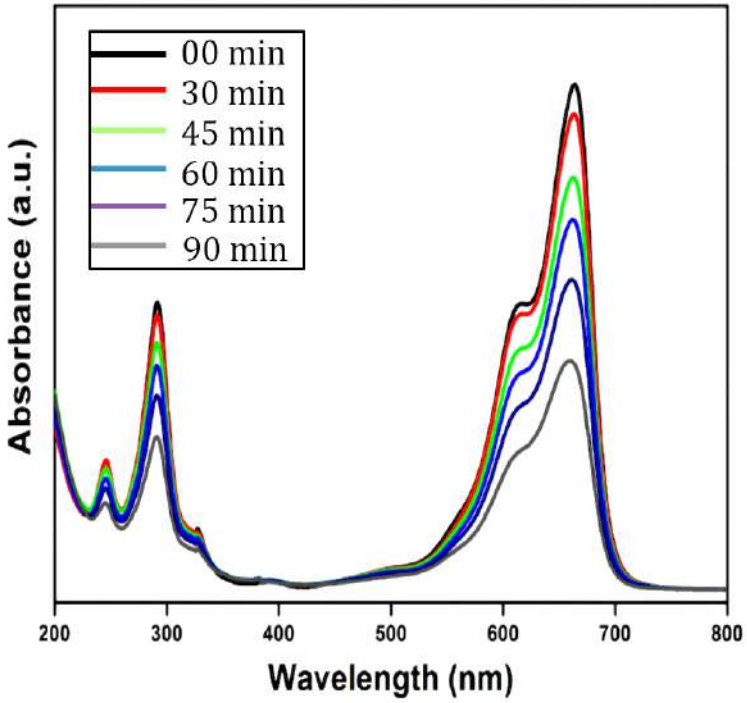

Figure 4.15: Variation of the absorbance spectra of MB solution in presence of undoped TiO_2 under UV illumination at specific time intervals.

However, better MB degradation efficiency was observed for both Cu- and Ag-doped TiO_2 nanoparticles. With the increase of doping percentage (from 0.5% to 2%), Cu-doped TiO_2 showed immense increase in the photocatalytic efficiency from 37.3% to 74.4%, respectively. Similar trend was found for Ag-doped TiO_2. Photocatalytic efficiency increased from 68.3% to 85.9% for the increase of doping percentage from 0.5% to 2%. It is evident that, compared to Cu-doped TiO_2 samples, Ag-doped ones exhibited better photocatalytic performance in terms of efficiency. The reason behind it might be the lower band gap energies [113][167] as well as the crystallites size [168] of the Ag-doped TiO_2 samples in comparison to Cu-doped TiO_2 samples. Figure 4.16 and figure 4.17 show the change of the absorbance spectra for Cu-doped and Ag-doped TiO_2 at various

time intervals. On the other hand, figure 4.18 and figure 4.19 shows the schematic representation of photo-degradation efficiency of Cu-doped and Ag-doped TiO_2 in terms of C/C_o plotted against time.

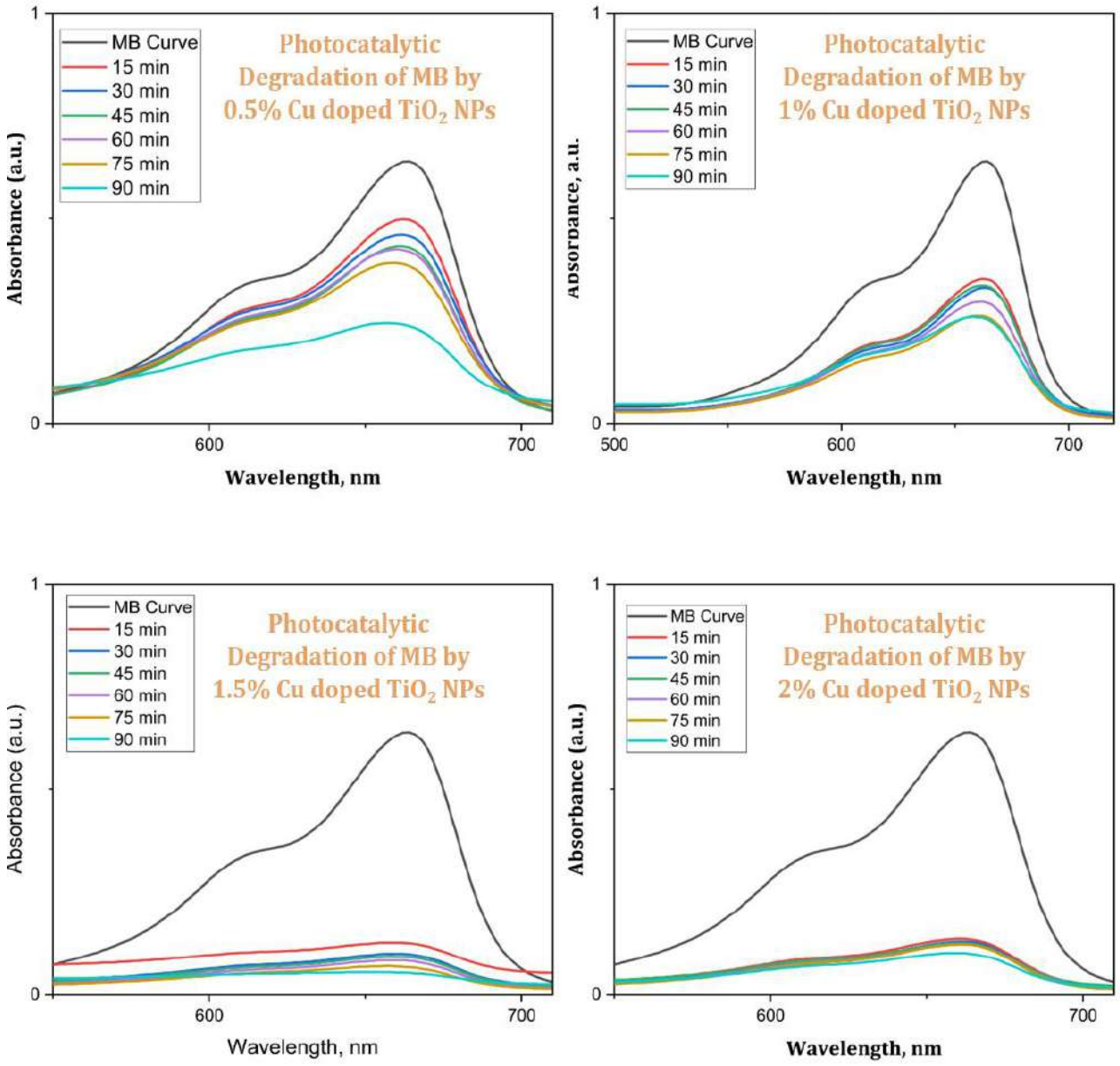

Figure 4.16: Variation of the absorbance spectra of MB solution in presence of 0.5%, 1%, 1.5%, and 2% Cu-doped TiO_2 under UV illumination at specific time intervals.

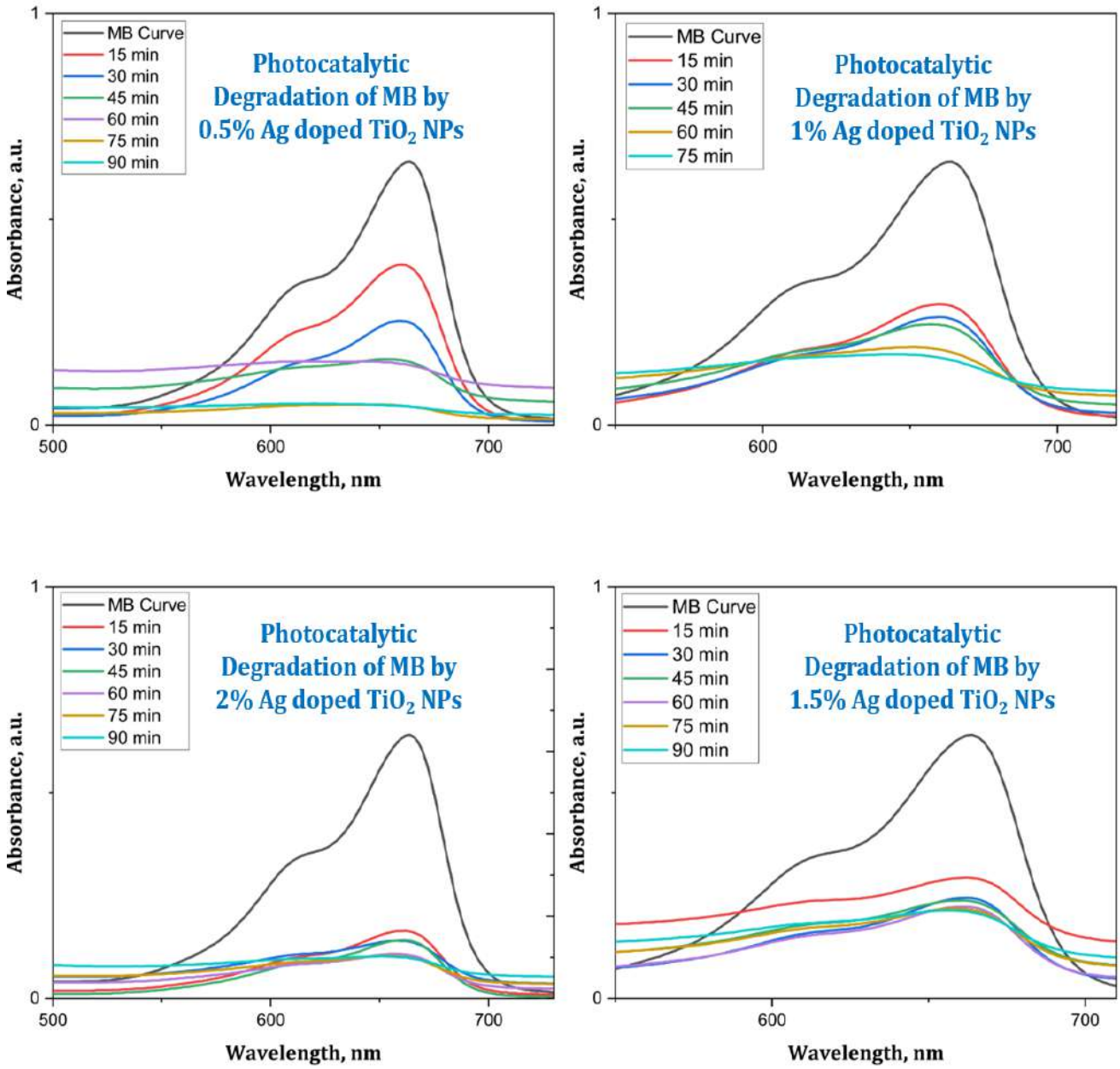

Figure 4.17: Variation of the absorbance spectra of MB solution in presence of 0.5%, 1%, 1.5%, and 2% Ag-doped TiO_2 under UV illumination at specific time intervals.

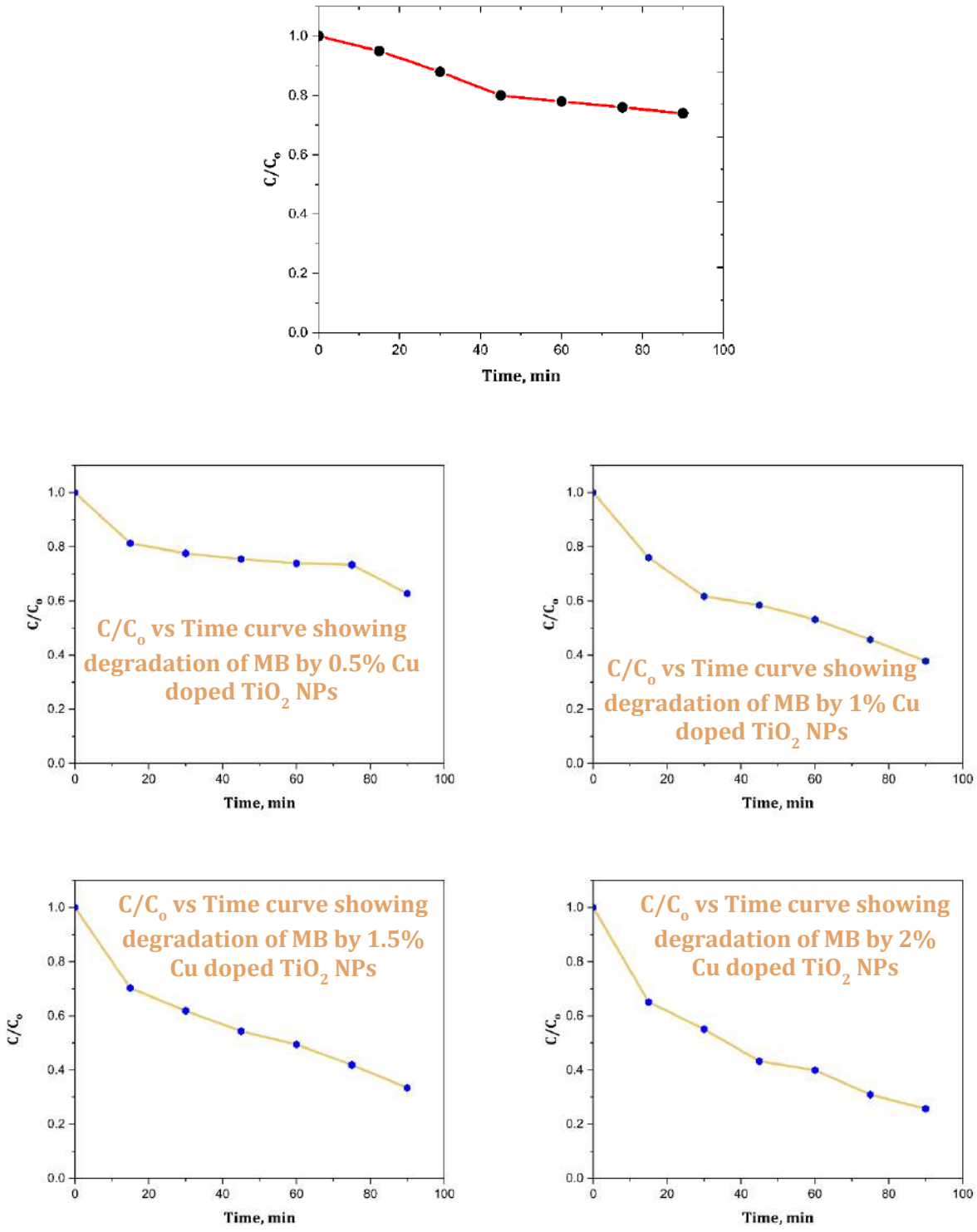

Figure 4.18: Photodegradation of MB solution under UV irradiation using Cu-doped TiO_2 with different Cu contents and undoped TiO_2 as catalysts.

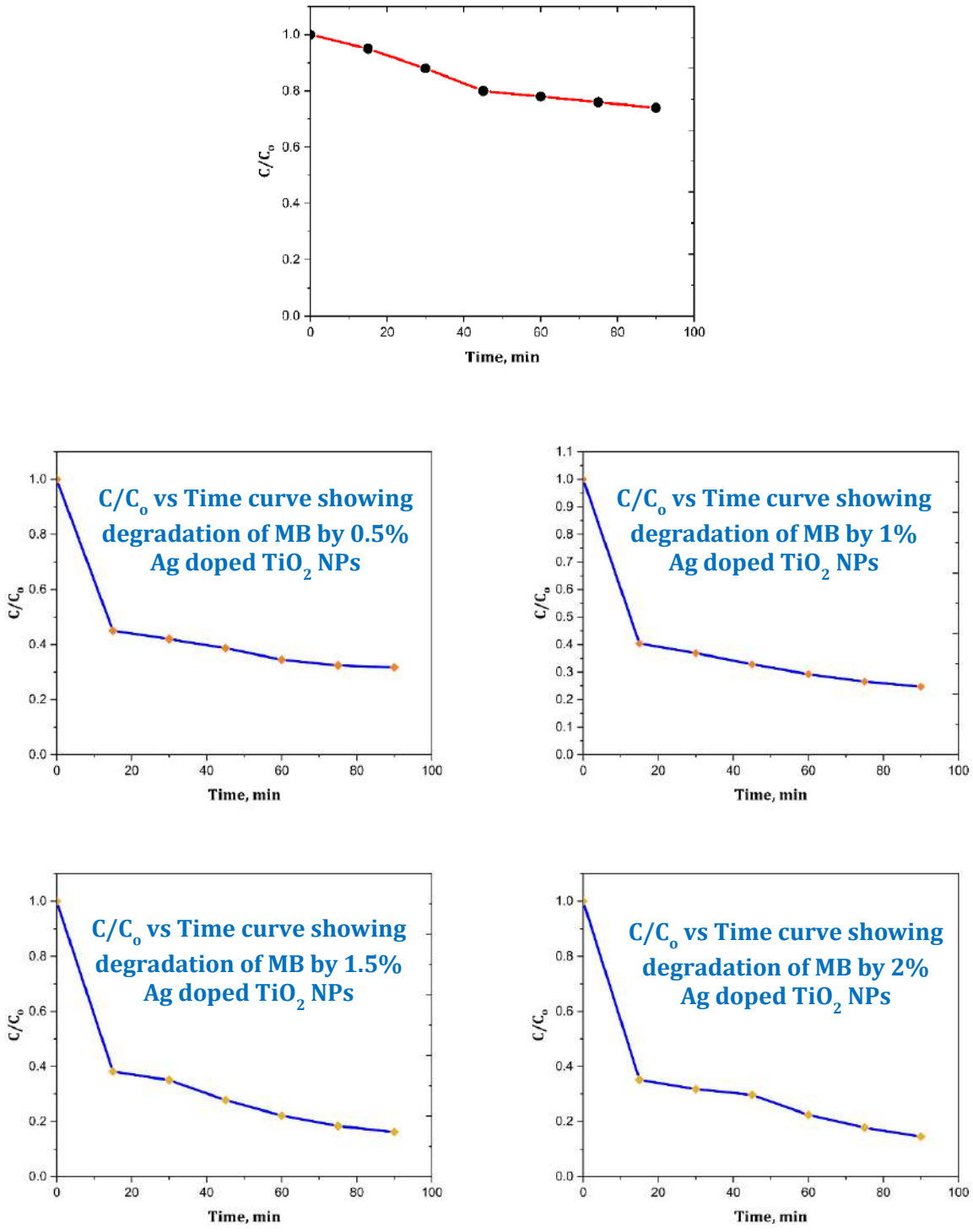

Figure 4.19: Photodegradation of MB solution under UV irradiation using Ag-doped TiO_2 with different Ag contents and undoped TiO_2 as catalysts.

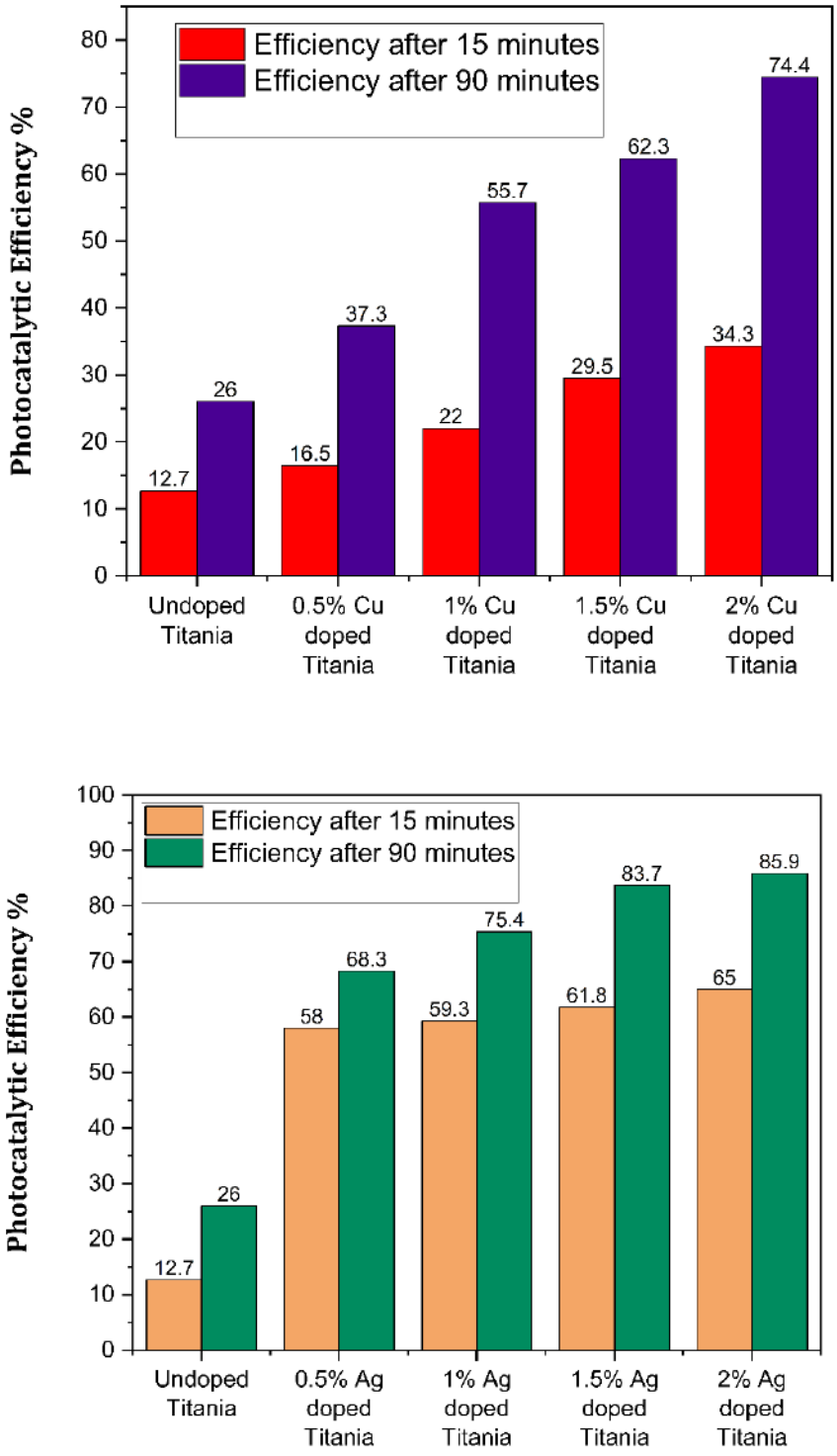

Figure 4.20: Comparison of photocatalytic efficiency of undoped, Cu doped and Ag doped TiO_2 nanoparticles.

The figure 4.20 demonstrates the photocatalytic efficiency comparison among the undoped, Cu-doped, and Ag-doped samples. It is obvious that both Cu-doped and Ag-doped TiO_2 nanoparticles showed better photocatalytic performance compared to undoped TiO_2. Moreover, better efficiency is obtained for Ag-doped TiO_2 in comparison to Cu-doped TiO_2. 15 minutes after equilibrium, 0.5% Ag-doped sample showed 58% efficiency whereas 0.5% Cu-doped sample exhibited only 16.5% efficacy. The reading taken after 90 minutes from equilibrium, showed almost similar scenario. Compared to the 68.3% efficiency of Ag-doped samples, the Cu-doped ones showed efficiency value of almost half of it. Identical trend followed for rest of the Cu- and Ag-doped samples (1%, 1.5%, 2%). The maximum efficiency obtained from 2% Ag-doped TiO_2 which is 85.9%, whereas for 2% Cu-doped TiO_2 it was 74.4%. The higher and better photocatalytic efficiency of Ag-doped samples compared to their Cu-doped counterparts can be attributed to the lower band gap energy of the Ag-doped samples. Table 4.4 summarizes the C/C_o value along with their respective photocatalytic efficiency after 15 and 90 minutes from the equilibrium for undoped, Cu-doped, and Ag-doped TiO_2 samples.

The following factors contribute to the improved photocatalytic activity of Cu- and Ag-doped TiO_2. First of all, the Cu- and Ag-doped TiO_2 absorbance spectra show increased light harvesting in both UV and visible light areas, allowing substantially more light energy to be used for photocatalysis. Secondly, because Cu and Ag species have a smaller band gap and a greater work function than bare TiO_2, electrons can move from TiO_2's conduction band to the metallic copper ion. This causes a Schottky barrier to form in the metal-semiconductor contact region, facilitating charge separation and hence improving TiO_2's photocatalytic activity. Moreover, the inducing impurity energy level due to doping by Ag and Cu also plays an important role in the effective separation of photo-induced electron−hole pair. Doping of Ag and Cu causes formation of oxygen vacancies since the valence of Ti^{4+} is greater than both Ag^{+} and Cu^{2+}. They act as active sites for water dissociation on the surface of TiO_2, and can also capture the holes to restrain the recombination of electron – hole pairs, thus improving photocatalytic efficiency [164]. However, there is a certain limit of doping after which efficiency starts to degrade. The excess amount of dopant buildup covers a portion of the photocatalyst surface, reducing the number of surface active sites and lowering photocatalytic activity.

A mechanism for the increased photocatalysis of Cu- and Ag-doped TiO_2 nanoparticles may be hypothesized by combining the results of this thesis work with the existing literature. When Cu- and Ag-doped TiO_2 was irradiated under UV light, electrons transferred from VB to CB of induced Cu/Ag particles, creating electron–hole pairs. MB solution was photo-sensitized when CB electron from Ag/Cu migrated to CB of doped titania. Subsequent to this, oxygen molecules (O_2) were reduced by migrated electrons into active oxygen radicals O_2*. At the same time, VB of Ag/Cu particles reacted with water molecules (H_2O) to produce hydroxyl radicals (OH*). Finally, produced radicals (O_2* and OH*) attacked MB* molecules. Consequently, decomposition of the molecules of dye occurred along with the formation of byproducts. Thus, the separation of the charge carriers was attributed to such trapping by Ag and Cu dopant in TiO_2 nanoparticles. As a result of the doping, the photoactivity of photocatalysts was significantly increased [156]. These findings suggest that Cu-doped as well as Ag-doped TiO_2 has a high potential for usage in polluted water purification and dye remediation. The photodegradation mechanism of MB solution by Cu- and Ag-doped TiO_2 nanoparticles can be explain with the help of following equations.

$$MB + h\nu \rightarrow MB^*$$

$$MB^* + \text{doped } TiO_2 \rightarrow MB + \cdot + \text{doped } TiO_2\,(e)$$

$$\text{Doped } TiO_2\ (e) + O_2 \rightarrow O_2^{-*}$$

$$O_2^{-*} + H^+ \leftrightarrow HO_2^*$$

$$HO_2^* + HO_2^* \rightarrow O_2 + H_2O$$

$$e^- + 2H^+ + O_2^{-*} \rightarrow H_2O_2$$

$$e^- + H_2O_2 \rightarrow OH^- + OH^*$$

$$MB^{+*} + O_2\left(O_2^{-*} \text{ or } OH^*\right) \rightarrow CO_2 + H_2O + \text{other products}$$

Table 4.4: Photocatalytic efficiency of the prepared undoped and doped TiO_2 nanoparticles.

Sample	**C/C_o after 15 min**	**C/C_o after 90 min**	**Efficiency after 15 min, $[1-(C/C_o)]*100\%$**	**Efficiency after 90 min, $[1-(C/C_o)]*100\%$**
Undoped TiO_2	0.873	0.74	12.7	26
0.5% Ag doped TiO_2	0.42	0.317	58	68.3
1% Ag doped TiO_2	0.407	0.246	59.3	75.4
1.5% Ag doped TiO_2	0.382	0.163	61.8	83.7
2% Ag doped TiO_2	0.35	0.141	65	85.9
0.5% Cu doped TiO_2	0.835	0.627	16.5	37.3
1% Cu doped TiO_2	0.78	0.443	22	55.7
1.5% Cu doped TiO_2	0.705	0.377	29.5	62.3
2% Cu doped TiO_2	0.657	0.256	34.3	74.4

4.4 **Antibacterial Analysis**

Antibacterial activity of the prepared undoped as well as Cu- and Ag-doped doped TiO_2 was investigated on both Gram positive and Gram negative bacteria strain using Kirby-Bauer disk diffusion method. Among the bacterial strain there were Staphylococcus aureus (Gram +ve), Bacillus subtilis (Gram +ve), Escherichia coli (Gram -ve), and Klebsiella pneumonia (Gram -ve). The zone of inhibition, measure in mm, was utilized to determine the antibacterial efficiency of the prepared undoped and doped TiO_2 nanoparticles. From the figure 4.20 and figure 4.21, it is evident that sample concentration, whether doped or undoped, has significant influence on the antibacterial performance of the nanoparticles. When sample concentration was minute in amount (0.1 mg/mL), none of the nanoparticles (undoped and doped) showed any kind of antibacterial activity. This was true for both Gram positive as well as Gram negative bacteria strain. However, as sample concentration on the antibiotic disk was increase to 2mg/mL, some of the nanoparticles showed zone of inhibition. Whether it was Cu- or Ag-doped TiO_2, doping percentage of 0.5 and 1 did not show any inhibition zone for Staphylococcus aureus (Gram +ve) and Escherichia coli (Gram -ve). However, with increasing percentage of doping (from 1.5% to 2%), both Cu- and Ag-doped TiO_2 showed narrow inhibition zone. Zone of inhibition for 1.5% Cu-doped TiO_2 was 3.1 mm and 3.6 mm for Staphylococcus aureus (Gram +ve) and Escherichia coli (Gram -ve), respectively. While for 2% Cu-doped TiO_2, the zone of inhibition was 4.2 mm and 4.5 mm for the same bacteria strain stated above. Similar trend was found for Ag-doped TiO_2 samples. 1.5% Ag-doped TiO_2 showed lower zone of inhibition compared to 2% Ag-doped TiO_2 for Staphylococcus aureus (Gram +ve) and Escherichia coli (Gram -ve), respectively. Another important feature, that is evident from the result is that, the zone of inhibition was much larger for Gram-positive bacteria strain compared to Gram-negative bacteria. As a result, it can be concluded that for synthesized undoped and Cu- as well as Ag-doped TiO_2, Gram-negative bacteria showed more resistant than their Gram-positive counterparts. The increased antibacterial activity of the samples is linked to the release metal ions producing an excessive amount of ROS. These ROS cause oxidative damage to numerous biological components, culminating in cell death [169]. Thus, the findings of this thesis work verified the efficacy of undoped TiO_2, Cu-doped TiO_2, and Ag-doped TiO_2 as bactericidal agent against both Gram-positive and Gram-negative bacterial.

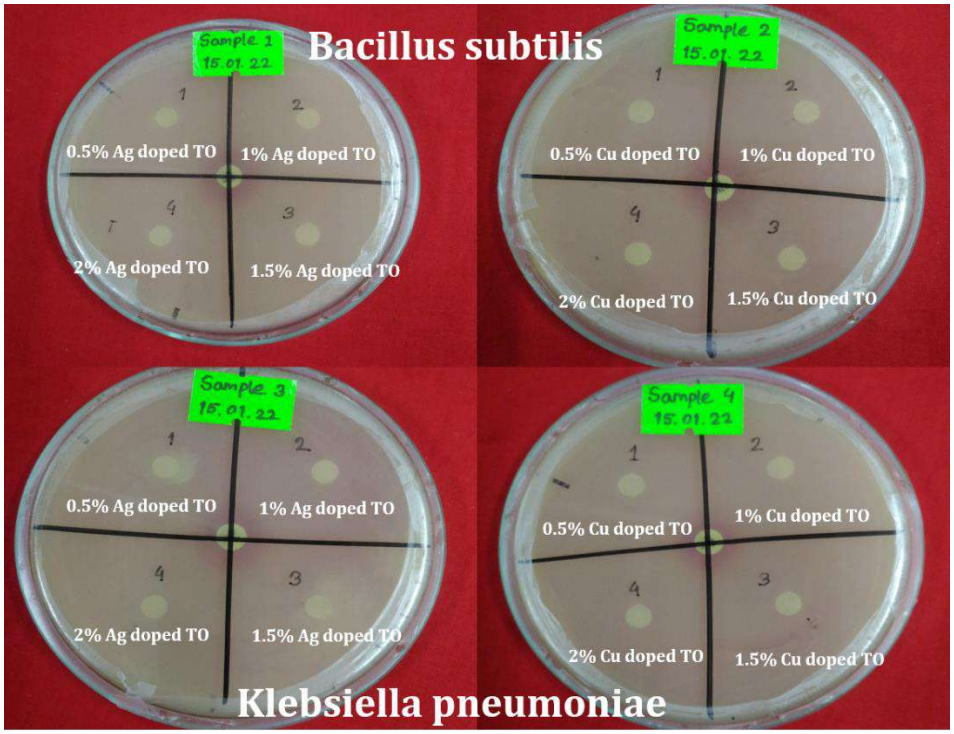

Figure 4.21: Antibacterial activity of undoped TiO_2, Cu-doped TiO_2, and Ag-doped TiO_2 NPs against Bacillus subtilis and Klebsiella pneumonia

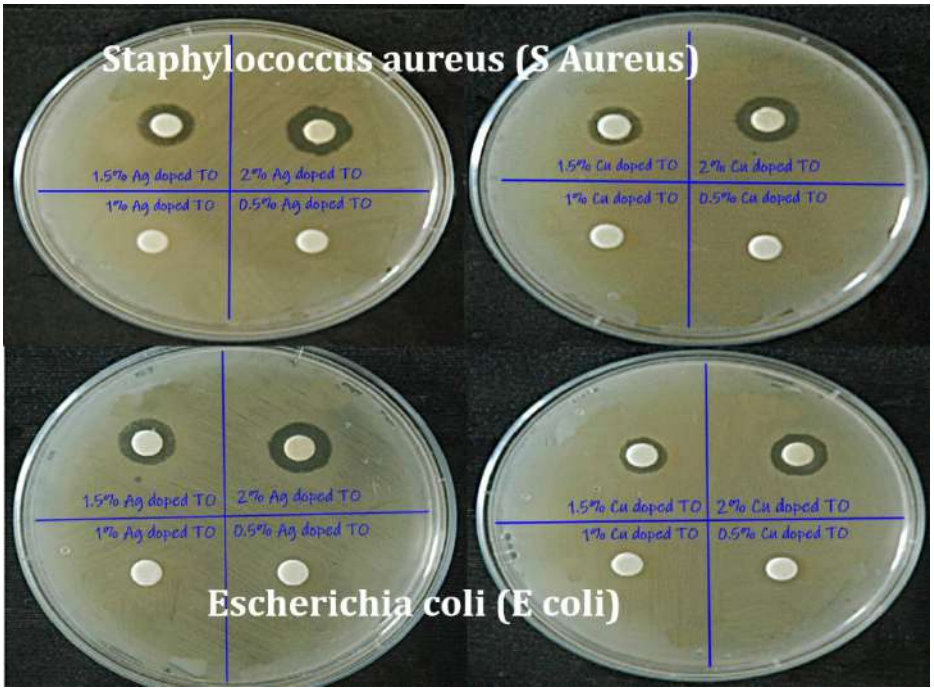

Figure 4.22: Antibacterial activity of undoped TiO_2, Cu-doped TiO_2, and Ag-doped TiO_2 NPs against Staphylococcus aureus and Escherichia coli.

Table 4.5: Zone of inhibition for different bacterial strain against undoped and doped TiO_2 samples.

Sample \ Bacteria Strain	**Zone of Inhibition, mm**			
	E. coli (Gram -ve)	**S aureus (Gram +ve)**	**K pneumoniae (Gram -ve)**	**B subtilis (Gram +ve)**
	Sample Concentration = 2 mg/mL		*Sample Concentration = 0.1 mg/mL*	
0.5% Ag doped TiO_2	0	0	0	0
1% Ag doped TiO_2	0	0	0	0
1.5% Ag doped TiO_2	4.2	4.4	0	0
2% Ag doped TiO_2	5.3	5.6	0	0
0.5% Cu doped TiO_2	0	0	0	0
1% Cu doped TiO_2	0	0	0	0
1.5% Cu doped TiO_2	3.1	3.6	0	0
2% Cu doped TiO_2	4.2	4.5	0	0

4.5 Comparison with Other Reported Studies

In this section a comparison has been done among the present thesis work and other reported studies. Table 4.6 summarizes the comparison of the undoped and Cu/Ag doped TiO_2 samples with other studies on the basis of synthesis route, crystallite size, photocatalytic efficacy, band gap energy, and antibacterial inhibition zone.

Table 4.6: A comparative study between this work and reported literature.

Sample	**Synthesis Route**	**Crystallite size, nm**	**Photocatalytic efficiency, %**	**Band gap energy, eV**	**Antibacterial Inhibition Zone, mm**		**Ref.**
					Gram +ve	**Gram -ve**	
TiO_2	Biogenic (Mango Leaf)	10.74	26	3.50	0	0	This Study
2% Ag doped TiO_2		9.25	85.9	2.91	5.6	5.3	
2% Cu doped TiO_2		10.63	74.4	3.05	4.5	4.2	
TiO_2	Biogenic (Cinnamon Powder)	70.1	-	3.20	-	-	[155]
TiO_2	Biogenic (Phyllanthus niruri)	32	-	3.16	-	-	[15]
2% Ag doped TiO_2	Sol-gel	12.20	80	2.90	-	18.7	[114]

Sample	Synthesis Route	Crystallite size, nm	Photocatalytic efficiency, %	Band gap energy, eV	Antibacterial Inhibition Zone, mm		Ref.
					Gram +ve	Gram -ve	
3% Cu doped TiO_2	Sol-gel	20.09	75	2.8	2.75	0	[113]
TiO_2	Biogenic (Acacia catechu)	25	80	-	-	-	[18]
TiO_2	Biogenic (Turmeric)	9.5	-	-	26	20	[19]
	Biogenic (Ginger)	10.5	-	-	22	18	
Ag/TiO_2	Biogenic	3	90	-	-	12	[167]
Gd doped TiO_2	Biogenic (Betel Leaf)	5.45	-	-	10	10	[170]
2% Ga doped TiO_2	Biogenic (Coffee Husk)	10	88	3.17	-	-	[153]
Ag-Cu co-doped TiO_2	Sol-gel	14	96	-	-	-	[171]
Sr-Ag co-doped TiO_2	Sol-gel	11	85	2.62	-	-	[172]

CHAPTER 5: CONCLUSION

The primary focus of this thesis was to biogenic synthesis of undoped as well as Ag and Cu doped TiO_2 nanoparticles utilizing mango leaf extract to study their morphology, structures, photocatalytic activity, and antibacterial performance. Although some limitations were faced, the principle goals of the investigation have been largely achieved. In summary, this research revealed the following concluding remarks:

I. This study reports the first example of a novel biogenic route by successful incorporation of mango leaf extract for the synthesis of undoped TiO_2 nanoparticles as well as Ag and Cu doped TiO_2 nanoparticles.

II. For all undoped and doped TiO_2 samples, XRD pattern ensured the absence of impurity phases such as Ag, Cu, or their oxides even at highest doping percentage. Thus, it is confirmed that anatase phase is not disturbed upon doping.

III. Undoped TiO_2 exhibited spherical shaped particles whereas both Ag doped and Cu doped samples showed agglomerated particles perhaps due to the lack of pH control.

IV. Large reduction in bandgap is observed for both Ag and Cu doped TiO_2 samples than their unmodified counterparts which enables them to be utilized in photocatalysis applications.

V. Compared to undoped TiO_2, both the Ag doped and Cu doped samples showed substantial increase in the photo-catalytic degradation efficiency ranging from almost 26% to almost 90%. However, Ag doped TiO_2 exhibited better photo-degradation efficiency than their Cu doped counterparts.

VI. According to the result of bactericidal activity, for both Ag and Cu doped TiO_2 particles, lower concentration (on the antibacterial disk) shows zero inhibition zone. At higher concentration level, both 1.5% and 2% Ag as well as Cu doped particles showed mentionable inhibition zone. Moreover, Gram-negative bacteria showed more resistant than their Gram-positive counterparts.

CHAPTER 6: SUGESSTION FOR FUTURE WORKS

This study has opened many dimensions for future works. Some of them are listed below:

I. The effect of increasing percentage of mango leaf extract concentration on the structural and morphological change of the nanoparticles could be studied.

II. Synthesis of Ag-Cu co-doped TiO_2 nanoparticles should be done utilizing this biogenic route with strong focus on their crystal structure and photocatalytic activity.

III. Doping can be done on higher level to study photocatalytic and antibacterial activities as well as to find out the optimum level for maximum efficiency.

IV. TiO_2 nanoparticles with similar composition and structure like this study should be biogenically synthesized utilizing other f-block and d-block elements such as (Ce, Gd, La, Zn, Co, Ni, etc.) to find out and compare their properties with present study.

V. The effect of both undoped and doped TiO_2 nanoparticles on Gram – positive as well as Gram – negative bacteria requires further elaborate study to find out the exact bacterial incapacitating mechanism by those nanoparticles.

REFERENCES

[1] I. Hussain, N. B. Singh, A. Singh, H. Singh, and S. C. Singh, "Green synthesis of nanoparticles and its potential application," *Biotechnol. Lett.*, vol. 38, no. 4, pp. 545–560, 2016, doi: 10.1007/s10529-015-2026-7.

[2] H. Bar, D. K. Bhui, G. P. Sahoo, P. Sarkar, S. P. De, and A. Misra, "Green synthesis of silver nanoparticles using latex of Jatropha curcas," *Colloids Surfaces A Physicochem. Eng. Asp.*, vol. 339, no. 1, pp. 134–139, 2009, doi: https://doi.org/10.1016/j.colsurfa.2009.02.008.

[3] M. Devi, S. Devi, V. Sharma, N. Rana, R. K. Bhatia, and A. K. Bhatt, "Green synthesis of silver nanoparticles using methanolic fruit extract of Aegle marmelos and their antimicrobial potential against human bacterial pathogens," *J. Tradit. Complement. Med.*, vol. 10, no. 2, pp. 158–165, 2020, doi: https://doi.org/10.1016/j.jtcme.2019.04.007.

[4] J. R. Peralta-Videa *et al.*, "Plant-based green synthesis of metallic nanoparticles: scientific curiosity or a realistic alternative to chemical synthesis?," *Nanotechnol. Environ. Eng.*, vol. 1, no. 1, p. 4, 2016, doi: 10.1007/s41204-016-0004-5.

[5] F. De Gaetano, L. Ambrosio, M. G. Raucci, A. Marotta, and M. Catauro, "Sol-gel processing of drug delivery materials and release kinetics.," *J. Mater. Sci. Mater. Med.*, vol. 16, no. 3, pp. 261–265, Mar. 2005, doi: 10.1007/s10856-005-6688-x.

[6] G. Zhao and S. E. Stevens, "Multiple parameters for the comprehensive evaluation of the susceptibility of Escherichia coli to the silver ion," *Biometals*, vol. 11, no. 1, pp. 27–32, 1998, doi: 10.1023/A:1009253223055.

[7] G. Singhal, R. Bhavesh, K. Kasariya, A. R. Sharma, and R. P. Singh, "Biosynthesis of silver nanoparticles using Ocimum sanctum (Tulsi) leaf extract and screening its antimicrobial activity," *J. Nanoparticle Res.*, vol. 13, no. 7, pp. 2981–2988, 2011, doi: 10.1007/s11051-010-0193-y.

[8] H. Nhung Tran *et al.*, "Optical nanoparticles: synthesis and biomedical application," *Adv. Nat. Sci. Nanosci. Nanotechnol.*, vol. 6, no. 2, p. 23002, 2015, doi: 10.1088/2043-6262/6/2/023002.

[9] D. Rueda, V. Arias, Y. Zhang, A. Cabot, A. C. Agudelo, and D. Cadavid, "Low-cost tangerine peel waste mediated production of Titanium Dioxide Nanocrystals: Synthesis and characterization," *Environ. Nanotechnology, Monit. Manag.*, vol. 13, no. January, p. 100285, 2020, doi: 10.1016/j.enmm.2020.100285.

[10] M. Nadeem *et al.*, "The current trends in the green syntheses of titanium oxide nanoparticles and their applications," *Green Chem. Lett. Rev.*, vol. 11, no. 4, pp. 492–502, 2018, doi: 10.1080/17518253.2018.1538430.

[11] W. Ahmad, K. K. Jaiswal, and S. Soni, "Green synthesis of titanium dioxide (TiO2) nanoparticles by using Mentha arvensis leaves extract and its antimicrobial properties,"

Inorg. Nano-Metal Chem., vol. 50, no. 10, pp. 1032–1038, Oct. 2020, doi: 10.1080/24701556.2020.1732419.

[12] E. Ismail, M. Khenfouch, M. Dhlamini, S. Dube, and M. Maaza, "Green palladium and palladium oxide nanoparticles synthesized via Aspalathus linearis natural extract," *J. Alloys Compd.*, vol. 695, pp. 3632–3638, 2017, doi: https://doi.org/10.1016/j.jallcom.2016.11.390.

[13] M. C. Edmundson, M. Capeness, and L. Horsfall, "Exploring the potential of metallic nanoparticles within synthetic biology," *N. Biotechnol.*, vol. 31, no. 6, pp. 572–578, 2014, doi: https://doi.org/10.1016/j.nbt.2014.03.004.

[14] R. Rajendhiran, V. Deivasigamani, J. Palanisamy, S. Masan, and S. Pitchaiya, "Terminalia catappa and carissa carandas assisted synthesis of Tio2 nanoparticles – A green synthesis approach," *Mater. Today Proc.*, vol. 45, pp. 2232–2238, 2021, doi: https://doi.org/10.1016/j.matpr.2020.10.223.

[15] S. Shanavas *et al.*, "Green synthesis of titanium dioxide nanoparticles using Phyllanthus niruri leaf extract and study on its structural, optical and morphological properties," *Mater. Today Proc.*, vol. 26, pp. 3531–3534, 2020, doi: https://doi.org/10.1016/j.matpr.2019.06.715.

[16] L.-L. Long, A.-Y. Zhang, J. Yang, X. Zhang, and H.-Q. Yu, "A Green Approach for Preparing Doped TiO2 Single Crystals," *ACS Appl. Mater. Interfaces*, vol. 6, no. 19, pp. 16712–16720, Oct. 2014, doi: 10.1021/am503661w.

[17] T. N. Rao *et al.*, "Green synthesis and structural classification of Acacia nilotica mediated-silver doped titanium oxide (Ag/TiO2) spherical nanoparticles: Assessment of its antimicrobial and anticancer activity," *Saudi J. Biol. Sci.*, vol. 26, no. 7, pp. 1385–1391, 2019, doi: https://doi.org/10.1016/j.sjbs.2019.09.005.

[18] K. Chand *et al.*, "Photocatalytic and antimicrobial activity of biosynthesized silver and titanium dioxide nanoparticles: A comparative study," *J. Mol. Liq.*, vol. 316, p. 113821, 2020, doi: https://doi.org/10.1016/j.molliq.2020.113821.

[19] P. Maheswari, S. Ponnusamy, S. Harish, M. R. Ganesh, and Y. Hayakawa, "Hydrothermal synthesis of pure and bio modified TiO2: Characterization, evaluation of antibacterial activity against gram positive and gram negative bacteria and anticancer activity against KB Oral cancer cell line," *Arab. J. Chem.*, vol. 13, no. 1, pp. 3484–3497, 2020, doi: https://doi.org/10.1016/j.arabjc.2018.11.020.

[20] B. Khodashenas and H. R. Ghorbani, "Synthesis of silver nanoparticles with different shapes," *Arab. J. Chem.*, vol. 12, no. 8, pp. 1823–1838, 2019, doi: https://doi.org/10.1016/j.arabjc.2014.12.014.

[21] A. E. Schwarz, "Green Dreams of Reason. Green Nanotechnology Between Visions of Excess and Control," *Nanoethics*, vol. 3, no. 2, pp. 109–118, 2009, doi: 10.1007/s11569-009-0061-3.

[22] J. E. Hutchison, "Greener Nanoscience: A Proactive Approach to Advancing Applications and Reducing Implications of Nanotechnology," *ACS Nano*, vol. 2, no. 3, pp. 395–402, Mar. 2008, doi: 10.1021/nn800131j.

[23] K. J. Klabunde and R. M. Richards, *Nanoscale Materials in Chemistry*. Wiley, 2009.

[24] D. Knopp, D. Tang, and R. Niessner, "Review: Bioanalytical applications of biomolecule-functionalized nanometer-sized doped silica particles," *Anal. Chim. Acta*, vol. 647, no. 1, pp. 14–30, 2009, doi: https://doi.org/10.1016/j.aca.2009.05.037.

[25] Z. P. Xu, Q. H. Zeng, G. Q. Lu, and A. B. Yu, "Inorganic nanoparticles as carriers for efficient cellular delivery," *Chem. Eng. Sci.*, vol. 61, no. 3, pp. 1027–1040, 2006, doi: https://doi.org/10.1016/j.ces.2005.06.019.

[26] F. Gu, S. F. Wang, M. K. Lü, G. J. Zhou, D. Xu, and D. R. Yuan, "Photoluminescence Properties of SnO2 Nanoparticles Synthesized by Sol−Gel Method," *J. Phys. Chem. B*, vol. 108, no. 24, pp. 8119–8123, Jun. 2004, doi: 10.1021/jp036741e.

[27] H. Zhang and J. F. Banfield, "Kinetics of Crystallization and Crystal Growth of Nanocrystalline Anatase in Nanometer-Sized Amorphous Titania," *Chem. Mater.*, vol. 14, no. 10, pp. 4145–4154, Oct. 2002, doi: 10.1021/cm020072k.

[28] C. Alexiou *et al.*, "Targeting cancer cells: magnetic nanoparticles as drug carriers.," *Eur. Biophys. J.*, vol. 35, no. 5, pp. 446–450, May 2006, doi: 10.1007/s00249-006-0042-1.

[29] H. Yu, X. Zheng, Z. Yin, F. Tag, B. Fang, and K. Hou, "Preparation of Nitrogen-doped TiO2 Nanoparticle Catalyst and Its Catalytic Activity under Visible Light* *Supported by the Science and Technology Research Program of Chongqing Education Commission (KJ050702), and the Natural Science Foundation Project of ," *Chinese J. Chem. Eng.*, vol. 15, no. 6, pp. 802–807, 2007, doi: https://doi.org/10.1016/S1004-9541(08)60006-3.

[30] G. Cao and Y. Wang, *Nanostructures and Nanomaterials*, vol. Volume 2. WORLD SCIENTIFIC, 2011.

[31] T. M. Tolaymat, A. M. El Badawy, A. Genaidy, K. G. Scheckel, T. P. Luxton, and M. Suidan, "An evidence-based environmental perspective of manufactured silver nanoparticle in syntheses and applications: a systematic review and critical appraisal of peer-reviewed scientific papers.," *Sci. Total Environ.*, vol. 408, no. 5, pp. 999–1006, Feb. 2010, doi: 10.1016/j.scitotenv.2009.11.003.

[32] W. Yan *et al.*, "A novel, practical and green synthesis of Ag nanoparticles catalyst and its application in three-component coupling of aldehyde, alkyne, and amine," *J. Mol. Catal. A-chemical*, vol. 255, pp. 81–85, 2006.

[33] M. L. Gulrajani, D. Gupta, S. Periyasamy, and S. G. Muthu, "Preparation and application of silver nanoparticles on silk for imparting antimicrobial properties," *J. Appl. Polym. Sci.*, vol. 108, no. 1, pp. 614–623, Apr. 2008, doi: https://doi.org/10.1002/app.27584.

[34] H. Korbekandi, S. Iravani, and S. Abbasi, "Production of nanoparticles using organisms," *Crit. Rev. Biotechnol.*, vol. 29, no. 4, pp. 279–306, Dec. 2009, doi: 10.3109/07388550903062462.

[35] F. E. Kruis, H. Fissan, and B. Rellinghaus, "Sintering and evaporation characteristics of gas-phase synthesis of size-selected PbS nanoparticles," *Mater. Sci. Eng. B*, vol. 69–70, pp. 329–334, 2000, doi: https://doi.org/10.1016/S0921-5107(99)00298-6.

[36] M. H. Magnusson, K. Deppert, J.-O. Malm, J.-O. Bovin, and L. Samuelson, "Gold Nanoparticles: Production, Reshaping, and Thermal Charging," *J. Nanoparticle Res.*, vol. 1, no. 2, pp. 243–251, 1999, doi: 10.1023/A:1010012802415.

[37] V. K. Sharma, R. A. Yngard, and Y. Lin, "Silver nanoparticles: green synthesis and their antimicrobial activities.," *Adv. Colloid Interface Sci.*, vol. 145, no. 1–2, pp. 83–96, Jan. 2009, doi: 10.1016/j.cis.2008.09.002.

[38] S. Gómez-Graña *et al.*, "Biogenic Synthesis of Metal Nanoparticles Using a Biosurfactant Extracted from Corn and Their Antimicrobial Properties.," *Nanomater. (Basel, Switzerland)*, vol. 7, no. 6, Jun. 2017, doi: 10.3390/nano7060139.

[39] R. Kumari, J. S. Singh, and D. P. Singh, "Biogenic synthesis and spatial distribution of silver nanoparticles in the legume mungbean plant (Vigna radiata L.).," *Plant Physiol. Biochem. PPB*, vol. 110, pp. 158–166, Jan. 2017, doi: 10.1016/j.plaphy.2016.06.001.

[40] J. Purohit, A. Chattopadhyay, and N. K. Singh, "Green Synthesis of Microbial Nanoparticle: Approaches to Application BT - Microbial Nanobionics: Volume 2, Basic Research and Applications," R. Prasad, Ed. Cham: Springer International Publishing, 2019, pp. 35–60.

[41] V. Kumar and S. K. Yadav, "Plant-mediated synthesis of silver and gold nanoparticles and their applications," *J. Chem. Technol. Biotechnol.*, vol. 84, no. 2, pp. 151–157, Feb. 2009, doi: https://doi.org/10.1002/jctb.2023.

[42] G. Marslin, R. K. Selvakesavan, G. Franklin, B. Sarmento, and A. C. P. Dias, "Antimicrobial activity of cream incorporated with silver nanoparticles biosynthesized from Withania somnifera.," *Int. J. Nanomedicine*, vol. 10, pp. 5955–5963, 2015, doi: 10.2147/IJN.S81271.

[43] S. Gunalan, R. Sivaraj, and V. Rajendran, "Green synthesized ZnO nanoparticles against bacterial and fungal pathogens," *Prog. Nat. Sci. Mater. Int.*, vol. 22, no. 6, pp. 693–700, 2012, doi: https://doi.org/10.1016/j.pnsc.2012.11.015.

[44] S. Sudhasree, A. Shakila Banu, P. Brindha, and G. A. Kurian, "Synthesis of nickel nanoparticles by chemical and green route and their comparison in respect to biological effect and toxicity," *Toxicol. Environ. Chem.*, vol. 96, no. 5, pp. 743–754, May 2014, doi: 10.1080/02772248.2014.923148.

[45] J. Singh, A. Mehta, M. Rawat, and S. Basu, "Green synthesis of silver nanoparticles using sun dried tulsi leaves and its catalytic application for 4-Nitrophenol reduction," *J. Environ. Chem. Eng.*, vol. 6, no. 1, pp. 1468–1474, 2018, doi: https://doi.org/10.1016/j.jece.2018.01.054.

[46] C.-G. Yuan, C. Huo, B. Gui, P. Liu, and C. Zhang, "Green Synthesis of Silver Nanoparticles Using Chenopodium aristatum L. Stem Extract and Their Catalytic/Antibacterial Activities," *J. Clust. Sci.*, vol. 28, no. 3, pp. 1319–1333, 2017, doi: 10.1007/s10876-016-1147-z.

[47] M. Nanoparticles *et al.*, "Secondary Metabolites in the Green Synthesis of," no. Figure 1, pp. 1–25, doi: 10.3390/ma11060940.

[48] N. A. Anjum *et al.*, “Jacks of metal/metalloid chelation trade in plants—an overview,” *Front. Plant Sci.*, vol. 6, 2015, doi: 10.3389/fpls.2015.00192.

[49] S. Branco-Neves *et al.*, “An efficient antioxidant system and heavy metal exclusion from leaves make Solanum cheesmaniae more tolerant to Cu than its cultivated counterpart,” *Food Energy Secur.*, vol. 6, no. 3, pp. 123–133, Aug. 2017, doi: https://doi.org/10.1002/fes3.114.

[50] M. K. Hasan, Y. Cheng, M. K. Kanwar, X.-Y. Chu, G. J. Ahammed, and Z.-Y. Qi, “Responses of Plant Proteins to Heavy Metal Stress—A Review,” *Front. Plant Sci.*, vol. 8, 2017, doi: 10.3389/fpls.2017.01492.

[51] G. Marslin, C. J. Sheeba, and G. Franklin, “Nanoparticles Alter Secondary Metabolism in Plants via ROS Burst,” *Front. Plant Sci.*, vol. 8, 2017, doi: 10.3389/fpls.2017.00832.

[52] G. Franklin, L. F. R. Conceição, E. Kombrink, and A. C. P. Dias, “Xanthone biosynthesis in Hypericum perforatum cells provides antioxidant and antimicrobial protection upon biotic stress,” *Phytochemistry*, vol. 70, no. 1, pp. 60–68, 2009, doi: https://doi.org/10.1016/j.phytochem.2008.10.016.

[53] V. V Makarov *et al.*, “‘Green’ nanotechnologies: synthesis of metal nanoparticles using plants,” *Acta Naturae*, vol. 6, no. 1, pp. 35–44, Jan. 2014, [Online]. Available: https://pubmed.ncbi.nlm.nih.gov/24772325.

[54] S. L. Smitha, D. Philip, and K. G. Gopchandran, “Green synthesis of gold nanoparticles using Cinnamomum zeylanicum leaf broth.,” *Spectrochim. Acta. A. Mol. Biomol. Spectrosc.*, vol. 74, no. 3, pp. 735–739, Oct. 2009, doi: 10.1016/j.saa.2009.08.007.

[55] J. Kim *et al.*, “Peptide-mediated shape- and size-tunable synthesis of gold nanostructures.,” *Acta Biomater.*, vol. 6, no. 7, pp. 2681–2689, Jul. 2010, doi: 10.1016/j.actbio.2010.01.019.

[56] P. Malik, R. Shankar, V. Malik, N. Sharma, and T. K. Mukherjee, “Green Chemistry Based Benign Routes for Nanoparticle Synthesis,” *J. Nanoparticles*, vol. 2014, p. 302429, 2014, doi: 10.1155/2014/302429.

[57] M. S. Akhtar, J. Panwar, and Y.-S. Yun, “Biogenic Synthesis of Metallic Nanoparticles by Plant Extracts,” *ACS Sustain. Chem. Eng.*, vol. 1, no. 6, pp. 591–602, Jun. 2013, doi: 10.1021/sc300118u.

[58] E. C. Njagi *et al.*, “Biosynthesis of Iron and Silver Nanoparticles at Room Temperature Using Aqueous Sorghum Bran Extracts,” *Langmuir*, vol. 27, no. 1, pp. 264–271, Jan. 2011, doi: 10.1021/la103190n.

[59] J. Pan *et al.*, “Bioactive phenolics from mango leaves (Mangifera indica L.),” *Ind. Crops Prod.*, vol. 111, pp. 400–406, 2018, doi: https://doi.org/10.1016/j.indcrop.2017.10.057.

[60] J. C. Barreto *et al.*, “Characterization and Quantitation of Polyphenolic Compounds in Bark, Kernel, Leaves, and Peel of Mango (Mangifera indica L.),” *J. Agric. Food Chem.*, vol. 56, no. 14, pp. 5599–5610, Jul. 2008, doi: 10.1021/jf800738r.

[61] M. Kumar *et al.*, “Mango (Mangifera indica L.) Leaves: Nutritional Composition, Phytochemical Profile, and Health-Promoting Bioactivities,” *Antioxidants* , vol. 10, no. 2.

2021, doi: 10.3390/antiox10020299.

[62] D. Sundeep, T. Vijaya Kumar, P. S. S. Rao, R. V. S. S. N. Ravikumar, and A. Gopala Krishna, “Green synthesis and characterization of Ag nanoparticles from Mangifera indica leaves for dental restoration and antibacterial applications,” *Prog. Biomater.*, vol. 6, no. 1, pp. 57–66, 2017, doi: 10.1007/s40204-017-0067-9.

[63] S. Dhuper, D. Panda, and P. P. L. Nayak, “Green Synthesis and Characterization of Zero Valent Iron Nanoparticles from the Leaf Extract of Mangifera indica,” vol. 13, no. 2, pp. 16–22, 2012.

[64] M. S. Al-Ruqeishi, T. Mohiuddin, and L. K. Al-Saadi, “Green synthesis of iron oxide nanorods from deciduous Omani mango tree leaves for heavy oil viscosity treatment,” *Arab. J. Chem.*, vol. 12, no. 8, pp. 4084–4090, 2019, doi: https://doi.org/10.1016/j.arabjc.2016.04.003.

[65] T. Muralikrishna, R. Malothu, M. Pattanayak, and P. L. Nayak, “Green Synthesis of Gold Nanoparticles Using Mangifera Indica (Mango Leaves) Aqueous Extract,” vol. 3, no. 2, pp. 66–73, 2014, doi: 10.5829/idosi.wjnst.2014.3.2.114.

[66] S. Rajeshkumar, S. V. Kumar, A. Ramaiah, H. Agarwal, T. Lakshmi, and S. M. Roopan, “Biosynthesis of zinc oxide nanoparticles usingMangifera indica leaves and evaluation of their antioxidant and cytotoxic properties in lung cancer (A549) cells,” *Enzyme Microb. Technol.*, vol. 117, pp. 91–95, 2018, doi: https://doi.org/10.1016/j.enzmictec.2018.06.009.

[67] S. Mahshid, M. Askari, and M. S. Ghamsari, “Synthesis of TiO2 nanoparticles by hydrolysis and peptization of titanium isopropoxide solution,” *J. Mater. Process. Technol.*, vol. 189, no. 1, pp. 296–300, 2007, doi: https://doi.org/10.1016/j.jmatprotec.2007.01.040.

[68] D. A. H. Hanaor, I. Chironi, I. Karatchevtseva, G. Triani, and C. C. Sorrell, “Single and mixed phase TiO2 powders prepared by excess hydrolysis of titanium alkoxide,” *Adv. Appl. Ceram.*, vol. 111, no. 3, pp. 149–158, Apr. 2012, doi: 10.1179/1743676111Y.0000000059.

[69] J.-M. Herrmann, “Titania-based true heterogeneous photocatalysis,” *Environ. Sci. Pollut. Res.*, vol. 19, no. 9, pp. 3655–3665, 2012, doi: 10.1007/s11356-011-0697-8.

[70] A. FUJISHIMA and K. HONDA, “Electrochemical Photolysis of Water at a Semiconductor Electrode,” *Nature*, vol. 238, no. 5358, pp. 37–38, 1972, doi: 10.1038/238037a0.

[71] D. Hariharan *et al.*, “Enhanced photocatalysis and anticancer activity of green hydrothermal synthesized Ag@TiO2 nanoparticles,” *J. Photochem. Photobiol. B Biol.*, vol. 202, no. September 2019, p. 111636, 2020, doi: 10.1016/j.jphotobiol.2019.111636.

[72] S. Middlemas, Z. Z. Fang, and P. Fan, “A new method for production of titanium dioxide pigment,” *Hydrometallurgy*, vol. 131–132, pp. 107–113, 2013, doi: https://doi.org/10.1016/j.hydromet.2012.11.002.

[73] R. Singh and H. S. Nalwa, “Medical applications of nanoparticles in biological imaging, cell labeling, antimicrobial agents, and anticancer nanodrugs.,” *J. Biomed. Nanotechnol.*, vol. 7, no. 4, pp. 489–503, Aug. 2011, doi: 10.1166/jbn.2011.1324.

[74] C. Garzella, E. Comini, E. Tempesti, C. Frigeri, and G. Sberveglieri, “TiO2 thin films by a

novel sol–gel processing for gas sensor applications," *Sensors Actuators B Chem.*, vol. 68, no. 1, pp. 189–196, 2000, doi: https://doi.org/10.1016/S0925-4005(00)00428-7.

[75] A. Mills, R. H. Davies, and D. Worsley, "Water purification by semiconductor photocatalysis," *Chem. Soc. Rev.*, vol. 22, no. 6, pp. 417–425, 1993, doi: 10.1039/CS9932200417.

[76] N. Serpone, D. Dondi, and A. Albini, "Inorganic and organic UV filters: Their role and efficacy in sunscreens and suncare products," *Inorganica Chim. Acta*, vol. 360, no. 3, pp. 794–802, 2007, doi: https://doi.org/10.1016/j.ica.2005.12.057.

[77] B. O'Regan and M. Grätzel, "A low-cost, high-efficiency solar cell based on dye-sensitized colloidal TiO2 films," *Nature*, vol. 353, no. 6346, pp. 737–740, 1991, doi: 10.1038/353737a0.

[78] D. Y. C. Leung *et al.*, "Hydrogen production over titania-based photocatalysts.," *ChemSusChem*, vol. 3, no. 6, pp. 681–694, Jun. 2010, doi: 10.1002/cssc.201000014.

[79] A. Fujishima, X. Zhang, and D. A. Tryk, "TiO2 photocatalysis and related surface phenomena," *Surf. Sci. Rep.*, vol. 63, no. 12, pp. 515–582, 2008, doi: https://doi.org/10.1016/j.surfrep.2008.10.001.

[80] A. Primo, A. Corma, and H. García, "Titania supported gold nanoparticles as photocatalyst," *Phys. Chem. Chem. Phys.*, vol. 13, no. 3, pp. 886–910, 2011, doi: 10.1039/C0CP00917B.

[81] D. C. Hurum, A. G. Agrios, K. A. Gray, T. Rajh, and M. C. Thurnauer, "Explaining the Enhanced Photocatalytic Activity of Degussa P25 Mixed-Phase TiO2 Using EPR," *J. Phys. Chem. B*, vol. 107, no. 19, pp. 4545–4549, May 2003, doi: 10.1021/jp0273934.

[82] U. Diebold, "The surface science of titanium dioxide," *Surf. Sci. Rep.*, vol. 48, no. 5, pp. 53–229, 2003, doi: https://doi.org/10.1016/S0167-5729(02)00100-0.

[83] C. Colbeau-Justin, M. Kunst, and D. Huguenin, "Structural influence on charge-carrier lifetimes in TiO2 powders studied by microwave absorption," *J. Mater. Sci.*, vol. 38, no. 11, pp. 2429–2437, 2003, doi: 10.1023/A:1023905102094.

[84] N. Sakai, Y. Ebina, K. Takada, and T. Sasaki, "Electronic Band Structure of Titania Semiconductor Nanosheets Revealed by Electrochemical and Photoelectrochemical Studies," *J. Am. Chem. Soc.*, vol. 126, no. 18, pp. 5851–5858, May 2004, doi: 10.1021/ja0394582.

[85] T. Luttrell, S. Halpegamage, J. Tao, A. Kramer, E. Sutter, and M. Batzill, "Why is anatase a better photocatalyst than rutile? - Model studies on epitaxial TiO2 films," *Sci. Rep.*, vol. 4, pp. 1–8, 2015, doi: 10.1038/srep04043.

[86] L. Liu, H. Zhao, J. M. Andino, and Y. Li, "Photocatalytic CO2 Reduction with H2O on TiO2 Nanocrystals: Comparison of Anatase, Rutile, and Brookite Polymorphs and Exploration of Surface Chemistry," *ACS Catal.*, vol. 2, no. 8, pp. 1817–1828, Aug. 2012, doi: 10.1021/cs300273q.

[87] N. Kislov, J. Lahiri, H. Verma, D. Y. Goswami, E. Stefanakos, and M. Batzill,

"Photocatalytic degradation of methyl orange over single crystalline ZnO: orientation dependence of photoactivity and photostability of ZnO.," *Langmuir*, vol. 25, no. 5, pp. 3310–3315, Mar. 2009, doi: 10.1021/la803845f.

[88] T. Ohno, K. Sarukawa, and M. Matsumura, "Crystal faces of rutile and anatase TiO2 particles and their roles in photocatalytic reactions," *New J. Chem.*, vol. 26, no. 9, pp. 1167–1170, 2002, doi: 10.1039/B202140D.

[89] M. Batzill, "Fundamental aspects of surface engineering of transition metal oxide photocatalysts," *Energy Environ. Sci.*, vol. 4, no. 9, pp. 3275–3286, 2011, doi: 10.1039/C1EE01577J.

[90] J. N. Wilson and H. Idriss, "Effect of surface reconstruction of TiO2(001) single crystal on the photoreaction of acetic acid," *J. Catal.*, vol. 214, no. 1, pp. 46–52, 2003, doi: https://doi.org/10.1016/S0021-9517(02)00172-0.

[91] M. Xu *et al.*, "Photocatalytic Activity of Bulk ${\mathrm{TiO}}_{2}$ Anatase and Rutile Single Crystals Using Infrared Absorption Spectroscopy," *Phys. Rev. Lett.*, vol. 106, no. 13, p. 138302, Mar. 2011, doi: 10.1103/PhysRevLett.106.138302.

[92] J. L. Giocondi, P. A. Salvador, and G. S. Rohrer, "The origin of photochemical anisotropy in SrTiO3," *Top. Catal.*, vol. 44, no. 4, pp. 529–533, 2007, doi: 10.1007/s11244-006-0101-y.

[93] S. G. Kumar and L. G. Devi, "Review on Modified TiO2 Photocatalysis under UV/Visible Light: Selected Results and Related Mechanisms on Interfacial Charge Carrier Transfer Dynamics," *J. Phys. Chem. A*, vol. 115, no. 46, pp. 13211–13241, Nov. 2011, doi: 10.1021/jp204364a.

[94] A. Mills and S. Le Hunte, "An overview of semiconductor photocatalysis," *J. Photochem. Photobiol. A Chem.*, vol. 108, no. 1, pp. 1–35, 1997, doi: https://doi.org/10.1016/S1010-6030(97)00118-4.

[95] M. Pelaez *et al.*, "A review on the visible light active titanium dioxide photocatalysts for environmental applications," *Appl. Catal. B Environ.*, vol. 125, pp. 331–349, 2012, doi: https://doi.org/10.1016/j.apcatb.2012.05.036.

[96] W. Y. Teoh, J. A. Scott, and R. Amal, "Progress in Heterogeneous Photocatalysis: From Classical Radical Chemistry to Engineering Nanomaterials and Solar Reactors," *J. Phys. Chem. Lett.*, vol. 3, no. 5, pp. 629–639, Mar. 2012, doi: 10.1021/jz3000646.

[97] F. Amano, O.-O. Prieto-Mahaney, Y. Terada, T. Yasumoto, T. Shibayama, and B. Ohtani, "Decahedral Single-Crystalline Particles of Anatase Titanium(IV) Oxide with High Photocatalytic Activity," *Chem. Mater.*, vol. 21, no. 13, pp. 2601–2603, Jul. 2009, doi: 10.1021/cm9004344.

[98] H. Tong, S. Ouyang, Y. Bi, N. Umezawa, M. Oshikiri, and J. Ye, "Nano-photocatalytic Materials: Possibilities and Challenges," *Adv. Mater.*, vol. 24, no. 2, pp. 229–251, Jan. 2012, doi: https://doi.org/10.1002/adma.201102752.

[99] S. M. Gupta and M. Tripathi, "A review of TiO2 nanoparticles," *Chinese Sci. Bull.*, vol. 56, no. 16, p. 1639, 2011, doi: 10.1007/s11434-011-4476-1.

[100] N. Aman, P. K. Satapathy, T. Mishra, M. Mahato, and N. N. Das, "Synthesis and photocatalytic activity of mesoporous cerium doped TiO2 as visible light sensitive photocatalyst," *Mater. Res. Bull.*, vol. 47, no. 2, pp. 179–183, 2012, doi: https://doi.org/10.1016/j.materresbull.2011.11.049.

[101] F. E. Oropeza, B. Mei, I. Sinev, A. E. Becerikli, M. Muhler, and J. Strunk, "Effect of Sn surface states on the photocatalytic activity of anatase TiO2," *Appl. Catal. B Environ.*, vol. 140–141, pp. 51–59, 2013, doi: https://doi.org/10.1016/j.apcatb.2013.03.043.

[102] C. Di Valentin, G. Pacchioni, and A. Selloni, "Origin of the different photoactivity of N-doped anatase and rutile ${\mathrm{TiO}}_{2}$," *Phys. Rev. B*, vol. 70, no. 8, p. 85116, Aug. 2004, doi: 10.1103/PhysRevB.70.085116.

[103] A. R., M. T., O. T., A. K., and T. Y., "Visible-Light Photocatalysis in Nitrogen-Doped Titanium Oxides," *Science (80-.).*, vol. 293, no. 5528, pp. 269–271, Jul. 2001, doi: 10.1126/science.1061051.

[104] R. M. MOHAMED and E. AAZAM, "Synthesis and characterization of P-doped TiO2 thin-films for photocatalytic degradation of butyl benzyl phthalate under visible-light irradiation," *Chinese J. Catal.*, vol. 34, no. 6, pp. 1267–1273, 2013, doi: https://doi.org/10.1016/S1872-2067(12)60572-5.

[105] R. Fateh, A. A. Ismail, R. Dillert, and D. W. Bahnemann, "Highly Active Crystalline Mesoporous TiO2 Films Coated onto Polycarbonate Substrates for Self-Cleaning Applications," *J. Phys. Chem. C*, vol. 115, no. 21, pp. 10405–10411, Jun. 2011, doi: 10.1021/jp200892z.

[106] M. V. Dozzi, S. Livraghi, E. Giamello, and E. Selli, "Photocatalytic activity of S- and F-doped TiO2 in formic acid mineralization," *Photochem. Photobiol. Sci.*, vol. 10, no. 3, pp. 343–349, 2011, doi: 10.1039/C0PP00182A.

[107] B. Viswanathan and K. R. Krishanmurthy, "Nitrogen Incorporation in TiO_2: Does It Make a Visible Light Photo-Active Material?," *Int. J. Photoenergy*, vol. 2012, p. 269654, 2012, doi: 10.1155/2012/269654.

[108] M. A. Henderson, "A surface science perspective on TiO2 photocatalysis," *Surf. Sci. Rep.*, vol. 66, no. 6, pp. 185–297, 2011, doi: https://doi.org/10.1016/j.surfrep.2011.01.001.

[109] Y. Niu, M. Xing, J. Zhang, and B. Tian, "Visible light activated sulfur and iron co-doped TiO2 photocatalyst for the photocatalytic degradation of phenol," *Catal. Today*, vol. 201, pp. 159–166, 2013, doi: https://doi.org/10.1016/j.cattod.2012.04.035.

[110] F. Amano, M. Nakata, K. Asami, and A. Yamakata, "Photocatalytic activity of titania particles calcined at high temperature: Investigating deactivation," *Chem. Phys. Lett.*, vol. 579, pp. 111–113, 2013, doi: https://doi.org/10.1016/j.cplett.2013.06.038.

[111] F. Zuo, L. Wang, T. Wu, Z. Zhang, D. Borchardt, and P. Feng, "Self-Doped Ti3+ Enhanced Photocatalyst for Hydrogen Production under Visible Light," *J. Am. Chem. Soc.*, vol. 132, no. 34, pp. 11856–11857, Sep. 2010, doi: 10.1021/ja103843d.

[112] Roshan, Nainani, Pragati, Thakur, Manohar, and Chaskar, "Synthesis of Silver Doped TiO2 Nanoparticles for the Improved Photocatalytic Degradation of Methyl Orange," 2012.

[113] M. Ikram *et al.*, "Dye degradation performance, bactericidal behavior and molecular docking analysis of Cu-doped TiO2nanoparticles," *RSC Adv.*, vol. 10, no. 41, pp. 24215–24233, 2020, doi: 10.1039/d0ra04851h.

[114] T. Ali, A. Ahmed, U. Alam, I. Uddin, P. Tripathi, and M. Muneer, "Enhanced photocatalytic and antibacterial activities of Ag-doped TiO2 nanoparticles under visible light," *Mater. Chem. Phys.*, vol. 212, pp. 325–335, 2018, doi: https://doi.org/10.1016/j.matchemphys.2018.03.052.

[115] S. Mathew *et al.*, "Cu-Doped TiO2: Visible Light Assisted Photocatalytic Antimicrobial Activity," *Applied Sciences* , vol. 8, no. 11. 2018, doi: 10.3390/app8112067.

[116] J. Bahadur, S. Agrawal, V. Panwar, A. Parveen, and K. Pal, "Antibacterial properties of silver doped TiO2 nanoparticles synthesized via sol-gel technique," *Macromol. Res.*, vol. 24, no. 6, pp. 488–493, 2016, doi: 10.1007/s13233-016-4066-9.

[117] M. Khatami, H. Q. Alijani, and I. Sharifi, "Biosynthesis of bimetallic and core-shell nanoparticles: their biomedical applications - a review.," *IET nanobiotechnology*, vol. 12, no. 7, pp. 879–887, Oct. 2018, doi: 10.1049/iet-nbt.2017.0308.

[118] G. Colón, M. Maicu, M. C. Hidalgo, and J. A. Navío, "Cu-doped TiO2 systems with improved photocatalytic activity," *Appl. Catal. B Environ.*, vol. 67, no. 1, pp. 41–51, 2006, doi: https://doi.org/10.1016/j.apcatb.2006.03.019.

[119] O. Zuas and H. Budiman, "Synthesis of Nanostructured Copper-doped Titania and Its Properties," *Nano-Micro Lett.*, vol. 5, no. 1, pp. 26–33, 2013, doi: 10.1007/BF03353728.

[120] M. A. Acheampong and D. M. B. Antwi, "Modification of Titanium Dioxide for Wastewater Treatment Application and Its Recovery for Reuse," *J. Environ. Sci. \& Eng.*, vol. 5, 2016.

[121] O. State, "Synthesis , Modification , Applications and Challenges of Titanium Dioxide Nanoparticles," vol. 3, no. 4, pp. 10–22, 2019.

[122] N. A. Órdenes-Aenishanslins, L. A. Saona, V. M. Durán-Toro, J. P. Monrás, D. M. Bravo, and J. M. Pérez-Donoso, "Use of titanium dioxide nanoparticles biosynthesized by Bacillus mycoides in quantum dot sensitized solar cells," *Microb. Cell Fact.*, vol. 13, no. 1, p. 90, 2014, doi: 10.1186/s12934-014-0090-7.

[123] A. Kumar, P. Choudhary, A. Kumar, P. H. C. Camargo, and V. Krishnan, "Recent Advances in Plasmonic Photocatalysis Based on TiO2 and Noble Metal Nanoparticles for Energy Conversion, Environmental Remediation, and Organic Synthesis," *Small*, vol. 18, no. 1, p. 2101638, Jan. 2022, doi: https://doi.org/10.1002/smll.202101638.

[124] W. Doerffler and K. Hauffe, "Heterogeneous photocatalysis II. The mechanism of the carbon monoxide oxidation at dark and illuminated zinc oxide surfaces," *J. Catal.*, vol. 3, no. 2, pp. 171–178, 1964, doi: https://doi.org/10.1016/0021-9517(64)90124-1.

[125] V. S. K, "Materials Science in Semiconductor Processing Solar light active biogenic titanium dioxide embedded silver oxide (AgO / Ag 2 O @ TiO 2) nanocomposite structures for dye degradation by photocatalysis," *Mater. Sci. Semicond. Process.*, vol. 132, no. October 2020, p. 105923, 2021, doi: 10.1016/j.mssp.2021.105923.

[126] J.-M. Herrmann, "Heterogeneous photocatalysis: fundamentals and applications to the removal of various types of aqueous pollutants," *Catal. Today*, vol. 53, no. 1, pp. 115–129, 1999, doi: https://doi.org/10.1016/S0920-5861(99)00107-8.

[127] K. Rajeshwar *et al.*, "Heterogeneous photocatalytic treatment of organic dyes in air and aqueous media," *J. Photochem. Photobiol. C Photochem. Rev.*, vol. 9, no. 4, pp. 171–192, 2008, doi: https://doi.org/10.1016/j.jphotochemrev.2008.09.001.

[128] S. Malato, P. Fernández-Ibáñez, M. I. Maldonado, J. Blanco, and W. Gernjak, "Decontamination and disinfection of water by solar photocatalysis: Recent overview and trends," *Catal. Today*, vol. 147, no. 1, pp. 1–59, 2009, doi: https://doi.org/10.1016/j.cattod.2009.06.018.

[129] K. Nakata and A. Fujishima, "TiO2 photocatalysis: Design and applications," *J. Photochem. Photobiol. C Photochem. Rev.*, vol. 13, no. 3, pp. 169–189, 2012, doi: https://doi.org/10.1016/j.jphotochemrev.2012.06.001.

[130] M. M. Khan, S. F. Adil, and A. Al-Mayouf, "Metal oxides as photocatalysts," *J. Saudi Chem. Soc.*, vol. 19, no. 5, pp. 462–464, 2015, doi: https://doi.org/10.1016/j.jscs.2015.04.003.

[131] U. I. Gaya and A. H. Abdullah, "Heterogeneous photocatalytic degradation of organic contaminants over titanium dioxide: A review of fundamentals, progress and problems," *J. Photochem. Photobiol. C Photochem. Rev.*, vol. 9, no. 1, pp. 1–12, 2008, doi: https://doi.org/10.1016/j.jphotochemrev.2007.12.003.

[132] Y. Kuwahara, T. Kamegawa, K. Mori, and H. Yamashita, "Design of New Functional Titanium Oxide-Based Photocatalysts for Degradation of Organics Diluted in Water and Air," *Current Organic Chemistry*, vol. 14, no. 7. pp. 616–629, 2010, doi: http://dx.doi.org/10.2174/138527210790963458.

[133] A. Fujishima, T. N. Rao, and D. A. Tryk, "Titanium dioxide photocatalysis," *J. Photochem. Photobiol. C Photochem. Rev.*, vol. 1, no. 1, pp. 1–21, 2000, doi: https://doi.org/10.1016/S1389-5567(00)00002-2.

[134] H. Honda, A. Ishizaki, R. Soma, K. Hashimoto, and A. Fujishima, "Application of Photocatalytic Reactions Caused by TiO2 Film to Improve the Maintenance Factor of Lighting Systems," *J. Illum. Eng. Soc.*, vol. 27, no. 1, pp. 42–49, Jan. 1998, doi: 10.1080/00994480.1998.10748209.

[135] R. R. Saravanan, F. Gracia, and A. Stephen, "Basic Principles, Mechanism, and Challenges of Photocatalysis," 2017.

[136] I. Bannat, K. Wessels, T. Oekermann, J. Rathousky, D. Bahnemann, and M. Wark, "Improving the Photocatalytic Performance of Mesoporous Titania Films by Modification with Gold Nanostructures," *Chem. Mater.*, vol. 21, no. 8, pp. 1645–1653, Apr. 2009, doi: 10.1021/cm803455k.

[137] V. Gombac *et al.*, "TiO2 nanopowders doped with boron and nitrogen for photocatalytic applications," *Chem. Phys.*, vol. 339, no. 1, pp. 111–123, 2007, doi: https://doi.org/10.1016/j.chemphys.2007.05.024.

[138] J. Zhang, Y. Wu, M. Xing, S. A. K. Leghari, and S. Sajjad, “Development of modified N doped TiO2 photocatalyst with metals{,} nonmetals and metal oxides,” *Energy Environ. Sci.*, vol. 3, no. 6, pp. 715–726, 2010, doi: 10.1039/B927575D.

[139] O. V Makarova, T. Rajh, M. C. Thurnauer, A. Martin, P. A. Kemme, and D. Cropek, “Surface Modification of TiO2 Nanoparticles For Photochemical Reduction of Nitrobenzene,” *Environ. Sci. Technol.*, vol. 34, no. 22, pp. 4797–4803, Nov. 2000, doi: 10.1021/es001109+.

[140] G. Williams, B. Seger, and P. V Kamat, “TiO2-Graphene Nanocomposites. UV-Assisted Photocatalytic Reduction of Graphene Oxide,” *ACS Nano*, vol. 2, no. 7, pp. 1487–1491, Jul. 2008, doi: 10.1021/nn800251f.

[141] O. Carp, C. L. Huisman, and A. Reller, “Photoinduced reactivity of titanium dioxide,” *Prog. Solid State Chem.*, vol. 32, no. 1, pp. 33–177, 2004, doi: https://doi.org/10.1016/j.progsolidstchem.2004.08.001.

[142] N. Nakayama and T. Hayashi, “Preparation and characterization of poly(l-lactic acid)/TiO2 nanoparticle nanocomposite films with high transparency and efficient photodegradability,” *Polym. Degrad. Stab.*, vol. 92, no. 7, pp. 1255–1264, 2007, doi: https://doi.org/10.1016/j.polymdegradstab.2007.03.026.

[143] G. Mascolo, R. Comparelli, M. L. Curri, G. Lovecchio, A. Lopez, and A. Agostiano, “Photocatalytic degradation of methyl red by TiO2: Comparison of the efficiency of immobilized nanoparticles versus conventional suspended catalyst,” *J. Hazard. Mater.*, vol. 142, no. 1, pp. 130–137, 2007, doi: https://doi.org/10.1016/j.jhazmat.2006.07.068.

[144] T. A. Gad-Allah, S. Kato, S. Satokawa, and T. Kojima, “Role of core diameter and silica content in photocatalytic activity of TiO2/SiO2/Fe3O4 composite,” *Solid State Sci.*, vol. 9, no. 8, pp. 737–743, 2007, doi: https://doi.org/10.1016/j.solidstatesciences.2007.05.012.

[145] F. Han, V. S. R. Kambala, M. Srinivasan, D. Rajarathnam, and R. Naidu, “Tailored titanium dioxide photocatalysts for the degradation of organic dyes in wastewater treatment: A review,” *Appl. Catal. A Gen.*, vol. 359, no. 1, pp. 25–40, 2009, doi: https://doi.org/10.1016/j.apcata.2009.02.043.

[146] M. Sökmen, D. W. Allen, F. Akkaş, N. Kartal, and F. Acar, “Photo-Degradation of Some Dyes using Ag-Loaded Titaniumdioxide,” *Water. Air. Soil Pollut.*, vol. 132, no. 1, pp. 153–163, 2001, doi: 10.1023/A:1012069009633.

[147] C. L. de Dicastillo, “Antimicrobial Effect of Titanium Dioxide Nanoparticles,” M. G. Correa, Ed. Rijeka: IntechOpen, 2021, p. Ch. 5.

[148] C. López de Dicastillo, C. Patiño, M. J. Galotto, J. L. Palma, D. Alburquenque, and J. Escrig, “Novel Antimicrobial Titanium Dioxide Nanotubes Obtained through a Combination of Atomic Layer Deposition and Electrospinning Technologies,” *Nanomaterials* , vol. 8, no. 2. 2018, doi: 10.3390/nano8020128.

[149] J. Podporska-Carroll, E. Panaitescu, B. Quilty, L. Wang, L. Menon, and S. C. Pillai, “Antimicrobial properties of highly efficient photocatalytic TiO2 nanotubes,” *Appl. Catal. B Environ.*, vol. 176–177, pp. 70–75, 2015, doi:

https://doi.org/10.1016/j.apcatb.2015.03.029.

[150] Y.-H. Tsuang, J.-S. Sun, Y.-C. Huang, C.-H. Lu, W. H.-S. Chang, and C.-C. Wang, "Studies of photokilling of bacteria using titanium dioxide nanoparticles.," *Artif. Organs*, vol. 32, no. 2, pp. 167–174, Feb. 2008, doi: 10.1111/j.1525-1594.2007.00530.x.

[151] Y. Yuan, J. Ding, J. Xu, J. Deng, and J. Guo, "TiO2 nanoparticles co-doped with silver and nitrogen for antibacterial application.," *J. Nanosci. Nanotechnol.*, vol. 10, no. 8, pp. 4868–4874, Aug. 2010, doi: 10.1166/jnn.2010.2225.

[152] B. Wu, R. Huang, M. Sahu, X. Feng, P. Biswas, and Y. J. Tang, "Bacterial responses to Cu-doped TiO_2 nanoparticles.," *Sci. Total Environ.*, vol. 408, no. 7, pp. 1755–1758, Mar. 2010, doi: 10.1016/j.scitotenv.2009.11.004.

[153] H. H. Mohamed, F. Al Qarni, and N. A. Alomair, "Design of porous Ga doped TiO2 nanostructure for enhanced solar light photocatalytic applications," *Mater. Res. Bull.*, vol. 133, no. May 2020, p. 111057, 2021, doi: 10.1016/j.materresbull.2020.111057.

[154] K. A. Ali, A. Z. Abdullah, and A. R. Mohamed, "Visible light responsive TiO2 nanoparticles modified using Ce and La for photocatalytic reduction of CO2: Effect of Ce dopant content," *Appl. Catal. A Gen.*, vol. 537, pp. 111–120, 2017, doi: https://doi.org/10.1016/j.apcata.2017.03.022.

[155] G. Nabi, W. Raza, and M. B. Tahir, "Green Synthesis of TiO2 Nanoparticle Using Cinnamon Powder Extract and the Study of Optical Properties," *J. Inorg. Organomet. Polym. Mater.*, vol. 30, no. 4, pp. 1425–1429, 2020, doi: 10.1007/s10904-019-01248-3.

[156] M. Aqeel *et al.*, "TiO2Co-doped with Zr and Ag shows highly efficient visible light photocatalytic behavior suitable for treatment of polluted water," *RSC Adv.*, vol. 10, no. 69, pp. 42235–42248, 2020, doi: 10.1039/d0ra08718a.

[157] A. Khlyustova, N. Sirotkin, T. Kusova, A. Kraev, V. Titov, and A. Agafonov, "Doped TiO2: The effect of doping elements on photocatalytic activity," *Mater. Adv.*, vol. 1, no. 5, pp. 1193–1201, 2020, doi: 10.1039/d0ma00171f.

[158] S. I. Mogal *et al.*, "Single-step synthesis of silver-doped titanium dioxide: Influence of silver on structural, textural, and photocatalytic properties," *Ind. Eng. Chem. Res.*, vol. 53, no. 14, pp. 5749–5758, 2014, doi: 10.1021/ie404230q.

[159] A. Ahmad, J. Thiel, and S. I. Shah, "Structural effects of niobium and silver doping on titanium dioxide nanoparticles," *J. Phys. Conf. Ser.*, vol. 61, pp. 11–15, 2007, doi: 10.1088/1742-6596/61/1/003.

[160] A. Weibel, R. Bouchet, F. Boulc', and P. Knauth, "The Big Problem of Small Particles: A Comparison of Methods for Determination of Particle Size in Nanocrystalline Anatase Powders," *Chem. Mater.*, vol. 17, no. 9, pp. 2378–2385, May 2005, doi: 10.1021/cm0403762.

[161] A. Burns, G. Hayes, W. Li, J. Hirvonen, J. D. Demaree, and S. I. Shah, "Neodymium ion dopant effects on the phase transformation in sol–gel derived titania nanostructures," *Mater. Sci. Eng. B*, vol. 111, no. 2, pp. 150–155, 2004, doi: https://doi.org/10.1016/j.mseb.2004.04.008.

[162] M. Hamadanian, S. Karimzadeh, V. Jabbari, and D. Villagrán, "Materials Science in Semiconductor Processing Synthesis of cysteine , cobalt and copper-doped TiO 2 nanophotocatalysts with excellent visible-light-induced photocatalytic activity," *Mater. Sci. Semicond. Process.*, vol. 41, pp. 168–176, 2016, doi: 10.1016/j.mssp.2015.06.085.

[163] C.-H. Yu, K. Tam, and E. S. C. Tsang, "Chapter 5 Chemical Methods for Preparation of Nanoparticles in Solution," in *Metallic Nanoparticles*, vol. 5, J. A. B. T.-H. of M. P. Blackman, Ed. Elsevier, 2008, pp. 113–141.

[164] X. J. Yang, S. Wang, H. M. Sun, X. B. Wang, and J. S. Lian, "Preparation and photocatalytic performance of Cu-doped TiO2 nanoparticles," *Trans. Nonferrous Met. Soc. China (English Ed.*, vol. 25, no. 2, pp. 504–509, 2015, doi: 10.1016/S1003-6326(15)63631-7.

[165] R. J. Alvaro, N. D. Diana, and A. M. Maria, "Effect of Cu on optical properties of TiO2 nanoparticles," *Contemp. Eng. Sci.*, vol. 10, pp. 1539–1549, 2017.

[166] K. Vijayalakshmi and D. Sivaraj, "Synergistic antibacterial activity of barium doped TiO2 nanoclusters synthesized by microwave processing," *RSC Adv.*, vol. 6, no. 12, pp. 9663–9671, 2016, doi: 10.1039/C5RA28125C.

[167] K. Tahir *et al.*, "Visible light photo catalytic inactivation of bacteria and photo degradation of methylene blue with Ag/TiO2 nanocomposite prepared by a novel method," *J. Photochem. Photobiol. B Biol.*, vol. 162, pp. 189–198, 2016, doi: https://doi.org/10.1016/j.jphotobiol.2016.06.039.

[168] R. S. Dariani, A. Esmaeili, A. Mortezaali, and S. Dehghanpour, "Optik Photocatalytic reaction and degradation of methylene blue on TiO 2 nano-sized particles," *Opt. - Int. J. Light Electron Opt.*, vol. 127, no. 18, pp. 7143–7154, 2016, doi: 10.1016/j.ijleo.2016.04.026.

[169] P. Saini, S. K. Saha, P. Roy, P. Chowdhury, and S. P. Sinha Babu, "Evidence of reactive oxygen species (ROS) mediated apoptosis in Setaria cervi induced by green silver nanoparticles from Acacia auriculiformis at a very low dose.," *Exp. Parasitol.*, vol. 160, pp. 39–48, Jan. 2016, doi: 10.1016/j.exppara.2015.11.004.

[170] S. M. Hunagund *et al.*, "Photocatalysis effect of a novel green synthesis gadolinium doped titanium dioxide nanoparticles on their biological activities," *J. Photochem. Photobiol. A Chem.*, vol. 346, pp. 159–167, 2017, doi: https://doi.org/10.1016/j.jphotochem.2017.06.003.

[171] A. Hernández-Gordillo and V. R. González, "Silver nanoparticles loaded on Cu-doped TiO2 for the effective reduction of nitro-aromatic contaminants," *Chem. Eng. J.*, vol. 261, pp. 53–59, 2015, doi: https://doi.org/10.1016/j.cej.2014.05.148.

[172] S. Naraginti, T. V. L. Thejaswini, D. Prabhakaran, A. Sivakumar, V. S. V Satyanarayana, and A. S. Arun Prasad, "Enhanced photo-catalytic activity of Sr and Ag co-doped TiO2 nanoparticles for the degradation of Direct Green-6 and Reactive Blue-160 under UV & visible light," *Spectrochim. Acta Part A Mol. Biomol. Spectrosc.*, vol. 149, pp. 571–579, 2015, doi: https://doi.org/10.1016/j.saa.2015.04.101.